DEVELOPMENT OF A PRELIMINARY DESIGN TOOL AND CFD SIMULATIONS FOR HYPERSONIC INTAKES

A THESIS SUBMITTED TO
THE GRADUATE SCHOOL OF NATURAL AND APPLIED SCIENCES
OF
MIDDLE EAST TECHNICAL UNIVERSITY

BY

CUMHUR SEFA DİKMEN

IN PARTIAL FULFILLMENT OF THE REQUIREMENTS
FOR
THE DEGREE OF MASTER OF SCIENCE
IN
AEROSPACE ENGINEERING

JANUARY 2023

Approval of the thesis:

DEVELOPMENT OF A PRELIMINARY DESIGN TOOL AND CFD SIMULATIONS FOR HYPERSONIC INTAKES

submitted by **CUMHUR SEFA DİKMEN** in partial fulfillment of the requirements for the degree of **Master of Science** i**n Aerospace Engineering, Middle East Technical University** by,

Prof. Dr. Halil Kalıpçılar
Dean, Graduate School of **Natural and Applied Sciences** _____

Prof. Dr. Serkan Özgen
Head of the Department, **Aerospace Engineering** _____

Prof. Dr. Sinan Eyi
Supervisor, **Aerospace Engineering, METU** _____

_____

Examining Committee Members:

Assoc.Prof.Dr. Nilay Sezer Uzol
Aerospace Eng, METU _____

Prof. Dr. Sinan Eyi
Aerospace Eng, METU _____

Asst. Prof. Dr. Özge Başkan Perçin
Aerospace Eng, METU _____

Assoc. Prof. Dr. Mustafa Kaya
Aerospace Eng., Ankara Yıldırım Beyazıt University _____

Asst. Prof. Dr. Sıtkı Uslu
Aerospace Eng., TOBB ETU _____

Date: 19.01.2023

I hereby declare that all information in this document has been obtained and presented in accordance with academic rules and ethical conduct. I also declare that, as required by these rules and conduct, I have fully cited and referenced all material and results that are not original to this work.

Name Last name : Cumhur Sefa Dikmen

Signature :

ABSTRACT

DEVELOPMENT OF A PRELIMINARY DESIGN TOOL AND CFD SIMULATIONS FOR HYPERSONIC INTAKES

Dikmen, Cumhur Sefa
Master of Science, Aerospace Engineering
Supervisor : Prof. Dr. Sinan Eyi

January 2023, 103 pages

Air-breathing scramjet engines promise very high speeds at special flight trajectories, which boost research on this field. Air intake is one of the most critical components during the design process of these engines. Not only it leads the overall performance of the scramjet cycle, but also geometry of the intake affects the survivability of the vehicle at hypersonic flight conditions. Although there are many types of intakes, the design of 2-D intake with ramps is investigated in present thesis. After validating CFD methodology with experimental data, results of the inviscid design tool are compared with viscous CFD results for design point and off-design points. Fluent is used as commercial CFD solver. It is observed that such a tool can be used for preliminary design process with acceptable differences before conducting intense viscous CFD analysis.

Keywords: Hypersonic, Scramjet, Intake, CFD, Design Tool

ÖZ

HİPERSONİK HAVA ALIKLARI İÇİN ÖN TASARIM ARACI GELİŞTİRİLMESİ VE HAD SİMÜLASYONLARI

Dikmen, Cumhur Sefa
Yüksek Lisans, Havacılık ve Uzay Mühendisliği
Tez Yöneticisi: Prof. Dr. Sinan Eyi

Ocak 2023, 103 sayfa

Hava solumalı scramjet motorları, özel uçuş güzergâhlarında çok yüksek hızları amaçladıkları için bu alandaki araştırmalara hız kazandırmaktadır. Hava alığı, bu motorların tasarım sürecindeki en kritik kısımlardan birisidir. Hava alığı sadece scramjet döngüsünün genel performansını yönetmekle kalmamakta, hava alığı geometrisi hipersonik uçuş koşullarında uçuşun başarısını etkilemektedir. Farklı hava alığı çeşitleri olmasına rağmen, bu tez çalışmasında iki boyutlu rampalı hava alığı tasarımı incelenmiştir. HAD metodunun deneysel verilerle geçerli kılınmasının ardından viskoz olmayan tasarım aracının sonuçları tasarım noktasında ve tasarım dışı noktalarda viskoz HAD sonuçlarıyla karşılaştırılmıştır. Ticari HAD çözücüsü olarak Fluent kullanılmıştır. Böyle bir tasarım aracının ön tasarım sürecinde yoğun HAD analizlerinden önce kabul edilebilir farklılıklarla kullanılabileceği gözlenmiştir.

Anahtar Kelimeler: Hipersonik, Hava Alığı, HAD, Scramjet, Tasarım Aracı

To my lovely family…

ACKNOWLEDGMENTS

I firstly would like to express my deepest gratitude to my thesis supervisor Prof. Dr. Sinan Eyi for his guidance and encouragement from the acceptance to the MSc. Program until the procedure of thesis writing. Also, I thank all jury members for their constructive recommendations.

During thesis studies, student licenses of commercial tools such as Ansys Fluent and MATLAB have been used intensely; therefore, I would like to thank my university and producers of these tools for supporting academic efforts.

I wish to thank my workplace, Roketsan for supporting its employees about graduate programs. Particularly, I need to mention Ünsal Gümüşlüol, Hasan Tahsin Kılıç, Atılay Nebi Çallı and Semih Soğancı for their encouragement and support during whole period.

In addition to them, I would like to mention all my teachers from the first primary school teacher, Nimet Akçay, to my university professors because I am able to write this thesis after a long educational story in my life.

Finally yet importantly, I wish to present my sincere feelings to my mother and my brother for their endless patience and fellowship. It always makes anyone determined to fulfil dreams or goals after feeling the support of family.

Lastly, I would like to share my deepest gratefulness to Gazi Mustafa Kemal Atatürk, who points the sky to the youth of this nation for a bright and promising future.

TABLE OF CONTENTS

LIST OF TABLES

TABLES

LIST OF FIGURES

FIGURES

LIST OF ABBREVIATIONS

ABBREVIATIONS

AoA	Angle of Attack
AUSM	Advection Upstream Splitting Method
CFD	Computational Fluid Dynamics
CR	Contraction Ratio
HLL	Harten-Lax-van Leer
L/H	Length-to-Height Ratio
LES	Large Eddy Simulation
ODE	Ordinary Differential Equations
PDE	Partial Differential Equations
RANS	Reynolds Averaged Navier-Stokes Equations
REST	Rectangular-to-Elliptical Shape Transition
SA	Spalart-Allmaras
SBLI	Shockwave Boundary Layer Interaction
SC-Ramjet	Supersonic Combustion Ramjet
SoL	Shock-on-Lip Condition
SoS	Shock-on-Shoulder
SST	Shear Stress Transport
TBM	θ-β-Mach

LIST OF SYMBOLS

SYMBOLS

Γ_x	Effective Diffusivity (x=k, ω)
S_x	User Defined Source Term (x= $\tilde{v}$, k, Ɛ)
$\tilde{v}$	Modified Turbulent Viscosity
$\sigma_{\tilde{v}}$	Constant for Transport Equation Formulation
c	Speed of Sound
C_x	Constant for Transport Equation Formulation ($x=_{1Ɛ, 2Ɛ, 3Ɛ, b2}$)
D_ω	Cross Diffusion Term
e	Specific Internal Energy
Ɛ	Rate of Dissipation
G_b	Generation of Turbulent Kinetic Energy due to Buoyancy
G_k	Generation of Turbulent Kinetic Energy due to Mean Velocity Gradients
G_v	Production of Turbulent Viscosity
G_ω	Generation of ω
h	Enthalpy of the Fluid
k	Turbulent Kinetic Energy
M	Mach Number
P	Static Pressure
Pr_L	Prandtl Number
P_t	Total Pressure

q_k	Heat Flux Vector
R	Ideal Gas Constant
Re	Reynolds Number
S_{ij}	Strain Rate Tensor
S_{ij}^*	Traceless Strain Rate Tensor
S_x	User Defined Source Terms (x=k, ω)
T	Static Temperature
T_{ij}	Viscous Stresses Acting on a Fluid
TPR	Total Pressure Recovery
T_t	Total Temperature
u	Velocity
Y_M	Contribution of Fluctuating Dilatation in Compressible Turbulence
Y_v	Destruction of Turbulent Viscosity
Y_x	Dissipation due to Turbulence (x=k, ω)
γ	Specific Heat Ratio
δ_{ij}	Kronecker Delta
μ	Dynamic Viscosity
μ_t	Turbulent Viscosity
ρ	Density
υ	Molecular Kinematic Viscosity
ω	Specific Dissipation Rate

CHAPTER 1

INTRODUCTION

In the history, the humankind has always pushed the limits of the technology, and science forward. In aerospace field, these limits are generally aerothermal or structural. Thanks to recent advancements in material science and computational technologies, impossible or unsuccessful concepts of the past are the state-of-art applications of today. One of these concepts is scramjet engine operating at hypersonic flow conditions, which makes the supersonic combustion possible. Developing such an engine starts with the design and analysis of its challenging air intake. This thesis will enlighten readers about scramjet intakes in terms of design and analysis.

1.1 Scramjet and Its Background

As computational power and materials science are developed more in 21st century, some concepts that are not feasible in the past have started to take more attention. This fact is even more visible for hypersonic flow and related systems.

An engine called ‘SC-Ramjet’ works at hypersonic flow conditions, and it is used as propulsion system of air-breathing hypersonic vehicles. It is a simple concept while making a complex propulsion work real. That concept is rooted from ramjet engines. Ramjet is an engine compressing the air using its geometric shape without movable mechanical compressors. This is a clever idea because there is no use of complex compressor-turbine systems of turbofans. Instead, the air is compressed by the geometry and oblique shock waves. However, ramjets can burn the incoming air in combustion chambers under subsonic flow conditions. This will create normal

shocks, high level of heat and structural loads for ramjet combustion chamber if the speed of incoming air is above certain levels such as scramjet flight speeds. [38]

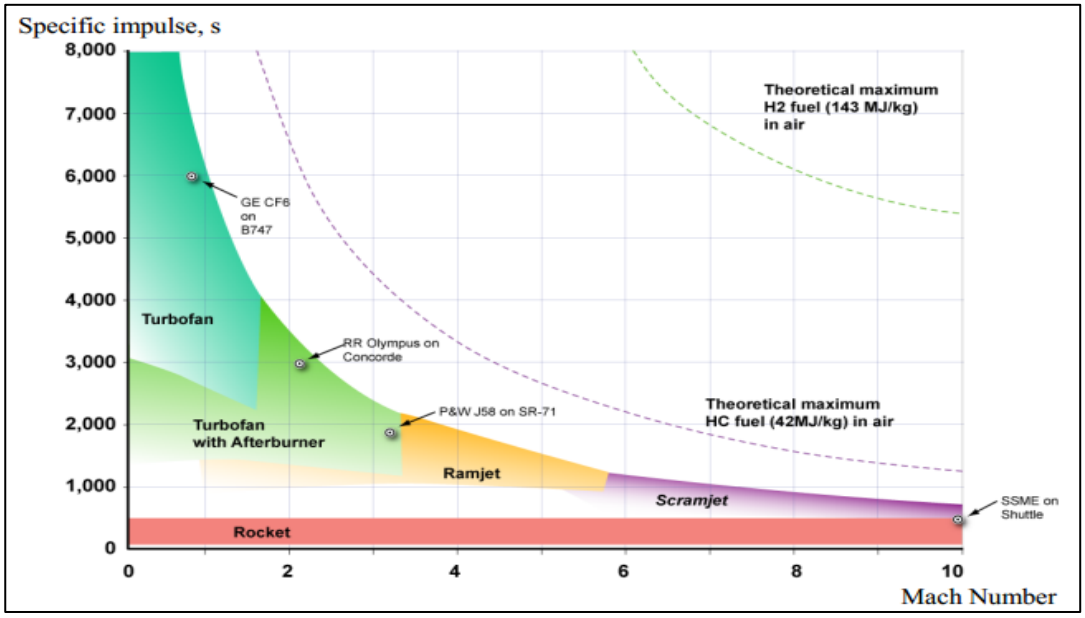

Figure 1.1. Comparison of Different Engine Types in Terms of Specific Impulse and Mach Number [57]

If the incoming air remains supersonic through the engine, and can be burned under supersonic conditions, this will decrease negative impacts of ramjet cycle at very high Mach numbers. In other words, scramjet engine can be defined as the propulsion system of hypersonic air-breathing vehicles. At some specific impulse and Mach number points, scramjets can be beneficial as it can be seen in Figure 1.1. Scramjet engine does not carry an internal oxidizer tank due to its air-breathing propulsions so that they are more efficient than rockets for equivalent Mach number. It should also be noticed that hydrocarbon fuels and hydrogen fuels make significant differences for the same Mach numbers.

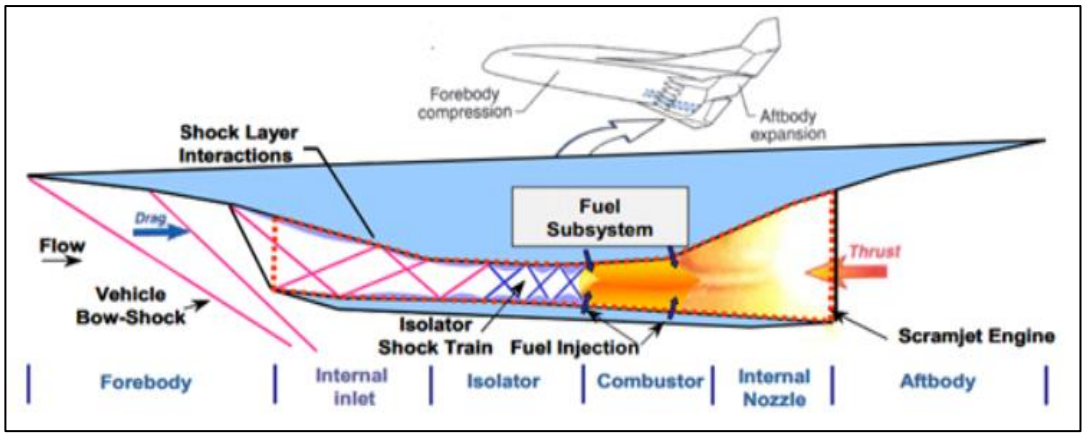

Figure 1.2. Illustration of Scramjet Propulsion System [44]

The theoretical base of the idea of scramjet cycle goes back to almost 60 years ago. According to [52]'s chronological systematic, the first scramjet concepts are podded engines and separated part of aircraft. NASA HRE and Russian NII-1 can be demonstrated as examples of this category. As a result of scientific observations about podded scramjet concepts, it has been decided to integrate scramjets into the vehicle. NASP (National Aero-Space Plane) program can be counted in this category. Due to the budget and technological feasibility issues of that time, the program has been stopped. However, scientific observations and experimental findings of such programs have been the base of current programs.

Especially after the development of air defense systems against well-known threats, scramjet powered missiles take the attention of many countries such as the USA, Russia, China, India, Japan and South Korea. In addition, research and development studies at scientific institutes and universities enhance the development of scramjet concepts because another aspect of usage of scramjets is space transportation. A detailed list of scramjet literature from open sources can be found in [42] and [57]. Some examples of scramjet application are demonstrated in Figure 1.3. and listed in Table 2.1.

Table 1.1 Examples of Scramjet Engines/Programs Worldwide [42]

Engine/Program	***Country***	***Era***	***M***	***C (kft)***	***State***
GASL SJ	The USA	1960s	3-12	-	CoT
Various	Russia	1980s	5-7	80-100	CT
HyTech	Russia	1995-…	7-10	50-130	CT
HyShot	Australia	2000s	7.6	75-120	FT
Hyper-X X-43	The USA	2000s	5-9.68	98+	FT
Boeing X-51	The USA	2010s	5	70	FT
14-X	Brazil	2020s	6+	-	FT
HSTDV	India	2020s	6	60-70	GT
3M22-Zircon	Russia	2020s	7	60-70	Operational
Spartan	Australia	2020s	5-12	-	Concept
HyCore	South Korea	2020s	5	60-70	Concept

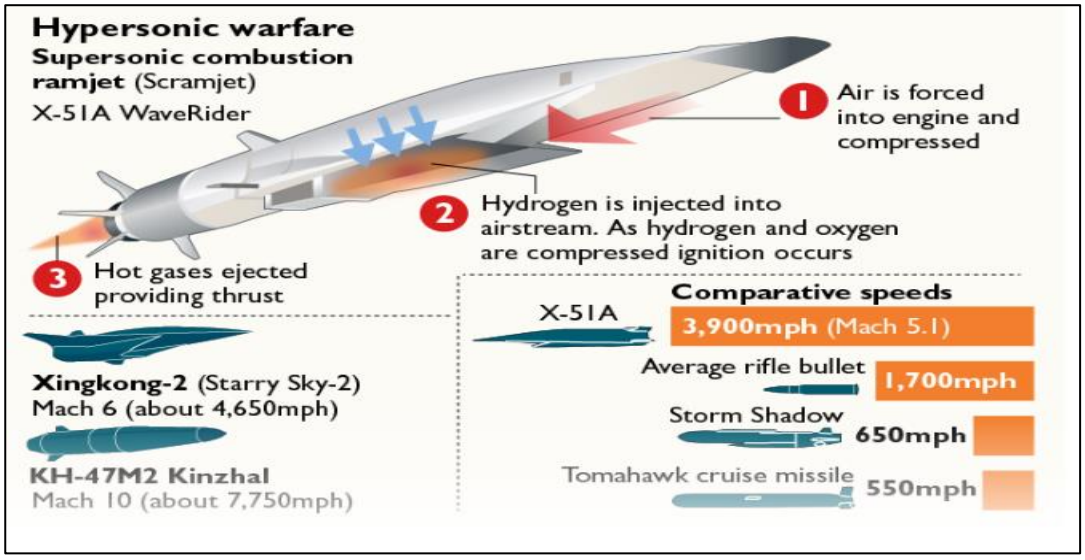

Figure 1.3. Comparison of Missile with Scramjet and Other Applications [66]

1.1.1 Scramjet Intakes

Air intake describes a wide field in aerospace applications. Every vehicle carrying the air-breathing propulsion system has the air intake to capture and then to burn the air. What makes air intakes hard to design is their strong trade-off relation with the rest of the system. Air intake should capture necessary amount of air with minimum pressure losses, and without exceeding tolerable drag levels of the system. [40]

However, scramjet air intakes may be separated from ordinary air intakes such as turbofans of commercial airplanes because scramjet engine and the carrier vehicle are fully integrated. Therefore, when scramjet air intakes are mentioned somewhere, it is directly related to vehicle forebody to receive required pressure increase and Mach decrease before the combustion process.

As stated in [56], different structure of scramjet intakes changes the techniques or solutions used in other type of intakes. Due to thicker boundary layers of scramjets, diverting and standard bleeding options are not used to prevent excessive drag. This situation is made detailed by [13]. Optimizing high amount of flow turning, cowl drag and internal aerodynamic performance require solutions such as the use of boundary layer bleed. In literature, there exists experimental research about the use of bleed at scramjet intakes. [20]

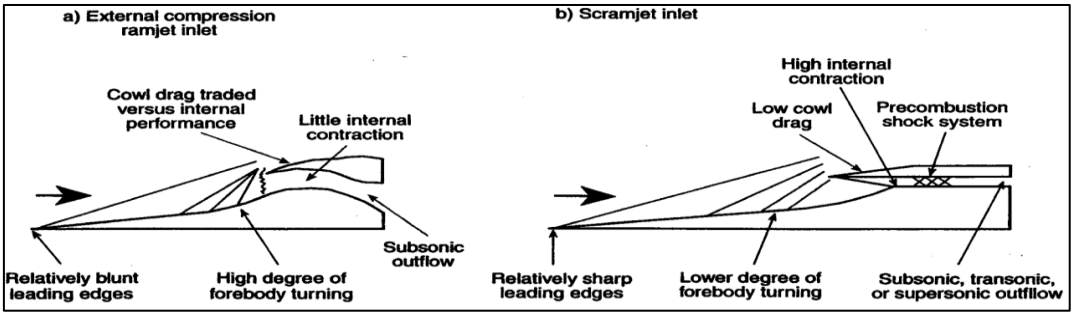

Figure 1.4. Comparison between External Compression Ramjet and Scramjet Models [13]

It is known that scramjet powered vehicles do not have a wide a range of AoA or sharp maneuvers as opposed to hypersonic gliders. This may be helpful to operate

fixed planar geometries; however, [46] explains that heat loads and flow separation around cowl lips may appear away from cruise design point of intake. Although fluctuations in the flow around these locations can be stabilized through isolator, it should be a design rule of thumb to have shock-on-lip condition for intake design to have better performance.

Figure 1.4., compares generic external compression ramjet intake and scramjet intake. As it can be seen from the figure, there are differences in both geometric properties and flow physics.

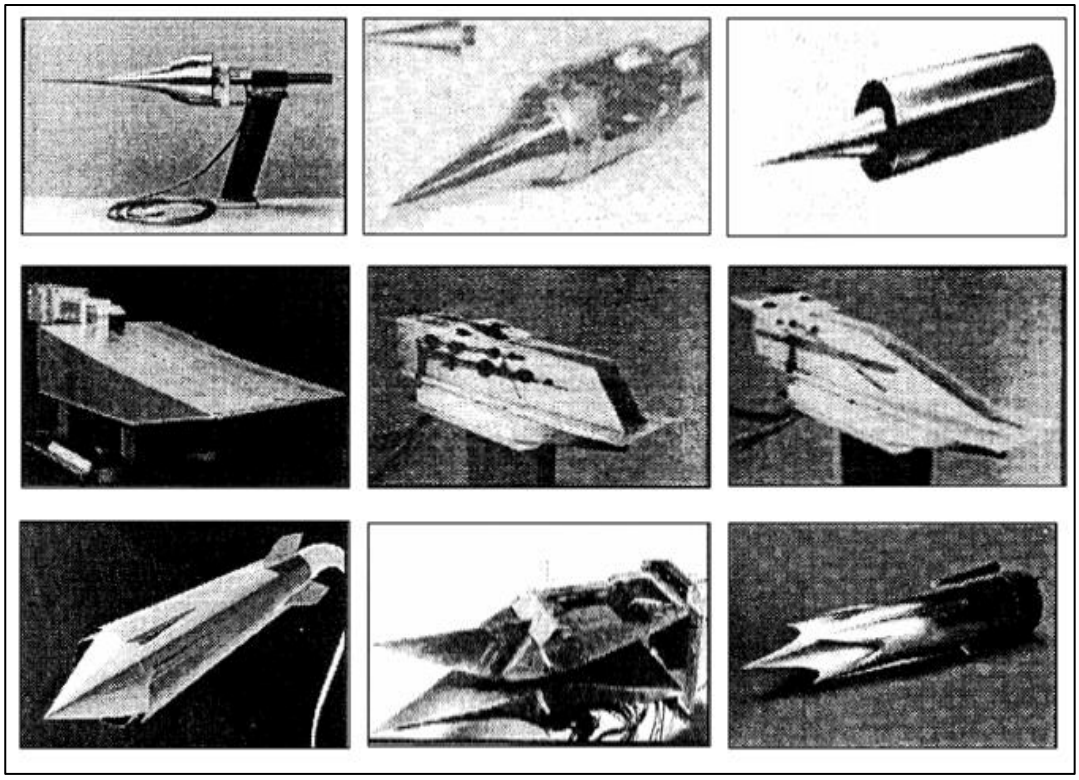

Figure 1.5. Examples of Different Intake Geometries Given in [13]

Figure 1.5 adopted from [13] reviews many intake design ideas from the literature. Their characteristics are quite different because intakes can be designed as axisymmetric, 2D, 3D, sidewall compression, Busemann type, Alligator type and spike depending on the design purpose.

The compression type, application type and the geometry can categorize all these intake types. This will be more detailed in the next section.

1.1.1.1 The Categorization of Intake Types

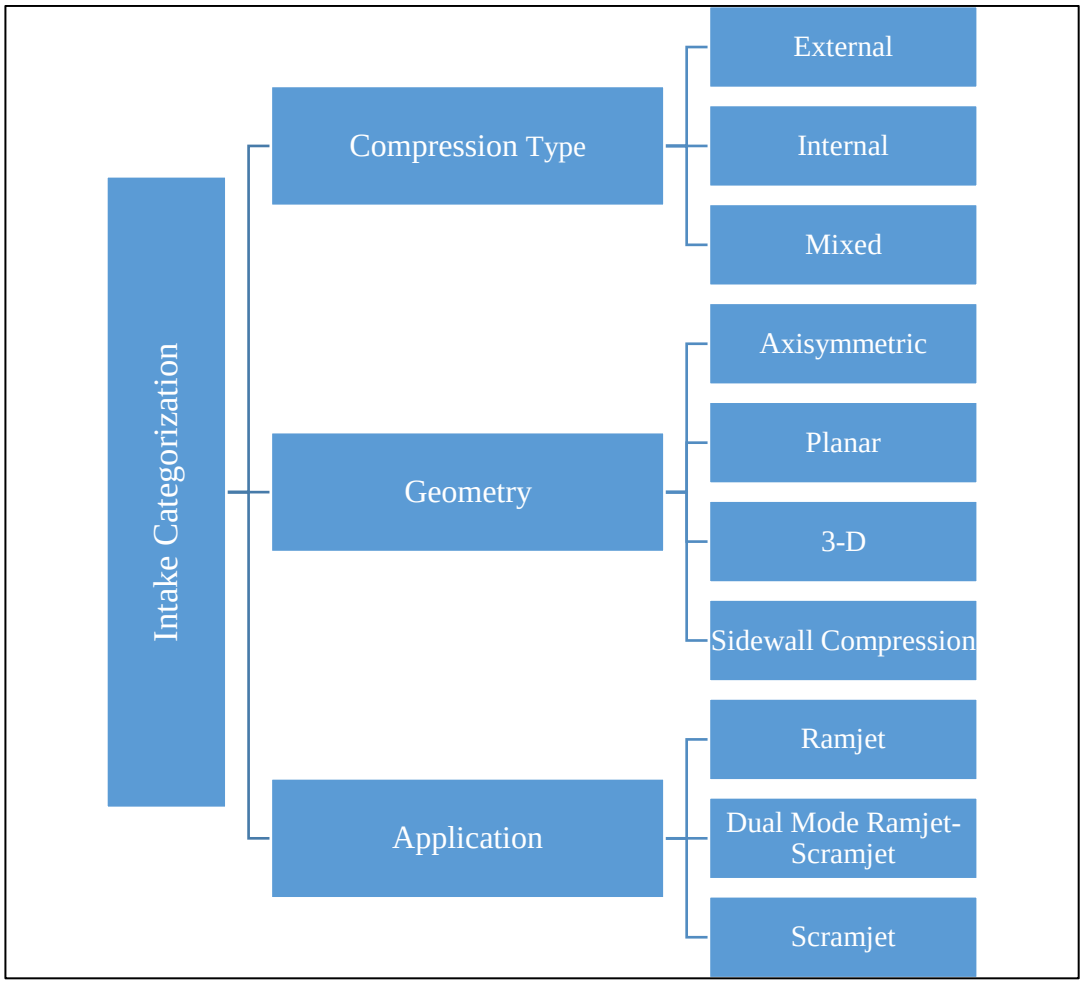

Figure 1.6. Intake Categorization Tree

The compression categorization of scramjet air intakes can be presented as given in Figure 1.6. These are external, internal and mixed compression intakes. All of them has some advantages and drawbacks. External compression type does not have engine start-unstart issue. Also, it does not suffer from operating away from its design point. However, cowl drag is quite high for external compression intakes because of flow entry angles.

Mixed compression intakes as illustrated in Figure 1.7. decreases the cowl drag compared to external ones. Yet, the drawback is the need of longer intake geometries. Flow spillage may occur away from the design point. Engine start-unstart issue is possible for mixed compression intakes depending on intake design. As a rule of thumb, mixed compression intakes can be considered as the most suitable design choice at hypersonic flow regime and scramjet engines. The use of isolators is beneficial for engine unstart issue related to backward pressure increase at the entry of combustor.

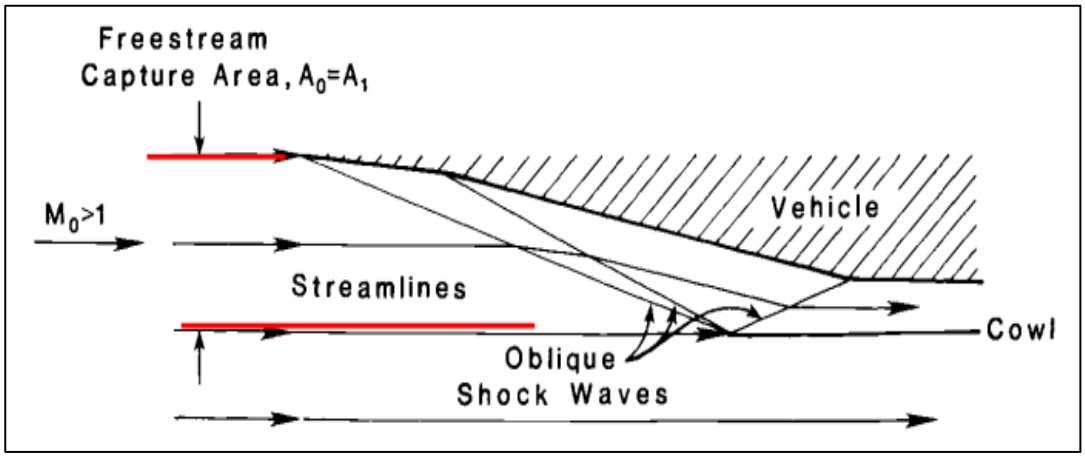

Figure 1.7. The Best Option for Scramjets: Mixed Compression Intake [22]

Although their use for hypersonic systems is scarce, internal compression intakes should be mentioned. They suffer from engine start-unstart issue. Therefore, they require variable geometric designs, and this fact brings more complexity for overall system integration. They are shorter than mixed compression intakes, and they are successful at capturing air flow below design point.

The second categorization can be made by application. The vehicle may be propelled by pure ramjet, dual mode ramjet-scramjet, pure scramjet or combined cycle propulsion such as turbojet-scramjet. However, only scramjet intakes are the scope of this thesis.

Lastly, intake types can be categorized by their geometry. Intake design may be purely two dimensional, axisymmetric, three dimensional. 3D intakes are more recent research topic compared to others, and there are innovative 3D concepts such as sugar-scoop and REST [46]. Some concepts such as sidewall compression may be combined as well. In this thesis, 2D geometries will be analyzed.

Figure 1.8: Illustration of REST Intake Installed on Hypersonic Vehicle [46]

1.1.1.2 Intake Ramp Geometries

Intake ramp geometries are critical for intake design choices. Their main purpose is generating oblique shock waves to compress air flow. The choice of the number of ramps and ramp angles dictate how much compression will be available for the engine. Therefore, all other choices are strongly connected to ramp design. For example, [58] investigates this topic. In this research, an intake with 4 ramps is

preferred instead of using common practices such as 2 ramps or 3 ramps. For a comparison, it is aimed to keep different intakes with the same total deflection angle, but a modification at ramp angles has to be needed for sufficient compression.

However, the design of intakes with 4 ramps is not common because it is a complex design. The benefit of higher number of ramps and shock waves is suppressed by the complexity of that design. Nevertheless, every kind of design choice needs a trade-off to have optimum level of compression, geometry simplicity and flow deflection.

As many scramjet research points out, [59] and [60] state that ideal compression ratio is around 50 through compression system. [59] and [60] also discuss that compression levels do not need to reach huge values such as 100 as given by previous studies.

Since ramp designs are mostly related to oblique shock wave relations, ramp angle choices or lengths are more or less similar for the same requirements. What makes ramp designs different from each other is optimization at the further steps of design. In the literature, there are some examples for this purpose. [11] changes straight ramps to the curved ones using multi-objective design optimization and Bezier curves for drag and pressure ratio goals. [5] uses gradient-based adjoint optimization to increase mass flow rate without increasing straight ramp length. Instead, the shape is changed.

1.1.1.3 Technical Challenges for Hypersonic Intakes

Properties of airflow at hypersonic flow regime are strongly dependent on flight Mach number and the altitude. This is quite valid for any aircraft and propulsion system; however, scramjet engines operate at a narrow band of the atmosphere, and changes from design point have significant impacts for the flight. Considering this fact, scramjet engines should not only focus on high speeds, but also, they should keep sufficient performance at lower speeds.

Formation of adverse pressure gradients along intake walls is another challenge. Experiments and numerical analyses demonstrate that shock waves caused by intake ramps can interact with the boundary layer [46]. This is a famous phenomenon for hypersonic flow dynamics called SBLI. These interactions cause flow separation, adverse pressure gradients and separation bubble. Depending on the size and location of them, the flow may be destabilized. Because of this destabilization, shock train along isolator may be affected negatively. This is a direct reason of performance losses of the engine, but also it may cause unstart of the intake and be fatal for the engine.

According to [52], momentum losses related to viscous forces cause that boundary layer cannot balance pressure increase in the direction of flow, and velocity profile of the flow changes. These changes are the reason of flow separation.

The issue of SBLI is significantly critical for scramjets and scramjet intakes because undesired pressure increases and changes at heat flux can create flow separation, flow unsteadiness and ultimately intake unstart condition.

Intake unstart condition is one of the most fatal event for scramjet operations. If the shock system (train) starts to move backwards due to the existence of pressure unbalance between the isolator and combustor, the shock train may be pushed away from the intake entrance. The stable movement of shock train towards combustor and the pressure balance through the channel are favorable because it is the best condition to capture air and spillage drag can be kept at minimum levels. Otherwise, shock waves will not be able to reach combustor, combustion will not be executed as designed, and the engine will experience performance losses and. For this reason, following conditions should be considered while designing the intake:

- Viscous effects: Boundary layer separation, which can create a blockage for air flow
- Non-viscous effects: Changes at freestream conditions (Mach number or AoA)

- Combustor effects: Increasing back-pressure and unbalance at the entrance of the combustor, which results in backwards movement of the shock train towards the intake entrance

Although it is not the scope of this thesis, 3D effects are another challenge for intake designs. Rectangular ducts may create additional flow separation near the corner surfaces. Both of sidewalls and viscous forces at the bottom of the channel triggers flow separation. As it is mentioned before, flow separations and shock waves interact with each other, and SBLI and bubbles appear.

All these effects destabilize the flow regime while moving along the channel. LES numerical studies demonstrate that sidewalls generate a secondary shock in addition to the main shock, and these two shocks interact with each other destabilizing the flow further.

[38] also points out that start-unstart challenge has different natures for ramjet and scramjet intakes. In ramjets, mechanisms stabilizing pressure fluctuations caused by the combustor are normal shock waves. However, same mechanism works with oblique shock waves at scramjets. It is harder to achieve this task with oblique shock waves than normal shock waves.

1.1.1.4 Isolators

Isolators can be thought as a part of intake design and analysis procedure. Scramjet intakes can require shock trains or pre-combustion shock systems. Heat release at relatively slower speeds can create thermal blockages, or high levels of heat release can push the shock train backwards. For this reason, the distance from the intake to the entrance of combustor should be stabilized, so isolators are used. Isolator can be defined as a constant area diffuser duct in short. Three main design criteria about isolator flow are as follows:

- Minimizing flow distortion
- Maximizing static pressure rise without causing the inlet unstart
- Maximizing stagnation pressure recovery

The length of the isolator is the main design driver for isolators because every scramjet engine design may require different lengths to stabilize the flow due to different intake flow conditions or combustor entry conditions. The length is strongly coupled with the height.

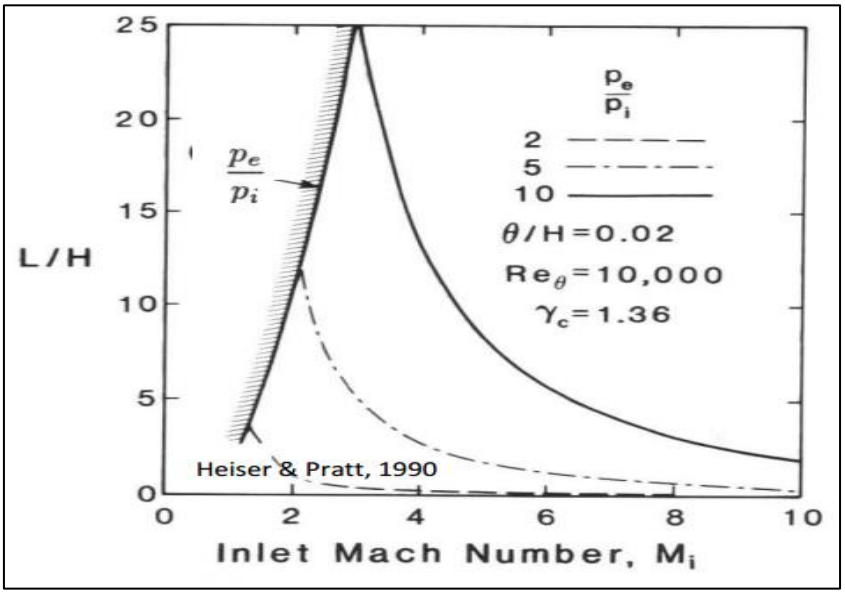

Figure 1.9: The Relation between L/H Ratio of Isolator and Inlet Mach Number [22]

As it can be seen from Figure 1.9, smaller inlet flow speed and high back pressure caused by combustor means higher L/H ratio. However, scramjet engines operate over Mach 4 speeds so that increasing Mach number means decreasing L/H ratio.

If intake and isolator design are not successful enough to reach a desired pressure distribution, unstart will probably occur and operation will fail. While designing isolator, different factors other than intake and combustor flow conditions such as intake cowl and surface roughness should be considered carefully.

[59] presents an example about how flow develops from the entrance of isolator towards the end of combustor. Isolator entrance Mach number drops slightly from M=2.65 to around M=2.5. Pressure and temperature slightly increase due to frictional heating through isolator. It should be noted that sudden changes of pressure, temperature, and Mach if there is a strong backpressure or enthalpy change caused by increasing fueling. Such effects will change isolator flow dynamics because flow separation and flow uniformity at the exit of isolator will change.

1.2 Literature Survey

Since hypersonic flow and scramjet intake fields are complex and less known compared to other fields of aerospace, an intensive literature survey has to be included in thesis studies. The literature survey can be divided into scramjet intake design, computational aerodynamics, and experimental aerodynamics and optimization categories.

1.2.1 Scramjet Intakes and Design Strategies

[69] proposes one of the most comprehensive and the oldest design guide about scramjet intakes. Definition of performance parameters, efficiency calculations, engine start-unstart conditions, Kantrowitz limits, the effect of leading-edge bluntness, the effect of viscosity, boundary layer separation are main topics in this publication. Van Wie also indicates the rule of thumbs about two-dimensional planar intake designs, which is critical for the scope of this thesis. At the end of the guide, there is an experimental chart including efficiencies of various 2-D, axisymmetric, Busemann and 3-D intakes from the real life.

Another intake design guide proposed by [59] considers the scramjet intakes operating from Mach 5 to Mach 12. This guide demonstrates flight corridor of air breathing hypersonic vehicles, which is used in the thesis task. As Van Wie does, Smart also has inlet efficiency experimental data from different references.

Especially, many scramjet articles and thesis refers Smart about the compression ratio requirement of scramjet intakes because there are limited information about this point other than Smart. The way about how to use stream thrust analysis and a sample scramjet calculation are also provided with charts. The critical information about combustor entrance pressure requirement, which is between 50 kPa and 100 kPa is given by this publication.

[67] demonstrates his 1-D analysis program for scramjet and ramjet flows in his MSc. Thesis, which can broaden the horizon of a scramjet researcher. Even if it includes a full flow path from the intake to the nozzle, the MATLAB model indicates how to create a similar design procedure for the intake. Also, the approach to design isolator by using Fanno flow relations is innovative.

The more recent Ph.D. study of [17] considers how to design and analyze the performance of 3-D scramjet air intakes. Although this study mostly covers 3-D case, the lessons can be also used for 2-D intake studies. The intake starting section of this study is well comprehensive, and it compares previous studies of Smart, Van Wie and Sun to current design in terms of Kantrowitz limit. [17] focuses on streamline tracing because this technique is suitable for 3D-GRK intake of DLR.

[32] designs a tool for performance estimations of a scramjet engine operating from Mach 5 to Mach 9 using MATLAB. Since 2-D planar type intake is considered, this article is examined carefully. Some design criteria in this article can be used for the current thesis. Boundary layer separation criteria, isolator Mach number criteria, area-Mach relationships, sizing of intake and isolator can be counted among critical design options. It should be noted that these criteria are not only proposed by [32], but they are a review from different references.

[65] has another hypersonic intake design code, and its numerical validation. It is simple, but efficient because the geometry of an intake and well-known θ-β-M relations are used for this purpose. Different flight altitudes and operating conditions are considered. This study underlines the use of shock-on-lip criteria. Although the study is numerically validated by inviscid flow, it is still accurate for a preliminary

design tool. The intake geometry used by [65] belongs to Brazilian 14-X vehicle and the same inviscid investigation is proposed by [45] The findings are almost the same, and these studies prove the efficiency of inviscid shock design methodology regardless of deviations caused by viscous effects. In the present thesis, viscous effects will be investigated as well.

1.2.2 Computational Aerodynamics

One of the main guides of the present thesis is [49]'s parametric analysis of hypersonic intakes. The solver is Fluent, so the detailed explanations can enlighten for any researcher. He investigates different shapes together with the intake, and cases are solved using chemical reaction effects because the parametric analysis starts from Mach 6 to Mach 20. Different cowl lengths to see differences for an axisymmetric intake model execute hypersonic intake analysis. However, one should note that the Fluent solver has changed since 2013, and necessary tuning is applied for present thesis.

[10] investigates scramjet intake and isolator from different perspectives using an in-house solver. This is quite beneficial to see differences of approaches. He compares axisymmetric and planar geometries for every case. One of the most significant findings is that the deviation caused by chemical reactions are very limited. In fact, this study is about Mach 10 flow, and such a finding is one of the proofs about why ideal gas assumption will be used in numerical analysis part of this thesis, and in many other publications around Mach 5-6. Other than this finding, he demonstrates the effect of compression ratio, isolator length, expansion corner edge, isolator-to-intake size ratio on scramjet intake performance.

Ph.D. thesis of [47] and [48] are examined to understand boundary layer flow and re-laminarization concepts deeper. None of these theses uses Fluent solver; however, mathematical background and numerical approaches are appreciated. [48] examines GRK 1095 intake model of RWTH Aachen University, and operating Mach number

of 6.7 is suitable for the scope of present thesis. In these studies, many computational decisions such as grid resolution, first layer thickness and turbulence model modifications are justified. [47] uses CFX solver, and it can be considered very close to Fluent. Effects of different flow conditions separation and SBLI issue are deeply investigated, and understanding these topics helps solving similar issues in this thesis.

[30] compares different solver setups (KW-SST and transition options) for scramjet intakes. The study is executed using Fluent and its user defined functions. The study is quite beneficial because it helps any researcher see what kind of differences exist for intake flow field and ramp surfaces when different solver setups of transition such as Gama-Transition and blended models are used. Present thesis is also investigated considering transition options of Fluent, and as it will be explained later, even transition options of KW-SST differ around cowl and shoulder. Moreover, [30] underlines the effect of turbulence intensity ratios on the result, and it is considered for the current thesis.

Since SBLI and separation issues are common for scramjet intakes, a good opportunity to investigate these issues is provided by [73]. Using [34]'s double-wedge intake configuration at Mach 7, numerical investigation is executed. The solver is CFX, which has similar properties with Fluent. This study compares its own results with QUADFLOW 2D and Flower 3D solvers for various turbulence models. At the end of the article, the effect of leading-edge radius is demonstrated, which is related to current thesis. The sharpness or bluntness has a significant effect on separation bubble and pressure recovery.

[55] validates the study of [26]'s experimental case using Fluent. What makes this study different from other studies using the same case is that pressure feedback options are investigated. Pressure feedbacks are between around the end of first ramp and shoulder separation region. The effect of feedback can be seen for pressure and Mach number results. Another point to state is that [55] presents a chart to

demonstrate isolator outlet Mach number distribution, and that chart can be used for validation purposes of the current thesis to compare.

1.2.3 Experimental Aerodynamics

The validation case of current thesis is taken from [25] at the High Supersonic Tunnel of the University of Manchester. It is widely used Ph.D. thesis in scramjet intake literature because there is limited resource giving open-source experimental data. Since he has experimental data from PSP and Kulite measurements at Mach 5, and Fluent is used to validate these measurements. For this reason, this research is preferred by many other articles, and thesis to validate numerical studies.

[6] makes another experimental research like [25]. The High Supersonic Tunnel at the University of Manchester is the place of where experiments are made at Mach 5. This experiment mainly focuses on hypersonic buzz phenomena, but many following research is based on it. Following this experiment, [11] uses this experiment to validate Fluent solver for shape optimization purposes. Both of [11] and [25] proves that Fluent can be used for the numerical needs of the current thesis.

Together with the University of Manchester test facilities, DLR H2K hypersonic wind tunnel is another place where scramjet intake research is intense. [21] investigates 2-D and 3-D scramjet intakes at Mach 7. This experiment is different from many others because different configurations of intake bleed exist. It is stated that the bleed can be used to remove separation bubble, but the location and the size of the bleed gap may vanish the purpose.

[34] executes the experimental study coupled by in-house numerical solver. This study uses two different facilities for different scramjet intake configurations. One of them is SWL of RWTH Aachen University, and the other one is DLR Cologne test facilities. The importance of these experiments is the uniqueness of different configurations.2-D intakes with converging or non-converging sidewall, no sidewall, 3-D intakes are investigated detailed at Mach numbers between 6-8. Especially

SCR02 and GK01 intake models are widely used for numerical studies in the literature. The main finding of this experiment is that there is not a clear winner among these design configurations, but 2D-I-WOS-CR and 3D-I-CS may be preferable regardless of where it will be used.

[28] experimentally investigates 14-X B hypersonic vehicle demonstrator, which is the example of one of the few open-source real-life scramjet application. Although the experiment is about a full-scale vehicle, there is sufficient data about intake part. 14-X B operates at Mach 7 and 30 km. IEAv T3 Hypersonic Shock Tunnel is used to see results from Mach 7 to Mach 8, which is low-to-middle hypersonic speed levels, and results are appreciated for the scope of current thesis. Fluent is used to couple the experiment numerically. There are some lessons from this study as follows. Pressure distributions for the ideal and real gas do not differ much, and inviscid case of Fluent solver agrees with the experimental Schlieren results. However, the research underlines the need of the improvement of the experimental procedure to vanish differences between the experiment, analytical and numerical results.

1.3 Thesis Objectives

In present thesis, the author aims to create a preliminary design tool for hypersonic scramjet intakes. The tool will include intake and isolator region. The designed geometry will be obtained using this tool and it will be analyzed using CFD. In this way, a design tool, an intake design and 2-D CFD results can be combined for comparisons and investigations.

Thesis outline can be divided into 4 main chapters. In the first chapter, introductory parts are given such as scramjet and its background, scramjet intakes, their categorization, technical challenges and literature survey of present thesis. In the second chapter, the methodology of present thesis is given. Mathematical

background of numerics, design considerations about the analytical tool, formulations used in the code can be found here. The next chapter includes the validation test case . Details of experimental study of [24] are provided and present CFD setup is presented with comparisons between the experiment , present results and additional reference for this setup. The fourth chapter discusses results of analytical tool and CFD. Analytical results include geometric dimensions of the designed intake and exit thermodynamic flow properties. CFD results include viscous and inviscid flow solutions. Then, the tool calculations and CFD results are compared . The fifth chapter is about parametric analysis to see how the design is affected from changes applied on on-design point.

1.4 Thesis Motivation

The technology changes and evolves into different concepts with time. Currently, there are increasing demand and attention for hypersonic flow and scramjet technologies. The author would be glad to part of this change.

Moreover, undergraduate propulsion classes generally have less focus on intake designs compared to compressors or turbines. However, the author has always been attracted to intakes so it has been an extra motivation to choose this topic.

CHAPTER 2

METHODOLOGY

In this chapter, the methodology of present thesis is given for both of computational and theoretical part. While computational part consists of the background of flow solver software such as governing equations, basics of fluid dynamics, turbulence modelling and CFD settings, theoretical part includes the design tool of present thesis and its mathematical formulations. Readers can easily follow results of CFD and design tool considering explanations given in this chapter.

2.1 General Discussions on Computational Fluid Dynamics

In this section, the author aims to provide fundamental theoretical knowledge about computational fluid dynamics because the methodology of this thesis is numerical, and practical usage of the numerical software should be supported by theoretical background of these topics. Therefore, Navier-Stokes equations, type of flow solvers and turbulence models will be summarized.

2.2 Approaches for Fluid Flow Problems

Fluid mechanics problems can be solved by three ways in engineering. These ways can be experimental, theoretical, or computational. These ways have advantages and drawbacks at the same time. Engineers try to use all of them depending on the case and conditions.

For example, this thesis somehow includes all these ways because analytical approach is used to create simple intake design using oblique shock relations. A sample experimental case is used to verify computational method. Ultimately,

computational approach is used for the solution of hypersonic intake flow and optimization.

Experimental approach is the most accurate and realistic one, and research studies on computational aerodynamics verify that research using an experiment. However, there does not exist an experimental setup available for every research. Most of the time, studies proceed using the setups in the literature. Equipment and facility requirements and operational costs make experiments less usable. Also, experimental setups may have scaling and tunnel correction problems, and measurement should be made carefully.

Computational approach aims to be more feasible than experimental approach. Sometimes it is not feasible to make experiments for complex flows many times during design process. For example, high-speed flows can be given as an example. Also, analytical calculations can just demonstrate general information for linear problems, while computational approach is not limited to that. However, computational approach has its own drawbacks such as computational errors and high-performance resource. More detailed discussions can be found in [72]

2.3 Governing Equations

In engineering, physical events are characterized by governing equations and computational resources are built on these equations. In this thesis, the field is fluid dynamics, and it is governed by Navier-Stokes equations. These equations are continuity (conservation of mass), momentum equations (x-y-z components depending on solution domain) and energy.

While continuity equation states the mass of the flow is conserved through the control volume, momentum equations state the 2nd Law of Newton. Forces of 2nd Law of Motion can be viscous forces, body forces, pressure differences or other forces. When viscous solution or inviscid solution is mentioned, the root of this sentence goes back to the governing equations and which components of the equation

are included or not. Energy equation is related to 1st Law of Thermodynamics, which state the internal energy of the system is composed of the net heat transfer to the system and the net work on the system.

- Mass Conservation Equation (Continuity)

$$\frac{\partial \rho u}{\partial t} + \frac{\partial}{\partial x_k}(\rho u_k) = 0 \qquad \text{Eq.1}$$

- Momentum Equation

$$\frac{\partial (\rho u_i)}{\partial t} + \frac{\partial}{\partial x_k}(\rho u_i u_k) = \frac{\partial \tau_{ik}}{\partial x_k} - \frac{\partial p}{\partial x_k} \qquad \text{Eq.2}$$

- Energy Equation

$$\frac{\partial}{\partial t}\left[\rho(\frac{1}{2}u_i u_i + e)\right] + \frac{\partial}{x_k}\left[\rho u_k(\frac{1}{2}u_i u_i + h)\right] = -\frac{\partial q_k}{\partial x_k} + \frac{\partial}{\partial x_k}(\tau_{ik} u_i) \qquad \text{Eq.3}$$

In Eq.1, Eq.2 and Eq.3, the Cartesian tensor notation and Einstein summation convention are preferred. However, these equations should be closed in terms of unknowns and the number of equations. This closure is satisfied by the equation of state. Detailed discussion about governing equations of fluid dynamics can be found in [50]. Eq.5 and Eq.6 define the specific internal energy and enthalpy.

- Equation of State

$p = \rho RT$ for ideal gas Eq.4

- Internal Energy Model

$e = C_v T$, constant C for calorically perfect gas Eq.5

- Enthalpy

$h = C_p T$, constant C_p for calorically perfect gas Eq.6

Viscous stresses for a Newtonian fluid, strain rate tensor, heat flux vector and laminar Prandtl Number can be determined from Eq.7, Eq.8, Eq.9 and Eq.10, respectively.

$$\tau_{ij} = 2\mu\left(S_{ij} - \frac{1}{3}S_{kk}\delta_{ij}\right) = 2\mu S_{ij}^{*} \quad \text{Eq.7}$$

$$S_{ij} = \frac{1}{2}\left(\frac{\partial U_i}{\partial x_j} + \frac{\partial U_j}{\partial x_i}\right) \quad \text{Eq.8}$$

$$q_k = -\lambda\frac{\partial T}{\partial x_k} \quad \text{Eq.9}$$

$$Pr_L = \frac{C_p\mu}{\lambda} \quad \text{Eq.10}$$

However, Navier-Stokes (N-S) equations are partial-differential equations. (PDE) These equations require initial condition and boundary conditions. When someone uses the initialization settings of Fluent, it gives initial conditions to the solver. When someone defines conditions of domain such as inlet, wall or outlet, the purpose is giving boundary conditions to the solver. Mathematically, these conditions can be Dirichlet type, Neumann type or Robin's combination of these two types. [70]

When aerospace problems are considered, one of the most critical topics is partial differential equations. All computational developments are related to PDEs and their understanding.

PDEs can be elliptic, parabolic, or hyperbolic mathematically. These equations physically symbolize equilibrium problems, eigenvalue problems or time-marching problems. Equilibrium problems are boundary value problems such as steady-state temperature problems, incompressible inviscid flows, or equilibrium stress problems. Eigenvalue problems may be structural buckling, resonance in circuits or vibration. Marching problems are related to time marching so transient problems such as initial value problems are in this category [50]. Present thesis works on a type of compressible steady flow problem at hypersonic speeds. Such a case is under the category of hyperbolic equations.

2.4 Turbulence Modelling

Previously, Navier-Stokes equations are described as the governing equations of such a flow motion. Due to different requirements or expectations to solve fluid flow problems, there are different approaches such as DNS, LES and RANS.

There is no modelling assumption for DNS, which makes it computationally expensive while solving the full scale of turbulent flow. Alternatively, LES is a bit less computationally expensive because only large scales of turbulent flow are considered in this approach. When only mean flow values are taken into account, the approach becomes RANS. RANS requires less computational power compared to DNS or LES but the accuracy decreases proportionally. Although DNS or LES has advantages in term of accuracy, RANS remains one of the most critical approaches for both academic and industrial applications due to its relatively fast and computationally cheaper nature.

Before diving into turbulence models, the reason why they are developed can be understood better investigating theoretical background of RANS.

The instantaneous flow variable is composed of two parts in RANS. One of them represents the mean variable and other one represents fluctuations at variable. Using these new systematic and some mathematical operations, new set of system of equations is obtained. Derivations and mathematical operations related to Reynolds Averaging or Favre Averaging can be found in [50]. In addition to standard mass conservation equation, three momentum equations exist for different directions. While there are four equations, there are ten unknowns because extra six Reynolds stress terms exist. These turbulent viscosity terms are related to fluctuations at variable. Since the closure of flow problem is required to proceed, new set of equations to solve turbulent terms are added. The famous turbulence models of RANS are developed and used for this purpose. Due to various modifications, there are many special turbulence models, but main model families are introduced in the present thesis.

- Spalart-Allmaras (SA) Model [3][43][50]

SA model is a RANS approach, which only solves one governing kinematic equation. Spalart and Allmaras proposed this model in 1992. [63] It is widely used in aerospace applications, especially in the industry. It is economical for large solution grids. In quasi-2-D flows, it performs well until some level to solve external/internal aerodynamic flows, boundary layers with adverse pressure gradients, stalled flows. However, SA model is not suitable for 3-D flows, rapidly changing flows, or complex geometries. This model family belongs to the one-equation turbulence models.

The transport equation for the SA turbulence model can be given as follows. Terms and coefficients in the Eq.11 can be found in [3].

$$\frac{\partial}{\partial t}(\rho\tilde{v}) + \frac{\partial}{\partial x_i}(\rho\tilde{v}u_i) = G_v + \frac{1}{\sigma_v}\left[\frac{\partial}{\partial x_j}\{\left(u + \rho\tilde{v}\right)\frac{\partial\tilde{v}}{\partial x_j}\right\} + C_{b2}\rho(\frac{\partial\tilde{v}}{\partial x_j})^2\right] - Y_v + S_{\tilde{v}} \qquad \text{Eq.11}$$

- Ƙ-Ɛ Model [3][43][50]

Because the exact Ɛ equation includes unknown and unmeasurable terms, Launder and Spalding proposed standard Ƙ-Ɛ model in 1974. [37] This model is widely used for its robustness for many industrially relevant flows. However, its performance is not sufficient for some aerospace applications such as rotating flows, unconfined flows, boundary layer flows and separations. This model family belongs to the two-equation turbulence models. This formulation is based on relating Ɛ with *k*.Turbulent kinetic energy and the rate of dissipation can be obtained using transport equations given in Eq.12 and Eq.13. Terms and coefficients in the equation can be found in [3].

$$\frac{\partial}{\partial t}(\rho k) + \frac{\partial}{\partial x_i}(\rho k u_i) = \frac{\partial}{\partial x_j}\left[(\mu + \frac{\mu_t}{\sigma_k})\frac{\partial k}{\partial x_j}\right] + G_k + G_b - \rho\varepsilon - Y_M + S_k \qquad \text{Eq.12}$$

$$\frac{\partial}{\partial t}(\rho\varepsilon) + \frac{\partial}{\partial x_i}(\rho\varepsilon u_i) = \frac{\partial}{\partial x_j}\left[(\mu + \frac{\mu_t}{\sigma_\epsilon})\frac{\partial\epsilon}{\partial x_j}\right] + C_{1\varepsilon}\frac{\varepsilon}{k}(G_k + C_{3\varepsilon}G_b) - C_{2\varepsilon}\rho\frac{\varepsilon^2}{k} + S_\varepsilon \qquad \text{Eq.13}$$

- Ƙ-ω and Ƙ-ω -SST Models [3][43][50]

Compared with Ƙ-Ɛ model, standard Ƙ-ω model is superior because low Reynolds flows, free shear and wall-bounded boundary layer flows and separation are solved better. However, the amount and the location of separation lack accuracy. For this reason, [43] proposed Ƙ-ω -SST model. Ƙ-ω -SST model has many improvements such as revised model constants, blending functions and limiters. This model family belongs to the two-equation turbulence models. The formulation change of this model is replacement of transport equation for Ɛ with ω. Transport equations presented in Eq.14 and Eq.15 give the turbulent kinetic energy and the specific dissipation rate for the standard model. Terms and coefficients in the equation can be found in [3].

$$\frac{\partial}{\partial t}(\rho k) + \frac{\partial}{\partial x_i}(\rho k u_i) = \frac{\partial}{\partial x_j}\left[\Gamma_k \frac{\partial k}{\partial x_j}\right] + G_k - Y_k + S_k \qquad \text{Eq.14}$$

$$\frac{\partial}{\partial t}(\rho \omega) + \frac{\partial}{\partial x_i}(\rho \omega u_j) = \frac{\partial}{\partial x_j}\left[\Gamma_\omega \frac{\partial \omega}{\partial x_j}\right] + G_\omega - Y_\omega + S_\omega \qquad \text{Eq.15}$$

For the KW-SST model, transport equations are like standard model with a small modification. However, there are some improvements for modelling some terms, constants, or functions in Menter's baseline model compared to Wilcox's model. [3]

$$\frac{\partial}{\partial t}(\rho \omega) + \frac{\partial}{\partial x_i}(\rho \omega u_j) = \frac{\partial}{\partial x_j}\left[\Gamma_\omega \frac{\partial \omega}{\partial x_j}\right] + G_\omega - Y_\omega + S_\omega + \boldsymbol{D_\omega} \qquad \text{Eq.16}$$

Considering improvements or refinements in baseline model of Menter, there is an additional improvement to calculate the transport of turbulent shear stress in KW-SST model. For this reason, it is widely used for flows including adverse pressure gradients compared to baseline model.

- Transition Shear Stress Transport [3][43][50]

This model is developed by the idea of coupling Ƙ-ω -SST transport equations and two other equations for intermittency and transition onset criteria. As it can be understood from its name, this model is directly specialized for laminar-to-turbulent transitions and flow separations. It is critical to have (y+=<1) for the mesh. Second order upwind discretization is suggested for this turbulence model. The model family belongs to the four-equation turbulence models. The model is also known as $\gamma - Re_{\Theta}$ model. Transport equation for intermittency is given by Eq.17, and transport equation for transition momentum thickness is given by Eq.18. Terms and coefficients in the equation can be found in [3].

$$\frac{\partial(\rho\gamma)}{\partial t} + \frac{\partial(\rho U_j \gamma)}{\partial x_j} = P_{\gamma 1} - E_{\gamma 1} + P_{\gamma 2} - E_{\gamma 2} + \frac{\partial}{x_j}\left[(\mu + \frac{\mu_t}{\sigma_\gamma})\frac{\partial \gamma}{\partial x_j}\right] \qquad \text{Eq.17}$$

$$\frac{\partial(\rho\widetilde{Re_{\theta t}})}{\partial t} + \frac{\partial(\rho U_j \widetilde{Re_{\theta t}})}{\partial x_j} = P_{\theta t} + \frac{\partial}{\partial x_j}\left[\sigma_{\theta t}(\mu_t + \mu)\frac{\partial \widetilde{Re_{\theta t}}}{\partial x_j}\right] \qquad \text{Eq.18}$$

- Reynolds Stress Model [3][43][50]

RSMs can be considered as the most general among well-known turbulence models. Initial or boundary conditions are sufficient for solution. Its accuracy is very high for many problems such as complex 3-D flows, swirling/rotating flows, curved ducts, cyclones. However, such advantages bring high computational cost and time, and convergence issues. Also, some problems such as axisymmetric jets and unconfined recirculating flows are not much suitable because these problems exist for Ƙ-Ɛ model. This model family belongs to the seven-equation turbulence models. RSM is not used in present thesis.

There are many more turbulence models, which are modification or improvement for widely used models explained in this section; however, understanding classical models is enough for the scope of this thesis.

2.4.1 Discussions on CFD Settings

In this section, some theoretical background about CFD methodology will be given. Since, the tool of this thesis is Fluent, topics will be related to settings of it. These topics are about the order of accuracy, the type of time integration, evaluation of gradient and discretization methods.

2.4.1.1 Discretization (Interpolation) Methods

In numerical methods, the solution is calculated on a solution domain. Then, this domain is divided into certain number of pieces. For example, the domain of a sample 2-D problem is divided into pieces along x and y axis. This process forms the computational grid (mesh) to solve the partial differential equations. In this way, discrete values are defined at the nodes of this grid through all of solution domain. Discretization schemes are based on how flow properties will flow from one place to another.

If the order increases, this brings higher accuracy to the solution. However, higher order may affect stability and the time to reach convergence. In this thesis, 2^{nd} order accuracy is mostly chosen; however, blending option of Fluent is used. Thanks to blending, accuracy of higher order, and the convergence speed of lower order can be combined for a better solution.

The solver can be used coupled implicit or coupled explicit. The term of coupling is related to the existence of strong interdependency of flow variables. It is suggested to use coupled solvers for high-speed compressible flows such as present scramjet intake flows. The memory requirement of coupled implicit solver is higher.

2.4.1.2 Flux Schemes

Approximate Riemann solvers are widely used solvers in the industry and the academia. In this section, categorization of them will be given, especially referring settings of Fluent. Approximate Riemann solvers are categorized as Finite Difference Splitting (FDS), Flux Vector Splitting (FVS) and Flux Splitting (FS).

Roe-FDS is one of the options in Fluent Density Based Solver. Roe-FDS is widely used to capture shock discontinuity with high resolution. Another FDS type is HLL schemes, which is not suggested for shock discontinuities. However, there are some modifications to improve this scheme such as HLLEM.

Well-known Steger-Warming and Van Leer FVS schemes are the other category. They are considered as more efficient than FDS schemes. In the literature, it is observed that schemes from this category is not used for hypersonic flows because they are not accurate enough to capture shock discontinuities despite their computational speed advantage.

The third category is FS schemes, which are proposed to combine the strengths of FDS and FVS schemes. AUSM Scheme is a FS scheme, which can be seen in Fluent solver settings. It should be noted that Fluent uses AUSM+ modification to boost robustness of AUSM.

At this point, it is critical to state that the scope of this thesis is not the improvement of flux schemes, and commercial solvers do not have the most accurate or the most robust properties because they are tuned to capture various flow cases. Therefore, their convergence or accuracy are not optimized. However, Fluent versions of Roe-FDS or AUSM are proved to give whatever a design or optimization study require.

During the literature survey, many comprehensive references are found, and some remarkable findings will be summarized for anyone who intends to dive into this topic. [29] compares flux schemes for different flow setups. Mach 5 hypersonic flow through scramjet inlet is evaluated using Roe, AUSM, AUSM+, HLLE, Van-Leer

and Rusanov schemes. In this study, AUSM+ is favorable scheme while Roe is stated as unstable. In this study, the author underlines the use of Roe scheme for supersonic flows while AUSM scheme family is the best trade-off for different properties. Moreover, some drawbacks of AUSM+ are vanished by some latest modifications.

Another review about this topic is proposed by [51] and this review demonstrates the modifications of AUSM such as AUSM+, AUSMPW+, E-AUSMPW, Roe-FDS, HLLE schemes. It is said that the state of art of this field focuses on the applicability of these solvers for all speeds. [36] discusses the applications of different flux schemes for high-speed flows.

In this study, AUSM, K-T and K-N-T schemes are compared, and these schemes are stated to be suitable for Mach 5 flow of the scramjet intake in terms of the accuracy and robustness. [39] proposes AUSMAS for all speed conditions, and it is claimed that AUSMAS performs outperforms the former ones of this family to increase robustness and accuracy.

2.5 Intake Design Tool

In the present thesis, it is aimed to develop a preliminary design tool and this section will explain the theoretical background of the tool. The tool is created by MATLAB and its results will be compared with CFD results in the following chapter.

2.5.1 Theoretical Background of Intake Design Tool

MATLAB code is created to calculate thermodynamic performance parameters and to obtain the intake geometry. For this purpose, oblique shock relations are used, and such a calculation is valid under inviscid flow conditions. Viscous effects cannot be included using simple relations. However, obtaining the geometry is sufficient to observe how it performs compared to CFD. Such a tool is beneficial to start a preliminary design and to have shock-on-lip and shock-on-shoulder conditions geometrically. If such a tool performs accurate enough, then the design process does not need the use of viscous CFD calculations at initial stage. Figure 2.1 demonstrates how the tool works in terms of inputs, outputs, and constraints.

2.5.2 Present Design Point (On-Design)

In the previous sections, what kind of physical challenges scramjet intakes have is explained. Considering these challenges, the design of scramjet intakes has some constraints and some goals. It is vital to create a design and performance box for this task. Design box of present thesis and its design tool can be summarized as follows:

- Flight Mach Number :7
- Flight Altitude: 27500 km
- Flight Dynamic Pressure: 58.75 kPa

Section 2.5.2.1 discusses the physical availability of this design point considering scramjet operational limits. Mach 7 flight can be accepted as a pure scramjet flow.

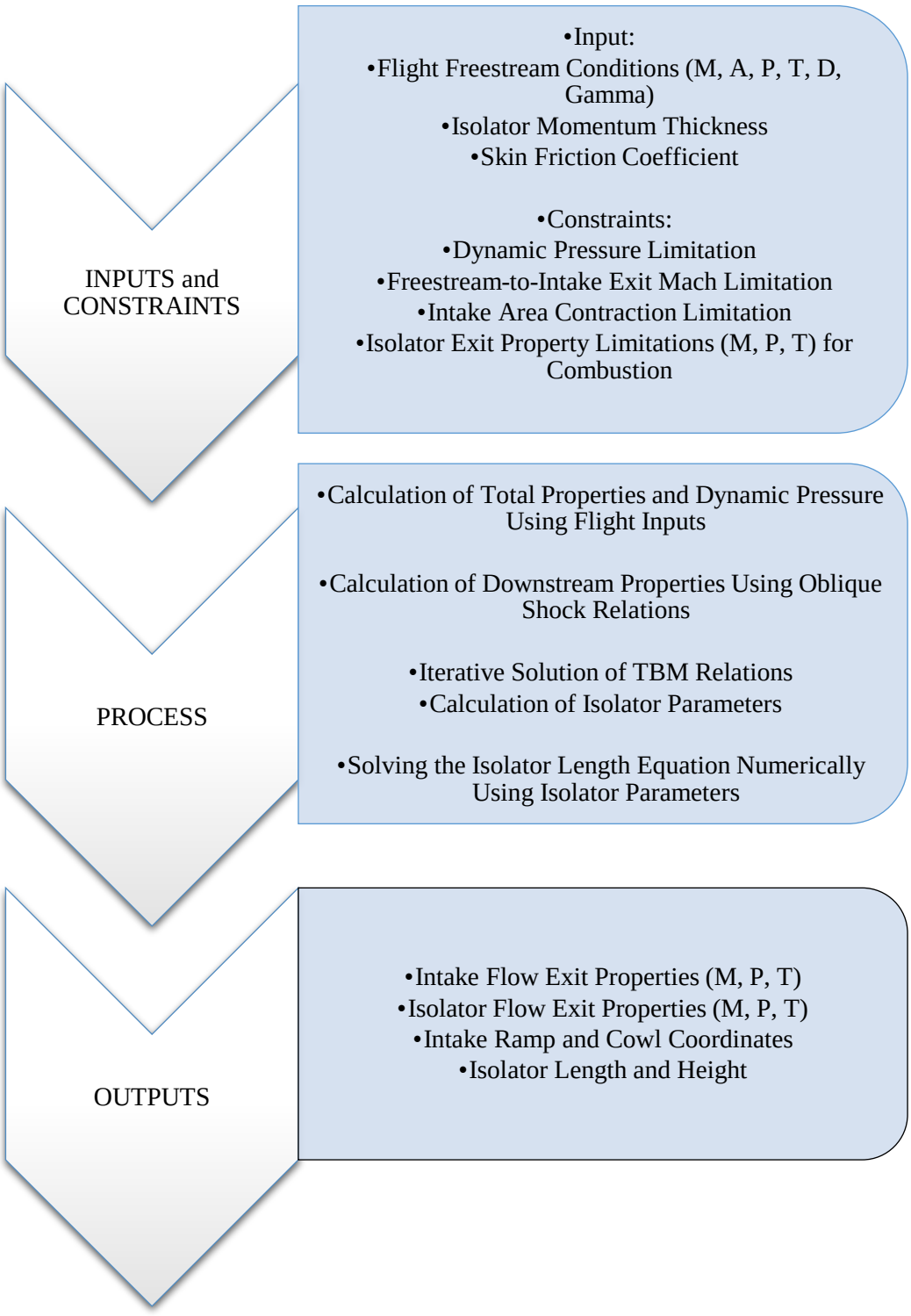

Figure 2.1: Flowchart of Simple Design Tool

2.5.2.1 Flight Corridor

Hypersonic airbreathing propulsion uses a narrow band to fly because low Mach numbers will prevent the proper scramjet operation. Until some point, it can be accepted as a dual-mode ramjet-scramjet propulsion but it is very hard task to sustain supersonic combustion and shock dynamics. High Mach numbers after a certain point is also problematic because designers must deal with low-density gas dynamics and thermo-structural issues. Therefore, ordinary scramjet operations are between Mach 6 and Mach 10. [68]

In addition to flight Mach number, flight altitude and flight dynamic pressure should be decided carefully. It is acceptable to be between 23.94 kPa and 95.76 kPa for dynamic pressure. When flight altitude, flight dynamic pressure, flight Mach number and total temperature are combined as a design box, Figure 2.2 can be obtained. Such a design box demonstrates the structural and thermal limits, proper combustion and engine unstart restrictions.

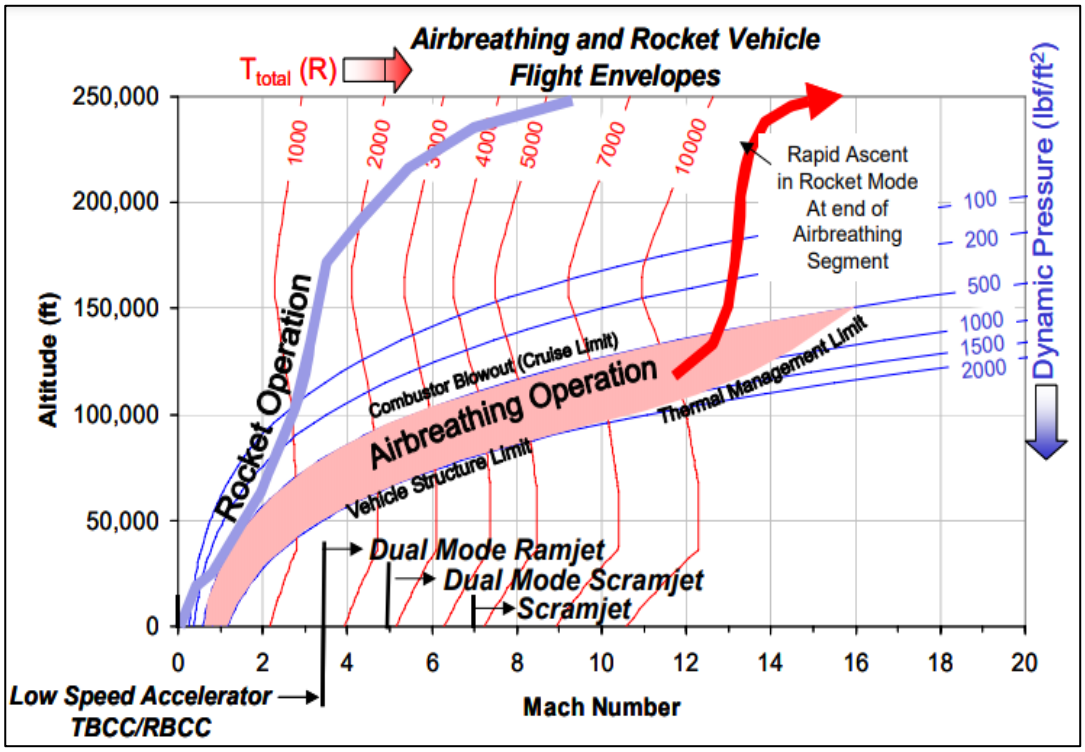

Figure 2.2: Flight Envelopes of Airbrathing Operation [2]

Also, scramjet engines are mostly developed for military purposes so the flight altitude decision should mirror possible requirements. There is another type of hypersonic vehicles called as gliding vehicles without the use of scramjet engines and flight altitude is one of the design constraint between them.

Air-breathing vehicles powered by scramjet engines combine the speed and relatively lower altitude to get rid of radar detection. As illustrated by [23], altitudes below 30 km during cruise are preferred. In present thesis, the design point is chosen considering this information. Figure 2.3 illustrates the differences between vehicles flying at hypersonic speeds with different trajectories.

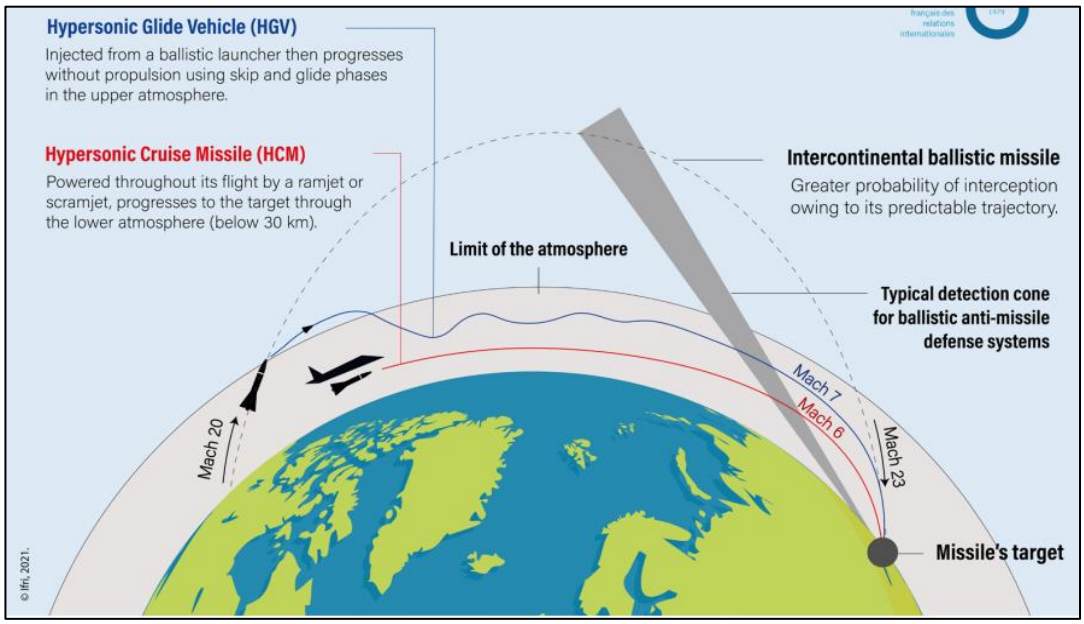

Figure 2.3: Illustration of Different Flight Trajectories, Altitudes and Speeds [23]

2.5.2.2 Isolator Exit Pressure and Temperature (Combustor Entrance)

Since scramjet concept does not have physical compressors, the only way to increase pressure for a proper combustion is the design of oblique shocks and isolator weak shock train. [59],[60],[61] state that the range between 50 kPa and 100 kPa is suitable for this purpose. Another reference [13] indicates the general rule of thumb of 0.5 atm for combustor entrance. Proper ignition can be obtained above 1000 K.

The information related to combustor entrance is generally rooted from T_3/T_0 ratio for certain flight altitudes given by [22] However, this generalized value can differ depending on fuel type or propulsion system design.

[68] reviews many references about this topic. Crossover temperature for hydrogen is given as 900-950-1000 K for 0.5-1.0-5.0 atm, respectively. There are many examples such as HiFire-2, HyShot-2, UVa, DLR for combustion entrance conditions in [68].

In an experiment, [14] presents inflow condition of 868.2 K while using the ethylene for combustion. Flight equivalent conditions are Mach 7.3, 53.5-kPa dynamic pressure and 28.7 km.

Moreover, [34] numerically investigates various 2-D intake-isolator models with Mach 8 and averaged isolator exit temperatures are between 862-1035. These values can be used for approximate judgements of present design.

In an old supersonic combustion thesis, [7] states that hydrogen-silane mixture can be used for ignition aid. Problematic ignition times at 900 K can be improved and can converge to 1000+ K results under suitable pressure conditions such as at least over 0.5 atm. Fuel and injection effects can be found in [27] with additional details.

2.5.2.3 Intake Exit Mach Number (Combustion Entrance)

Since the exit Mach number and flow profile at the end of isolator strongly affects the combustion, freestream Mach number, shock system design and resultant exit Mach number should be decided carefully. [41] states that the range between 2.2 and 5.0 is suitable for proper combustion. Lower limit is significant not to drop below supersonic conditions and upper limit is significant not to exceed flammability of air-fuel mixture.

Also, the ratio of entrance Mach number and exit Mach number is vital for boundary layer flow conditions through isolator.[22] explains that if the ratio is below 0.762, flow will separate. Nevertheless, flow separation depends on many conditions, and design will not be limited to these criteria only.[21] presents results of Mach 7 scramjet experiment and the Mach number at the entrance of combustor around 2.7, which agrees the theoretical expectations. [4] discusses inflow requirements for different flight trajectories and required entrance Mach number at given temperature and pressure conditions is approximately around Mach 2.5.

2.5.2.4 Shock-on-Lip (SoL) and Shock-on-Shoulder (SoS) Conditions

Since the hypersonic flight corridor is narrow and little changes make big differences, scramjet intake designs aim SoL condition, which means all external oblique shock waves impinge on cowl lip point. When the following shock from lip impinge on shoulder point, this means SoS condition. When SoL condition is not satisfied, the shock may pass the cowl lip and mass flow leakage occur or the windward shock may enter the intake. Both events are not desired considering pressure recovery, efficiency, additional aerothermal loads or even unstart condition.

However, it is not possible to keep scramjet intake exactly at on-design condition during flight. Also, inviscid based designs mostly deviate from flight conditions due to viscous effects. Geometry optimization, addition of bleed flow, energy techniques and variable cowl designs help off-design conditions overcome these issues. In the scope of this thesis, the design starts from inviscid flow and SoL condition. Figure 2.4 illustrates what SoL and SoS conditions mean on a generic geometry.

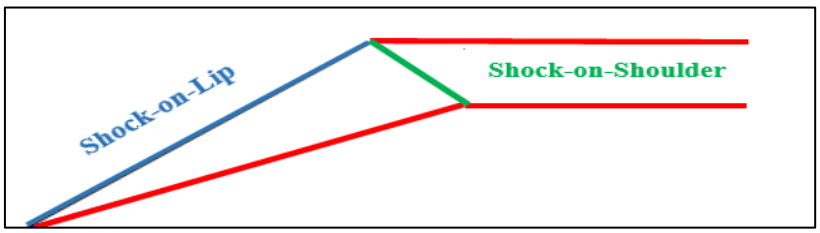

Figure 2.4. Schematic of SoL and SoS Conditions

2.5.2.5 Contraction Ratio and Intake Area Relations

As it is mentioned in intake design challenges, start-unstart conditions of an intake drive the design process. Geometrical features of the intake have a significant impact on starting of the intake. Internal Contraction Ratio (ICR) should be such that the intake should operate as desired under certain free stream Mach number and AoA conditions.

In the intake design literature, one of the most mentioned ICR criterion is given by Kantrowitz. Using this criterion, the intake design can be evaluated if it is self-starting or not. In addition to Kantrowitz limit, [33] reviews different ICR criterions in the same Kantrowitz Plot as given in Figure 2.5.

In the present thesis, the design also checks Kantrowitz Plot. The intake geometry stays within the safe region of this plot. Mach number at cowl lip generally cannot be detected by analytical methods so averaged value taken from CFD calculations is suitable for this purpose.

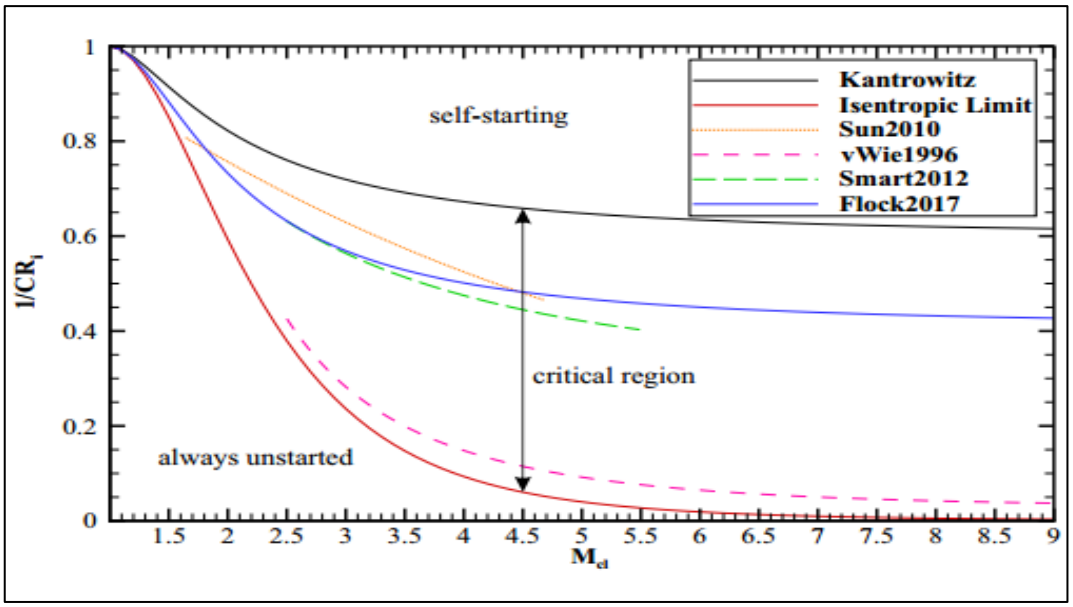

Figure 2.5. Combined Kantrowitz Criterion Plot Given By [33]

It is necessary to stay away from 'always unstarted' region. The present design aims to stay at least between always unstarted and self-starting region at first. Then, the design can be improved by size or shape optimizations after preliminary design if there is a need. Most of the time, SoL-SoS conditions and self-starting are not possible to obtain at the same time under viscous flow conditions. Currently, design aims to obtain SoL and SoS conditions at first because there is a need for a baseline to make comparisons between inviscid flow and viscous flow.

2.5.2.6 Theoretical Formulations of the Design Tool

Design tool fundamentally uses OSW and TBM relations for the intake ramp region.

- TBM Relations

$$tan\theta_1 = 2cot\beta \frac{M_1^2 sin^2\beta_1 - 1}{M_1^2(\gamma + cos2\beta_1) + 2} \quad \text{Eq.19}$$

TBM relations are strong tools of aerodynamics if there are calculations related to shocks. Shocks may exist in forms of strong or weak, and present thesis is interested in weaker oblique shocks and supersonic downstream flow. TBM relations can be solved in an iterative manner as it is done in present tool. The flow is assumed as perfect gas, steady and inviscid for these calculations.

- Total Thermodynamic Relations

$$Pressure: \frac{P_0}{P} = (1 + \frac{\gamma-1}{2}M^2)^{\frac{\gamma}{\gamma-1}} \quad \text{Eq.20}$$

$$Density: \frac{\rho_0}{\rho} = (1 + \frac{\gamma-1}{2}M^2)^{\frac{1}{\gamma-1}} \quad \text{Eq.21}$$

$$Temperature: \frac{T_0}{T} = 1 + \frac{\gamma-1}{2}M^2 \quad \text{Eq.22}$$

- Thermodynamic Relations Considering Oblique Shock Wave

$$Pressure: \frac{P_2}{P_1} = 1 + \frac{2\gamma}{\gamma+1}(M_1^2 sin^2\beta - 1) \quad \text{Eq.23}$$

$$Density: \frac{\rho_2}{\rho_1} = \frac{(\gamma+1)(M_1^2 sin^2\beta - 1)}{(\gamma+1)(M_1^2 sin^2\beta - 1)+2} \quad \text{Eq.24}$$

$$Temperature: \frac{T_2}{T_1} = \frac{\rho_1}{\rho_2}\frac{P_2}{P_1} \quad \text{Eq.25}$$

- Downstream Mach Number

$$M_2 = \frac{1}{\sin(\beta-\theta)}\sqrt{\frac{1+\frac{\gamma-1}{2}M_1^2 sin^2\beta}{\gamma M_1^2 sin^2\beta - \frac{\gamma-1}{2}}} \quad \text{Eq.26}$$

- Sample ICR Formulation (Isentropic)

$$\frac{A_{cl}}{A_{th}} = \frac{1}{M_{cl}}\left[\frac{2}{\delta-1}\left(1 + \frac{\gamma-1}{2}M_{cl}^2\right)\right]^{\frac{\gamma+1}{2(\delta-1)}} \quad \text{Eq.27}$$

TBM relations are solved iteratively until a certain convergence criterion is found. In the tool, 1E-3 criteria are chosen, and it is sufficient for such an analytical calculation. These relations are solved for each ramp. In the present thesis, 2-ramp intake design is chosen, and there will be 2 external ramp shocks. After these ramp shocks, there will be another oblique shock for cowl-shoulder region because the design is intended to have both SoL and SoS conditions. At the end of these loops, thermodynamic performance values can be obtained at the end of intake (at the entrance of isolator.

These formulations are about the aerodynamic performance of the designed intake geometry. However, the tool should also give the x-y coordinates of the geometry to use it further CFD analysis. The tool gives the location of these points where SoL and SoS conditions are satisfied together after a set of loops.

In the next phase, the length of the isolator is decided. [20] The topic of isolator depends on what kind of isolator flow exists. In the pure scramjet mode, isolator is considered as shock free without interactions between combustor back-effects and isolator flow. In this way, no flow separation is expected. Otherwise, there will be clear shock trains to suppress backpressure effects and to stabilize the flow.

The tool will assume that there will not be pure scramjet condition because the tool is developed to work from low Mach numbers such as 4-5 to pure scramjet such as 7-8. If there occurs a pure scramjet condition, it is easier to continue by carrying flow profile of isolator entrance to the exit.

However, if there is a dual-mode scramjet case at low Mach numbers, shock train will change flow profile through isolator. Pressure will increase and Mach number will decrease. For this reason, the isolator tool is created considered the worst-case scenario.

Pseudo-shock train length for isolator can be found using the empirical relation of [Eq.28]. This relation is firstly created by [71] for axisymmetric ducts. Then, [64] has modified this relation for rectangular ducts as given in [Eq.29] The limitation of this relation is the incoming Mach number at the entrance of isolator. [Eq.28] relation is obtained by experimental data of Mach 2.85. Such a value still can be considered acceptable for the present thesis. [19]

- Base L/H Formulation

$$\frac{S_t(M_2^2-1)Re_\theta^{0.25}}{D^{0.5}\theta^{0.5}} = 50(\frac{P_3}{P_2}) + 170(\frac{P_3}{P_2}-1)^2 \qquad \text{Eq.28}$$

- Modified L/H Formulation for Rectangular Ducts

$$\frac{S_t(M_2^2-1)Re_\theta^{0.2}}{H^{0.5}\theta^{0.5}} = 50(\frac{P_3}{P_2}) + 170(\frac{P_3}{P_2}-1)^2 \qquad \text{Eq. 29}$$

- Back-Pressure Ratio for $(\frac{P_3}{P_2})$ Ratio

Back-pressure is a critical aspect of isolator design. Although isolator is not the focus of present thesis, a special attention is given because isolator exit conditions are strongly coupled with intake flow.

Back-pressure ratio is expected to be larger for higher Mach numbers, especially for real flights to prevent possible unstart issue.

$$\frac{P_3}{P_2} = \frac{2\gamma_c}{\gamma_c+1} M_2^2 - \frac{\gamma_c-1}{\gamma_c+1} \qquad \text{Eq. 30}$$

- Determination of Skin Friction Coefficient

Skin friction coefficient makes remarkable differences for overall solution because all of ODEs of isolator uses it in equation. There are many formulations or correlations for C_f and [16] is used for this input.

- Momentum Thickness

Isolator momentum thickness is taken as 0.02 considering [22]'s explanation.

- ODE Set of Isolator Flow Properties

The isolator flow properties can be found using the equations developed by [15]. However, only frictional effects will be included as opposed to the reference for simplification. In present thesis, the isolator is preferred as constant area isolator so there is no inclination angle or area change. Heat transfer effects are neglected because the confirmation will be done by Fanno flow technique for ducts. Also, CFD wall BCs are constant wall temperature.

Mach number Equation: $\frac{dM}{dx} = \left(\frac{\gamma M^2\left(1+\frac{\gamma-1}{2}M^2\right)}{2(1-M^2)}M\right)\frac{4C_f}{D_h}$ Eq. 31

Static Pressure Equation: $\frac{dP}{dx} = \left(-\frac{\gamma M^2[1+(\gamma-1)M^2]}{2(1-M^2)}P\right)\frac{4C_f}{D_h}$ Eq. 32

Static Temperature Equation: $\frac{dT}{dx} = \left(-\frac{\gamma(\gamma-1)M^4}{2(1-M^2)}T\right)\frac{4C_f}{D_h}$ Eq. 33

These equations can be initialized by the inviscid exit Mach condition as mentioned before. Intake exit to freestream flow Mach number have a ratio of 0.5 and isolator condition given by [22] should be 0.762 to prevent separated flow for turbulent cases. This means that the isolator exits to freestream Mach number have a ratio of 0.38. If Mach 7 flow is considered, the iterations should aim 2.66 ideally. It should be remembered viscous flow can naturally deviate from this because centerline flow properties and near-wall flow properties are not the same.

- Fanno Flow Approach as a Back Test

Compressible inviscid flows can be modelled considering frictional effects. For this simple model, the flow is assumed as steady, 1-D, and adiabatic. The flow property is ideal gas and specific heat is constant. The flow goes through a constant area duct.

When these properties are evaluated carefully, it is sensible to think about isolators. Fanno flow relates to different location in the flow using sonic conditions. In a sufficiently long duct, supersonic flow can decelerate with friction and can be choked in theory. [12]

For example, Mach 3.5 and Mach 1 flow have their own relations. Also, Mach 2.65 and Mach 1 flow their own relations. Using this, pressure rise, temperature rise and required length can be predicted if skin friction coefficient, hydraulic diameter of the duct is known.

$$\Delta \frac{4C_f L^*}{D_H} = \left(\frac{4C_f L^*}{D_H}\right)_1 - \left(\frac{4C_f L^*}{D_H}\right)_2 \quad \text{Eq. 34}$$

$$\frac{P}{P^*} = \frac{1}{M}\left[\frac{\gamma+1}{2\left(1+\frac{\gamma-1}{2}M^2\right)}\right]^{\frac{1}{2}} \quad \text{Eq. 35}$$

$$\frac{T}{T^*} = \frac{\gamma+1}{2\left(1+\frac{\gamma-1}{2}M^2\right)}\Big] \quad \text{Eq. 36}$$

Considering skin friction can be between 0.002 and 0.008 for isolator duct flows like present one and hydraulic diameter can be taken as rectangular duct, $\Delta \frac{4C_f L^*}{D_H}$ can be calculated. Naturally, this is just a rough estimation, but the length obtained from the design tool can be roughly checked whether it is sensible or not. Other than these rough estimations, intake-isolator models and their length ratios are already checked.

CHAPTER 3

RESULTS FOR VALIDATION CASE

In this section, results from verification studies, simple performance code and optimized geometry will be presented. In Section 3.1, verification of ANSYS Fluent commercial code is demonstrated using an open-source experimental database. In Section 3.2, outputs of design tool developed in MATLAB are given. In Section 3.3, inviscid and viscous CFD simulations executed by ANSYS Fluent are given in contours, wall-exit profiles and averaged values. In Section 3.4, comparisons between analytical and numerical results are presented. In Section 3.5, parametric studies away from design point are conducted using CFD.

3.1 Validation Test Case Simulations

Every numerical study should start by verifying the flow solver because RANS simulations are one of the ways to replicate the real life conditions. Sometimes, capabilities of commercial codes themselves are already verified by many users in the literature, but the verification study is also the proof of the defined solver settings boundary conditions and computational grid. A model scramjet intake taken from the Ph.D. thesis of [24] is used, and the solver performance, settings and required tunings of the software are investigated. As mentioned before, the solver and required settings are critical to capture any part of the flow. Flow separation, bubble locations, peaks at pressure distribution should not be missed for intake design, and verification of the scramjet model will be vital for this purpose.

3.1.1 Geometry Generation for Validation Test Case [24]

Since it is not common to publish detailed scramjet experimental data in the literature, one of the most used open source setup belongs to the Ph.D. thesis of [24]. The High Supersonic Tunnel of the University of Manchester is capable of tests for hypersonic experiments. Freestream conditions are given in Table 3.1. as follows.

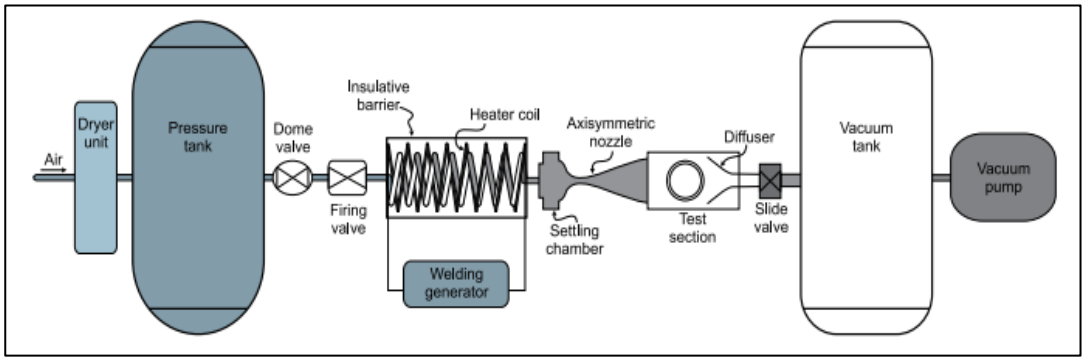

Figure 3.1. Schematic of the Tunnel of Experimental Case [24]

Table 3.1. Freestream Parameters of Experimental Setup

Parameter	Value
Mach Number	5 ± 0.1
Freestream Static Temperature	62.5 K
Freestream Static Pressure	1228.5 Pa
Baseline AoA	0°
Stagnation Pressure	6.5 ± *0.05 bar*
Stagnation Temperature	375 ± *5 K*
Reynolds Number	13.2E6

Pressure measurements of this experiment are made using PSP technique and Kulite pressure transducers. Visualization technique is colour schlieren. The detailed explanation about experimental setup can be found in [24].

The experimental model includes 2 ramps having 10° and 22°, isolator channel and a cowl. The cowl has a slope of 30°. Total intake and isolator length is 135 mm, and the designed model is a self-starting one. The geometry of the verification case is given in Figure 3.2.

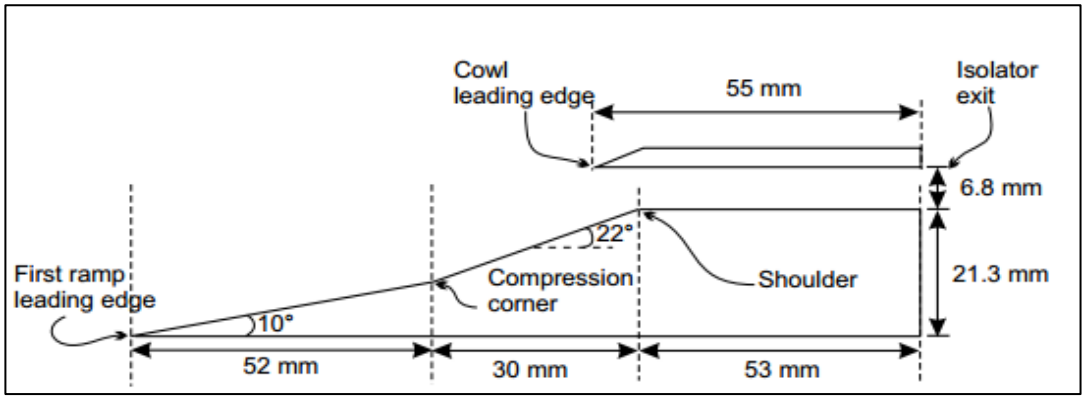

Figure 3.2. Reference Intake-Isolator Model

The proposed intake model satisfies the shock-on-lip condition, which is a vital condition to get rid of excessive thermodynamic conditions and performance losses.

In the verification study, S-A, kw-SST and transition-SST turbulence models are investigated. The verification aims to prove reproducing the shocks, re-attachments, 3 separation regions, bubbles with correct locations. The proof is not only quantitative contours, but also exit Mach number, exit pressure, exit temperature parameters and pressure distributions along x-axis. These parameters are numerically provided in the reference.

The convergence criterias to understand whether iterations are sufficient and they no longer improve the solution quality are residuals and physical quantites at the exit. As suggested in [24] E-4 is aimed for residuals. Other than the statement of reference, it is observed that continuity residual holds the rest of residuals for every case. When continuity reaches order of 3.5, energy residual already passes through order of 5. Also, results about residuals in [35]'s hypersonic intake study is around the order of 4 after thousands of iterations.

It is known that residuals do not mirror the convergence everytime. They mean nothing if physical quantities do not converge through a certain level. For this reason, mass or area averaged Mach numbers, static pressure and net mass flow rate are observed at the outlet of the domain. Ultimately, if net mass flow rate between pressure farfields and outlet of the domain converges to zero, this is the physical sign of converged solution.

The boundary conditions are pressure farfield at the inlet and at top of the domain, symmetry between domain and the start of ramps, no-slip wall at ramps, at cowl and at isolator, pressure outlet at isolator exit, and at cowl exit. The schematic of boundary conditions and domain is given in Figure 3.3.

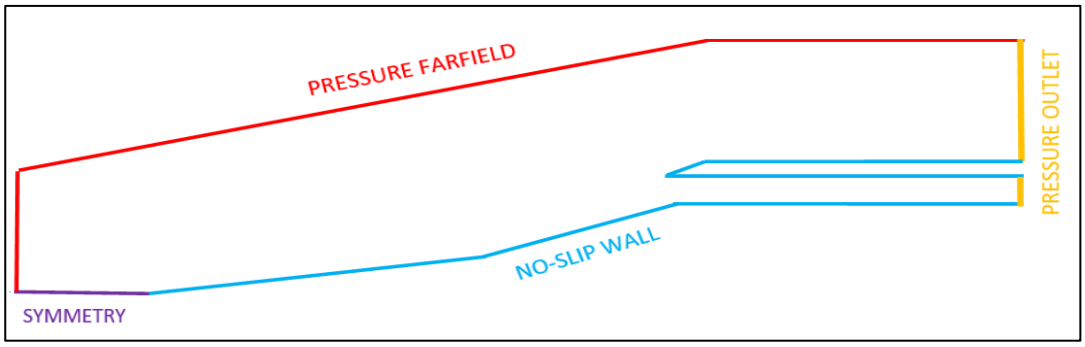

Figure 3.3. Boundary Conditions and Domain of Validation Case

3.1.1.1 Grid Generation for Validation Test Case

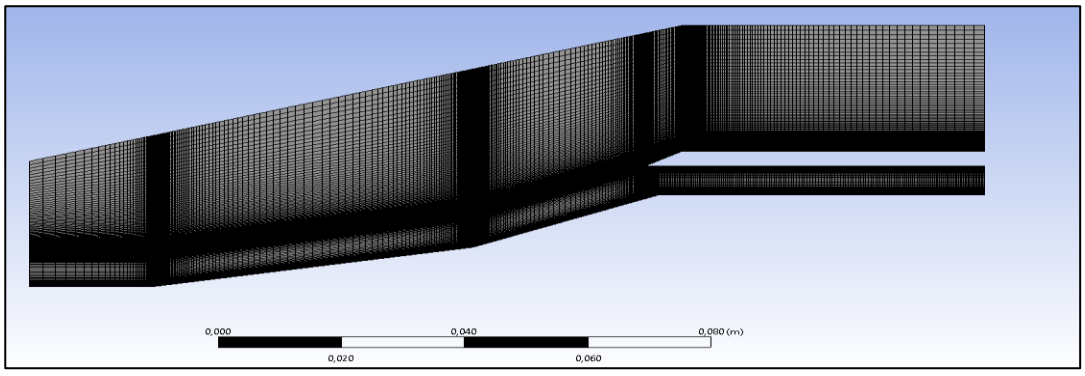

Figure 3.4: Base Grid of CFD Validation Case Created by Structured Meshing

3.1.1.2 Mesh Independence Study

When there is a use of CFD analysis, one of the most vital aspects is making the solution independence from the chosen grid. Especially, solving special flows such as the present thesis require the accurate modelling of little jumps or fluctuations in wall pressure or exit velocity profiles, and the intensity of the mesh should not affect the solution after a certain intensity.

In the validation study, the grid is created considering the criteria of (y+ <1) and the first layer thickness of 2E-6 m. The first layer thickness may change depending on the geometry or flow conditions, but the chosen value is able to satisfy the criteria of y+ and to calculate boundary layer solution accurately.

The independence is checked using 5 different mesh intensity for the same turbulence model. While GRID 1 indicates the coarser mesh, GRID 5 indicates the finest mesh. The grid independence study is executed using KW-SST turbulence model. Starting from the coarse mesh to finer meshes, normalized pressure plot is investigated. It is required to see pressure rise around the end of ramps, shoulder and through isolator. When the literature is examined in addition to experimental reference of this geometry, every CFD solution has little differences at peak and bottom pressures, but the trend is consistent with experimental PSP and Kulite data.

These 5 different grid setups are created by using 27200, 56800, 109860, 216830 and 433460 cells, respectively. Maximum sizes are iterated from 1E-3 m to 4.2E-4 m from coarser to finer grids. During these iterations, boundary layer resolution is also iterated using bias options.

In the present result, GRID 4 is suitable for further use because it predicts the critical fluctuation at isolator, and the result is almost the same with GRID 5 while there is a balance between the accuracy and computational cost. GRID 5 mesh does not create a significant difference on results while it dramatically increases the computational cost. Therefore, GRID 4 is considered as grid independent. After creating a base grid for further runs, the effect of turbulence models is also

investigated. Figure 3.5 demonstrates quantitative comparison of grids. The clear change depending on the grid type can be observed around X/L= 0.85-0.95 region. Double bottom like pressure trend on the plot is getting more visible from the worst grid to the best grid. Moreover, this pressure change location is shifted from the right to the left. The second proof about the grid resolution can be observed around X/L= 0.70-0.75, where the peak of pressure occurs. GRID 4 and GRID 5 grids have almost the same trend for normalized pressure, while GRID 3 grid predicts slightly lower pressure.

Physically, the convergence of mesh independence study can also be observed using averaged exit values of flow properties. For example, averaged static temperature at the isolator exit is 201.1 and 200.8 K respectively for GRID 4 and GRID 5, which makes the difference well below %1. These values agree with experimental data of 194.92 K with only %3 difference.

It should be remembered that [26] the experiment underlines the uncertainty level between experimental measurement techniques and CFD around %6. Therefore, it is sufficient to follow main trend, peak and bottom locations other than looking for diamond-precise numerical comparisons.

Table 3.2. Freestream Parameters of Experimental Setup

Grid Type	Exit Static Temperature [K]	Peak Normalized Wall Static Pressure [Pa]	Exit Static Pressure [Pa]
Present Base CFD	200.83	41789	21671
[25] Experiment	194.92	-	22000
[25] CFD	-	Appx. 42500	-

Table 3.2. compares where the present CFD stands quantitatively in addition to plots. [25] CFD only states the exit Mach and normalized wall static pressure data and other parameters are given from the experimental measurements. Temperature and pressure data seems consistent with present CFD. Ph.D. thesis of this experiment

[25] and following article [26] have two different exit Mach data as 2.01 and 2.088 respectively. Present CFD has Mach number of 2.0558 at the exit. Both present CFD and [25]'s CFD underestimates experimental exit Mach around %11. [26] explains that this difference gets smaller with higher AoA flows.

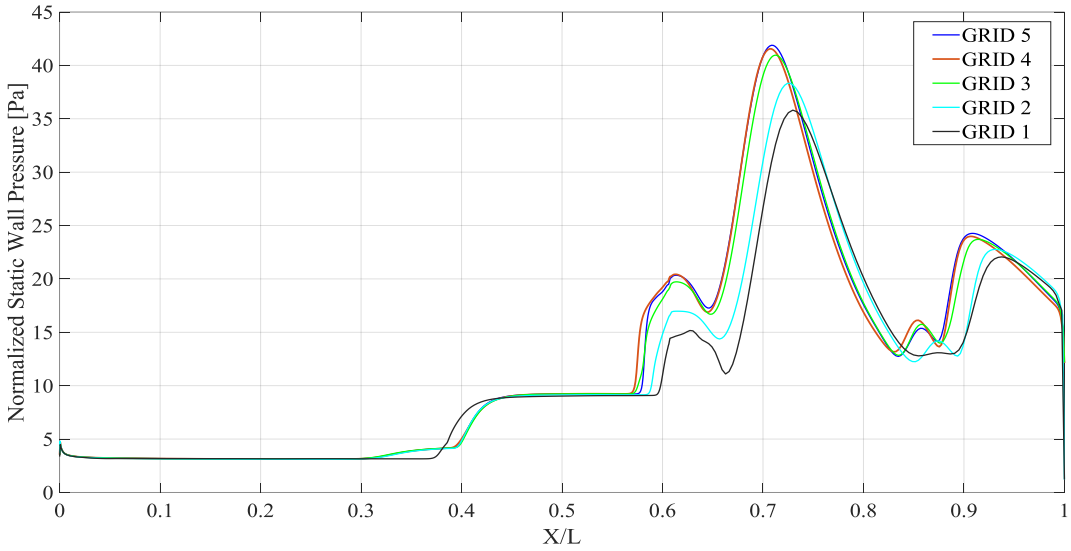

Figure 3.5. Comparison of Different Grids for Normalized Pressure

3.1.1.3 CFD Results for Different Turbulence Models

After choosing GRID 4 in the previous independence study, different turbulence models and their effect on the result are investigated. Different viscous options with SA, K-KL-W Transition, KW-SST and SST Transition models are chosen for this study. It should be noted that Low-Re Corrections and Compressibility Effects are not included in KW-SST model by considering suggestions of [43] Decreasing stability and convergence issues when these settings are applied in present study prove the sense of that suggestion. Viscous heating is chosen for all models.

When normalized pressure plot is examined, the first finding is that K-KL-W Transition model is not suitable for this case. Both the trend and numerical result clearly do not agree with experimental data. SA model is closer to experimental data and mostly successful, but it is lack of accuracy at two aspects. The double bottom

shape of normalized pressure at isolator around X/L=0.8 cannot be captured by SA model. [5] states that SA Model with Edwards's correction solves this issue but Fluent does not have this option as embedded. Secondly, slight pressure rise around at the end of first ramp is not parallel with experimental data and successful models.

KW-SST and Transition SST are in strong agreement with experimental data and other CFD validations in the literature. There are slight differences among these models. They successfully predict the double bottom shape around X/L=0.8 and the end of the first ramp is suitable to experimental data. However, KW-SST seems closer to the experimental data and [25] CFD investigations at the peak of this plot around X/L=0.72. There is around %3 difference. It is valid for X/L=0.62 location as well. Therefore, the choice is KW-SST turbulence model. KW-SST model is used together with transition options of Fluent. Figure 3.6 compares present CFD with turbulence models, [25]'s CFD and experimental data on the same plot. Moreover, results obtained by present thesis is in strong agreement with the CFD results of [5], which is conducted using SU2 solver. This is another indicator about the validation of present CFD setup.

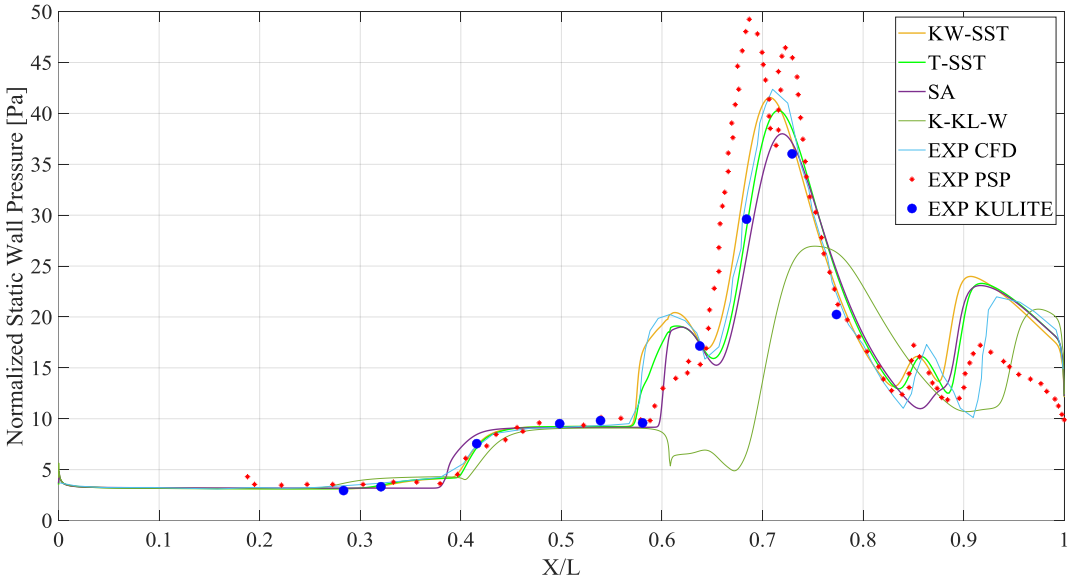

Figure 3.6: Comparison of Different Turbulence Models for the Same Grid

3.1.1.4 CFD Results for Validation Test Case

In this section, contour plots of validation case are given for Mach number and static pressure for a qualitative comparison in addition to quantitative normalized pressure plot. Explanations can be found at the end of this section.

Figures between 3.7 and 3.14 compare different turbulent models and their flowfield predictions. K-KL-W turbulence model fails to predict accurate flow field compared to experimental Schileren visuals in [25]. This is clearly related to cowl shock and separation region. K-W SST model and Transition SST models predict shoulder separation accurately because bubble spills towards the upstream of shoulder as proven in experimental case. SA model predicts the bubble at fully downstream of shoulder.

Figure 3.15 and Figure 3.16 demostrate the velocity vector field of selected K-W-SST model with gamma-transition setting. As it can be seen, there are 3 separation region with adverse velocity vectors. The shape of boundary layer profile also proves that boundary layer region is well resolved.

Another observation is that shoulder bubble is remarkably big and it interacts with cowl shock. Therefore, there is a high level of pressure increase around cowl wall surface. These are great examples of theoretical explanations given in previous sections.

Also, it should be noted that there is a thin separation region predicted by KW-SST and Transition SST around the intersection locations of 1^{st} and 2^{nd} ramps, which is also demonstrated the [25]'s own KW-SST results.

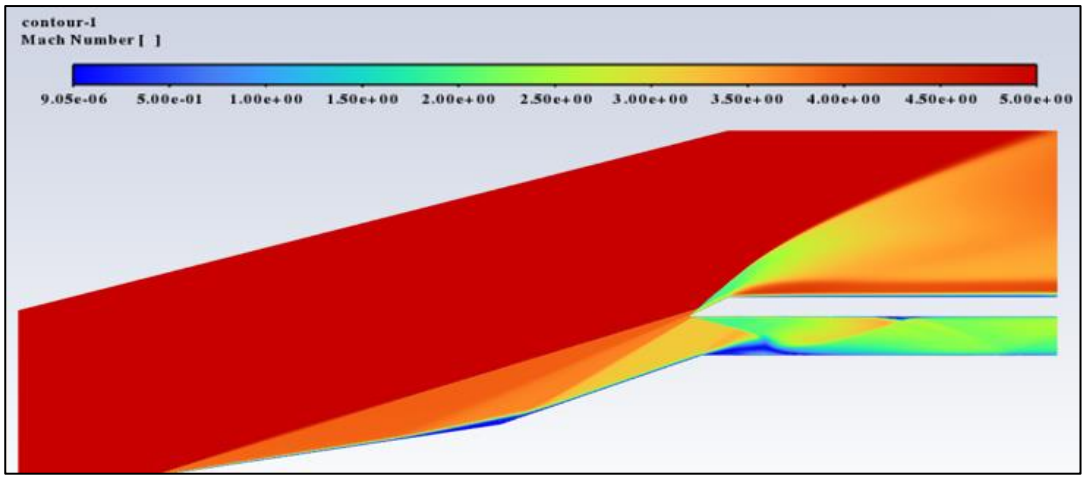

Figure 3.7. Mach Contour of K-KL-W Turbulence Model

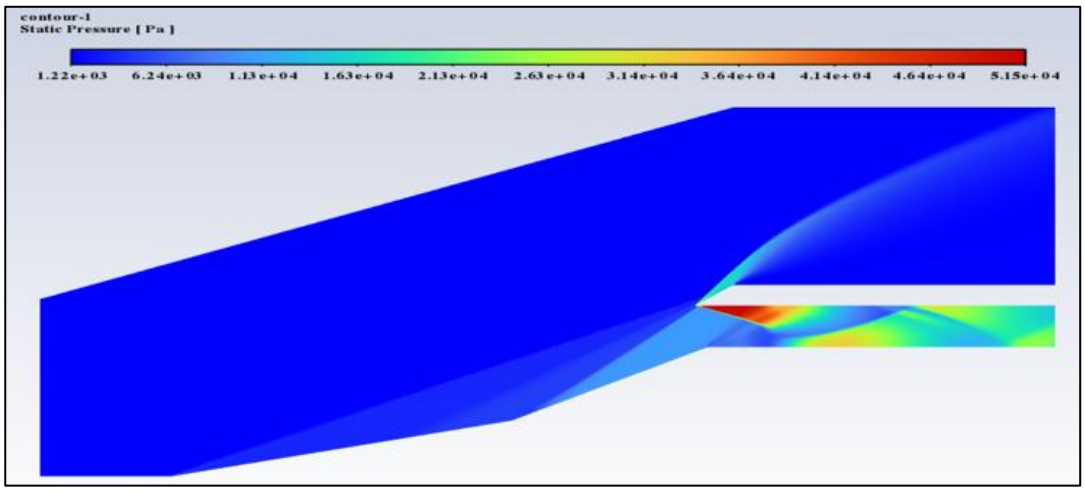

Figure 3.8. Static Pressure Contour of K-KL-W Turbulence Model

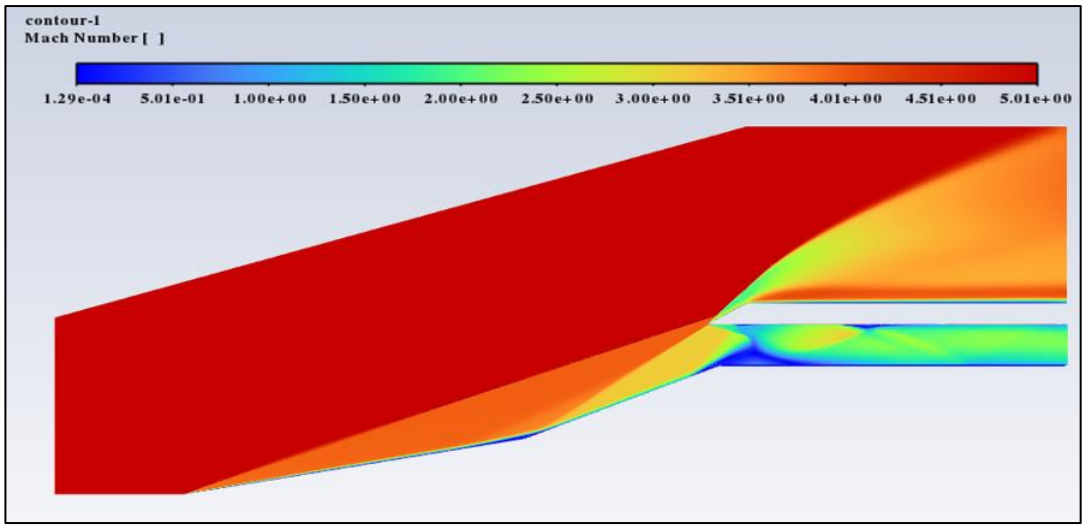

Figure 3.9. Mach Contour of KW-SST Turbulence Model

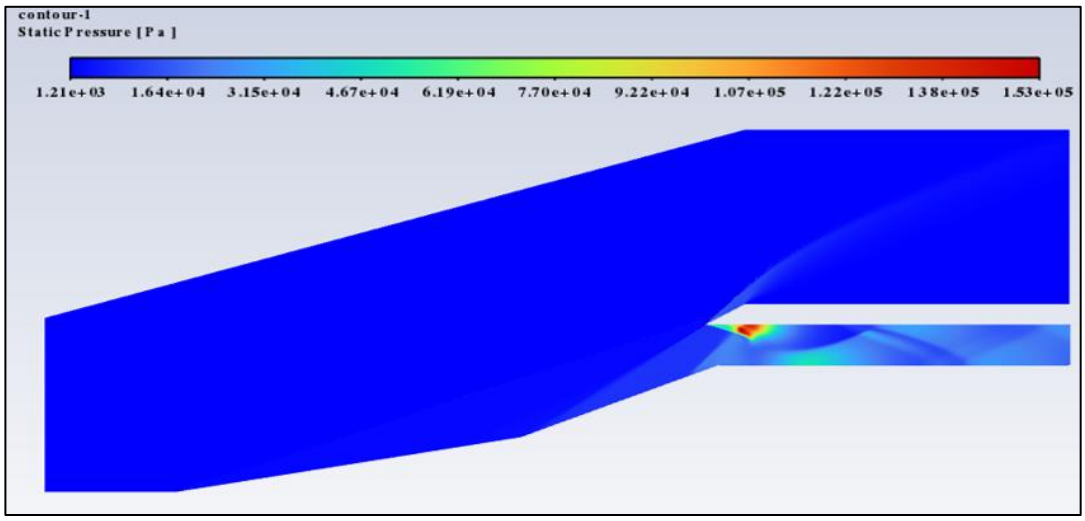

Figure 3.10. Static Pressure Contour of KW-SST Turbulence Model

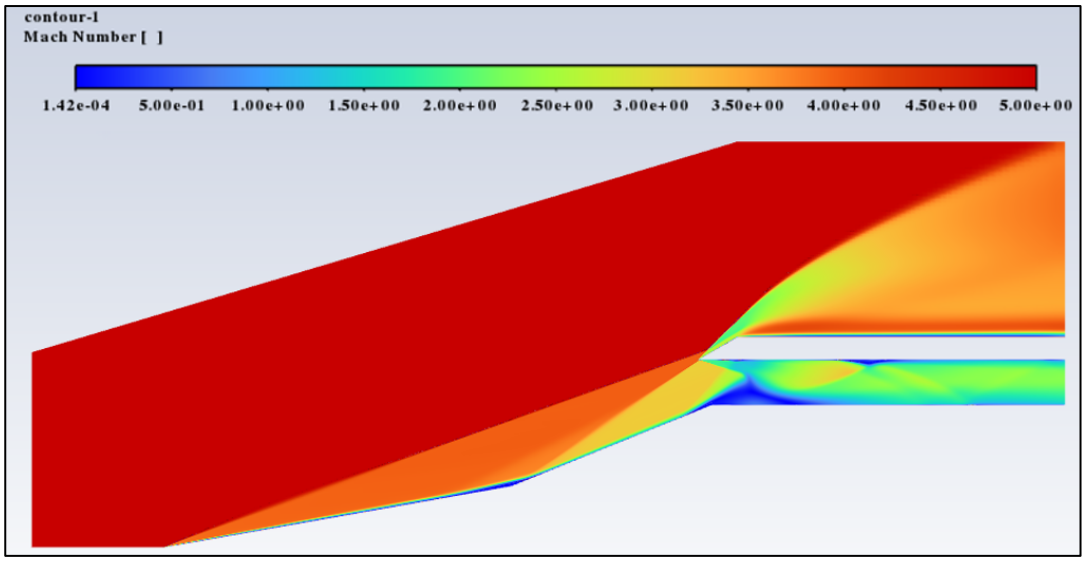

Figure 3.11. Mach Contour of Transition SST Model

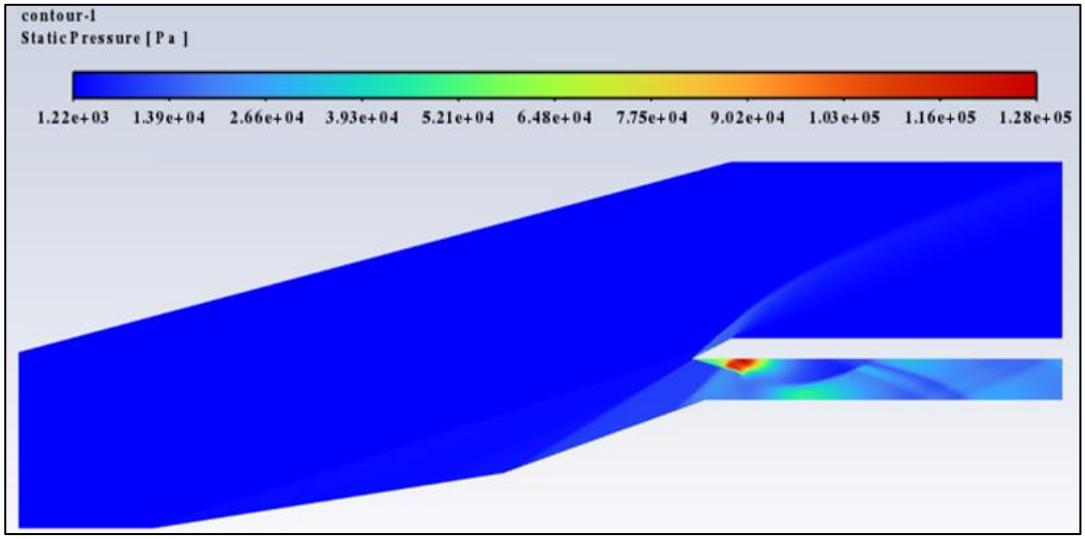

Figure 3.12. Static Pressure Contour of Transition SST Model

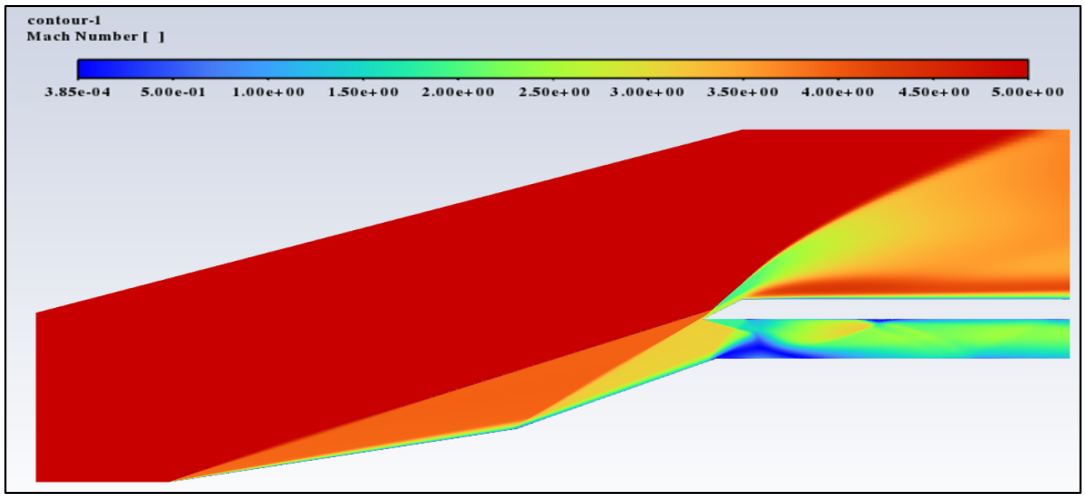

Figure 3.13. Mach Contour of SA Turbulence Model

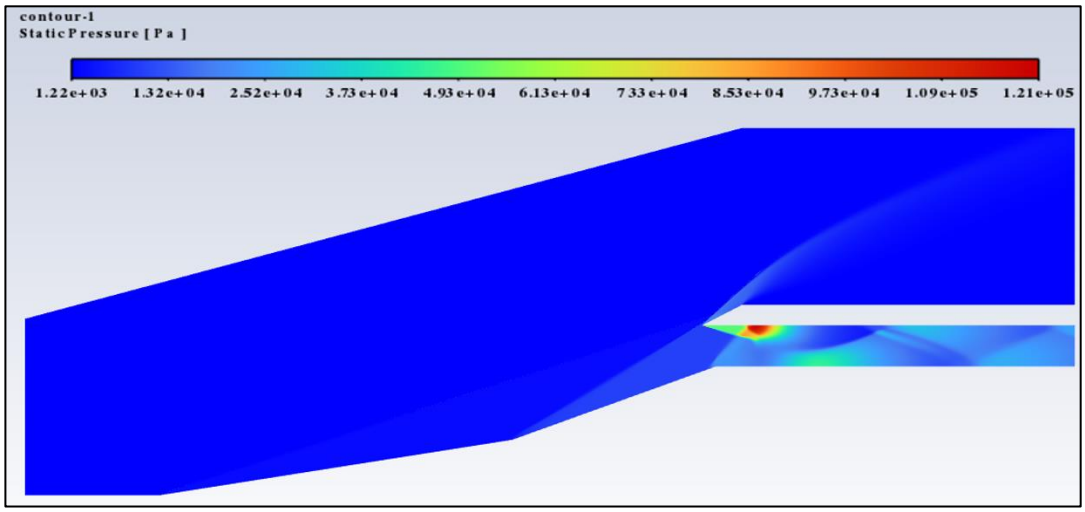

Figure 3.14. Static Pressure Contour of SA Turbulence Model

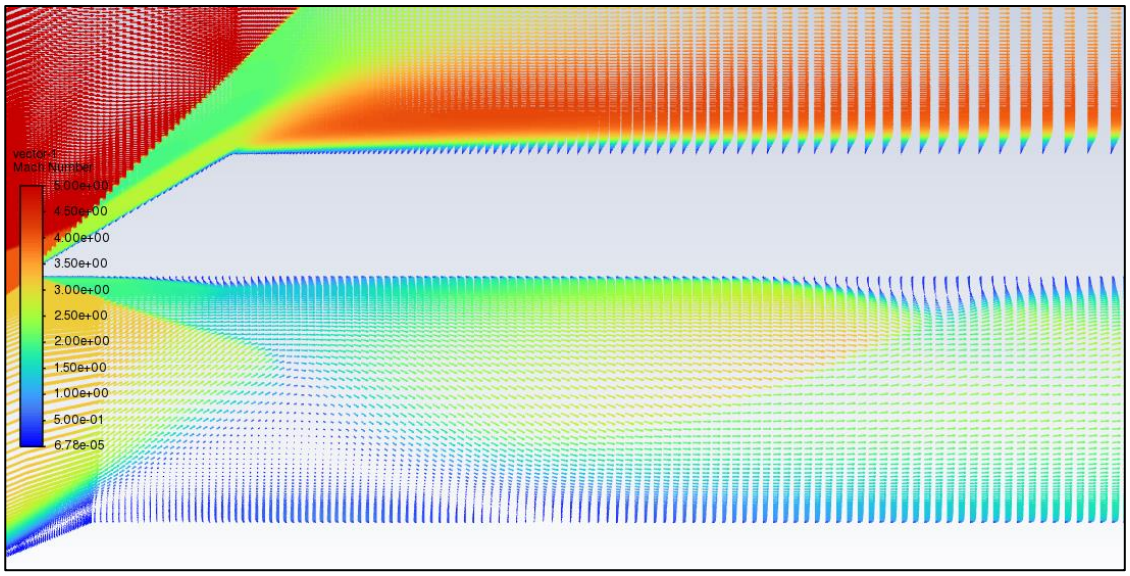

Figure 3.15. Velocity Vectors around Separation Regions

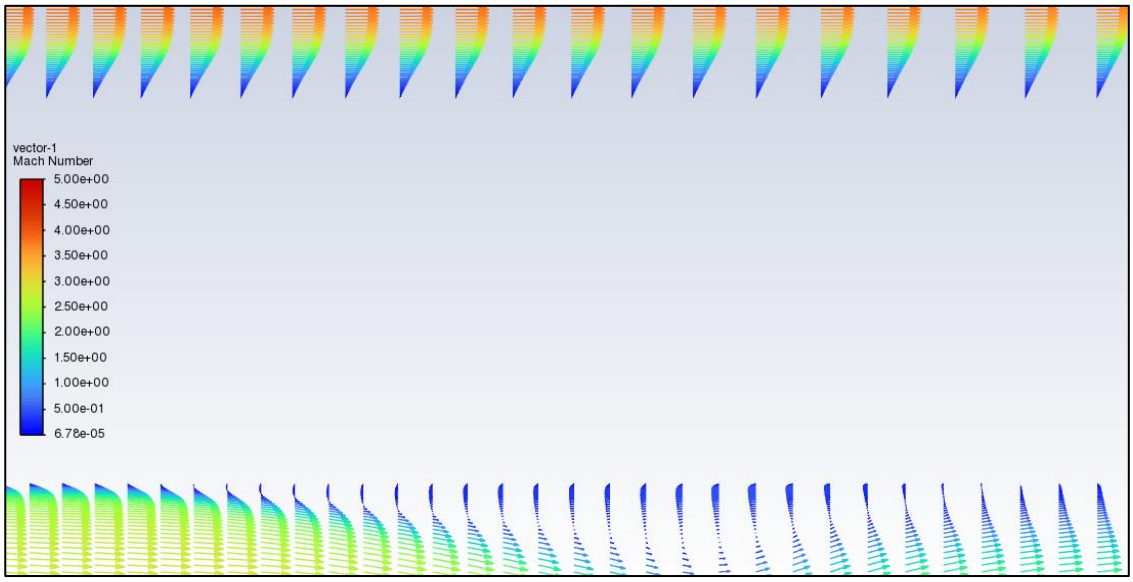

Figure 3.16. Zoomed Version of Velocity Vectors around 3rd Separation Bubble

CHAPTER 4

RESULTS FOR SCRAMJET INTAKE DESIGN

4.1 Scramjet Intake-Isolator Design Tool

Details of intake design tool is given in previous chapter. The code receives outputs and constraints and gives geometric outputs and thermodynamic outputs. Geometry is created by considering SoL and SoS conditions for the inviscid flow. The code gives everything about the geometry except for the cowl angle and cowl thickness, which are not the scope of design tool. In CFD part, these two geometric parameters are defined according to literature. Table 4.1, Table 4.2, and Table 4.3 summarizes design inputs and outputs.

Table 4.1. Design Inputs

Parameter	Design Value
Mach Number	7
Altitude [m]	27500
Freestream Static Temperature [K]	224.2
Freestream Static Pressure [Pa]	1711.8
Flight AoA [°]	0°
Stagnation Pressure [kPa]	702.7
Stagnation Temperature [K]	2427.5
Flight Dynamic Pressure [Pa]	58750
Number of Intake Ramps	2

Table 4.2. Geometric Outputs for CFD

Parameter	Design Value
Ramp 1 Angle [°]	6.43°
Ramp 2 Angle [°]	14.09°
Cowl Surface Length [mm]	1030.30
Intake Length [mm]	1488.7
Isolator Length [mm]	838.8
Intake Height [mm]	267.20
Isolator Height [mm]	32.81

Table 4.3. Performance Outputs of Design Tool

Parameter	Output
Intake Exit Mach	3.51
Intake Exit Pressure [Pa]	55160
Intake Exit Temperature [K]	699
Intake Exit Total Pressure [kPa]	1900
Isolator Exit (Burner Entry) Mach	2.65
Isolator Exit (Burner Entry) Pressure [Pa]	8789
Isolator Exit (Burner Entry) Temperature [K]	1005

Isolator Exit (Burner Entry) Axial Velocity [m/s]	1689
Total Pressure Recovery Factor at Intake Exit	0.606

Thermodynamic outputs confirms that initial constraints about the design are applied correctly because intake exit Mach, intake/isolator exit Mach ratio, isolator exit pressure and temperature values are within design limits as expected.

4.2 Scramjet Intake-Isolator CFD Simulations

After obtaining outputs from the MATLAB design tool, CFD methodology will be used for the checking these inviscid outputs to understand whether the tool is sufficiently accurate and beneficial for preliminary design. Since the tool can be considered fully inviscid until isolator, intake ramp regions and downstream regions of shocks can be compared by inviscid CFD and viscous CFD together. However, isolator calculations include skin friction effect and there are no fully inviscid formulations in theory, it is wise to compare this part with viscous CFD results. As it is mentioned in previous chapter, isolator flow dynamics is different than intake ramp region.

4.2.1.1 Geometry Generation for Scramjet Intake Design

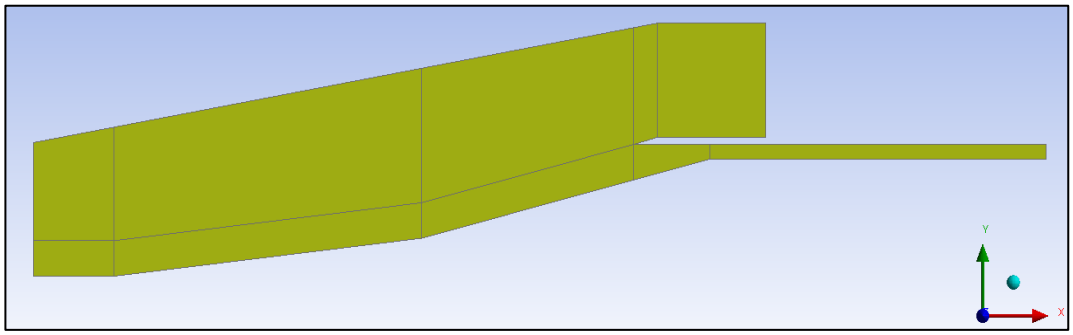

Figure 4.1. The Intake Model Created by Design Tool Results

The design tool creates the geometry considered pre-defined constraints. There are 2 intake ramps because this is the design decision of the author. Mach 7 flows are generally handled by 2 intake ramps in the literature and results of this thesis also confirm that. Detailed sizing information can be found in Table 4.2. It should be noted that the design tool gives ramp, cowl, and isolator surface. The region above the cowl is created for the development of the flow from pressure far field condition to pressure outlet condition so it is not a part of the tool.

4.2.1.2 Grid Generation for Scramjet Intake Design

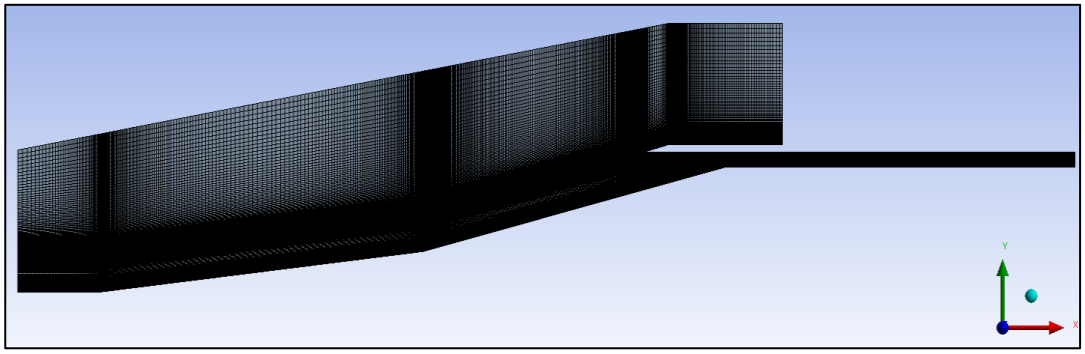

Figure 4.2. Grid Generation for Scramjet Intake Design

The grid is created by the same methodology, which is explained in validation case. However, validation case is a short experimental model with total length around 150 mm. Design point model is much longer with total length more than 2300 mm. For this reason, a scaling is followed.

The first layer thickness and minimum cell edge size are adopted. The first layer thickness is 1E-5 and maximum size is 4E-3 in the grid. According to these settings, the domain includes 292600 cells in total. Another adaptation is applied for the isolator region. Figure 4.3 demonstrates a detailed view of isolator mesh.

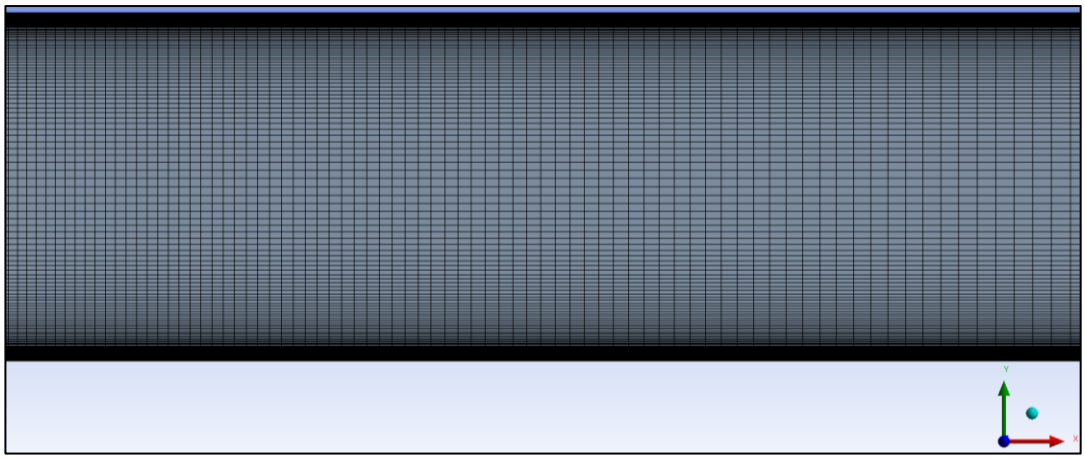

Figure 4.3. Zoomed View for the Boundary Layer Meshing

In the validation case, the isolator is short, and relatively less dense meshing is sufficient. In the present case, isolator is expected to have weak-shock train towards the exit and the flow should be resolved much better along whole isolator. Therefore, the intensity of isolator mesh is increased. All these arrangements satisfy the y+<1 requirement of boundary layer.

In the solution domain, boundary conditions are created as given in Figure 4.4. Symmetry BC along the first 200 mm is beneficial to obtained well-developed flow until ramp shock and to have stable iterations. For the inlet and top far field regions, pressure-far field BC is preferred. Walls have no-slip condition and constant temperatures of 300 K. Especially, no heat flux or adiabatic condition is not chosen because it affects the physical accuracy of the solution negatively. This is explained in the thesis of [10] and it will also be discussed in the parametric study of present thesis. Outlet conditions at isolator and top cowl are pressure outlet conditions.

Fluent solve the supersonic flow field using far field or inlet conditions so outlet BC does not drive the iteration. Free stream conditions are defined for the outlet. Intermittency, turbulence intensity and viscosity values are conservatively defined as %1, %0.5 and %1 respectively.

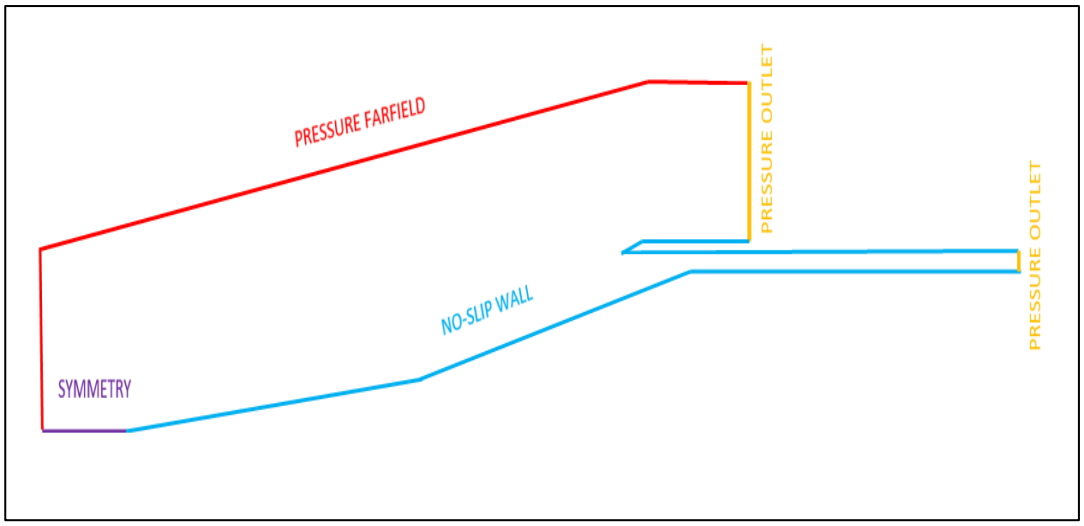

Figure 4.4. Boundary Conditions of the CFD Setup

4.2.1.3 CFD Results for Scramjet Intake Design

Settings of a solver is the most vital part of CFD methodology after obtaining a proper grid. The convergence speed, successful convergence to required criteria and solution accuracy depend on correct solver settings.

Solver is selected as steady DBNS solver for present study because ordinary approach for hypersonic flow regimes is DBNS solver. As a side note, [31] demonstrates that Fluent PBNS is also capable of solving high speed compressible flows such as Mach 6+ with the latest upgrades of the code. Readers of this thesis may consider this information if needed.

Turbulence model of present thesis is KW-SST with activated gamma-transport equation. Low-Re corrections or compressibility effects should be avoided because a training document of Fluent [43] does not suggest the use of them for such a flow.

Fluid material is air as ideal-gas and viscosity is calculated by Sutherland's Law with three coefficients. Solid material is standard aluminum. Reference values are calculated from far field.

Solution formulation is implicit, and flux type is AUSM. These selections are widely discussed in previous chapter. Spatial discretization setting for gradient is Green-Gauss Node Based. The ordinary and computationally less expensive option is Least Squared Cell Based, but the present choice is more accurate.

Flow, intermittency, TKE and specific dissipation rate schemes are 2nd order upwind. It should be noted that 1st order upwind for TKE is a sensible choice if convergence issues appear, then it may be switched to 2nd order upwind again.

Higher order term relaxation is beneficial because the present flow includes many shock waves, SBLI and very high flow speed. Such effects create issues to reach convergence and relaxation is required.

Courant number is kept at 0.5 for initial phase, then it is gradually increased to 2. More of this value such as 5 create stability issues. Theoretically, implicit formulation is unconditionally stable, but the choice of Courant number affects the stability significantly as suggested by [23].

As a side note for interested readers, if PBNS [31] will be used as an alternative, coupled Rhie-Chow: distance-based solver can be used as pseudo transient. Other settings can be kept the same. Starting with DBNS solver and continuing with PBNS can accelerate the solution speed.

In this section, settings of Fluent solver are given very detailed to guide future scramjet intake flow students. However, it should not be forgotten that versions of the software change with time and tuning of settings may be required in the future.

4.2.1.4 Inviscid Flow Results for Scramjet Intake Design

In this section, qualitative contour plots are presented to observe inviscid flow field in Figure 4.5, Figure 4.6 and Figure 4.7. Since there is no viscous effect from the walls, ramp shocks and cowl shock imping on corners. This fact confirms the SoL and SoS conditions of inviscid flow. At downstream of cowl shock (3rd shock), there is pure flow field and properties are carried all along the isolator.

Another finding is that static pressure contour demonstrates very weak reflection after shoulder. This is an acceptable state because a diamond precise SoS requires very detailed geometric design within a few mm margins, and cowl tip should be designed just for this purpose. Ultimately, the flow profile is uniform from isolator entrance towards exit as it should be.

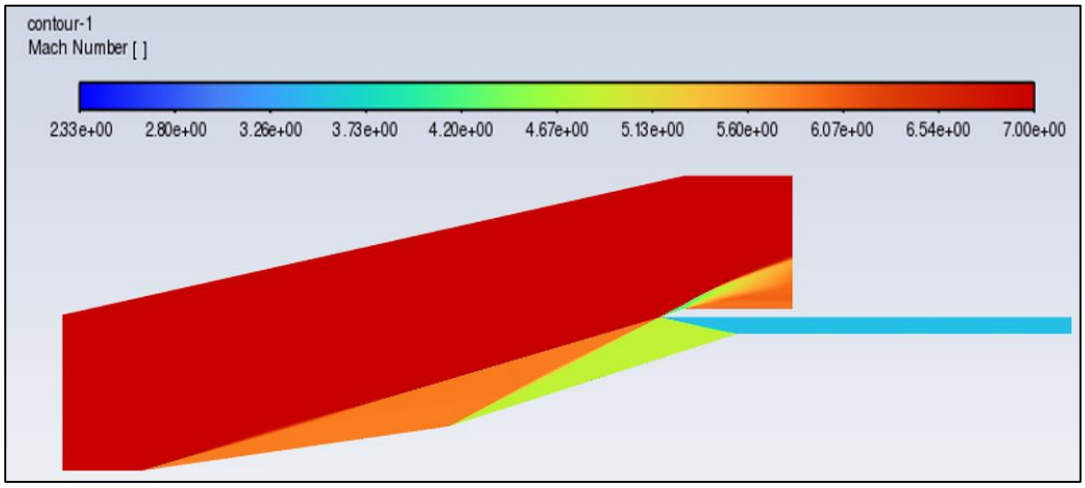

Figure 4.5. Mach Contour of Inviscid CFD Result

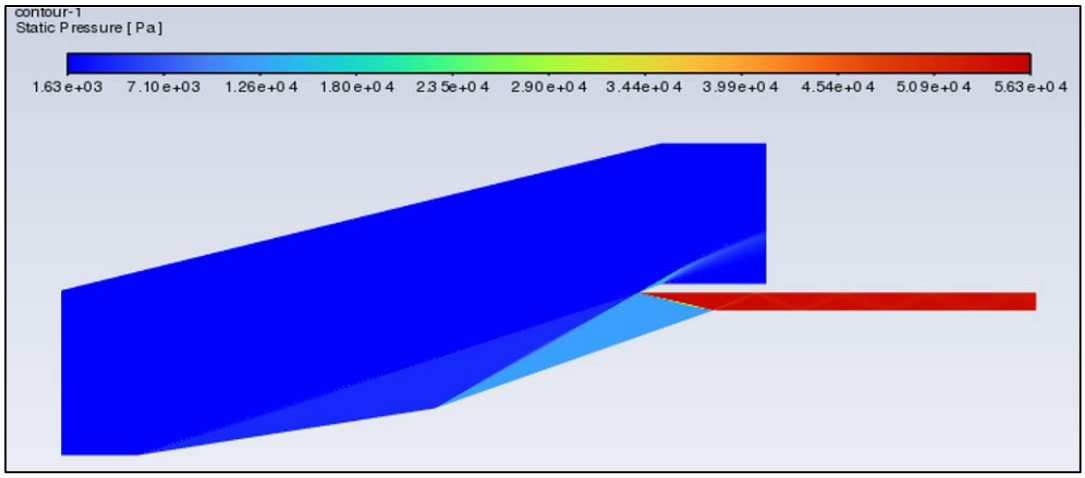

Figure 4.6. Static Pressure Contour of Inviscid CFD Result

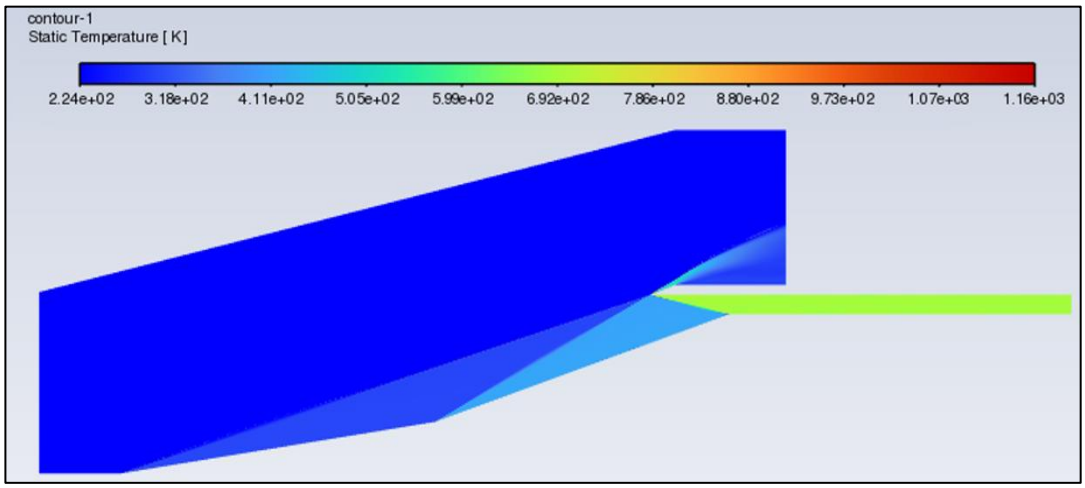

Figure 4.7. Static Temperature Contour of Inviscid CFD Result

Quantitative results about inviscid flow are given in comparison section. Readers should remind that design tool and inviscid CFD results are coupled until isolator exit. Design tool considers viscous effects and properties change along isolator. However, inviscid flow properties are naturally the same along the isolator.

4.2.1.5 Viscous Flow Results for Scramjet Intake Design

In this section, viscous CFD results of KW-SST turbulence model with gamma-transition option are presented in Figures from 4.8 to 4.15. Since viscous effects are in action now, zoomed views are added to observe separation regions and isolator regions.

Figure 4.9 indicates that there exists a separation bubble now around shoulder and shocks slightly deviate from the cowl tip. Observing these effects and how much they deviate viscous results from inviscid design tool are main scope of this thesis. Also, this bubble interacts with following weak shock waves in the isolator.

What this fact causes can be seen in Figure 4.10, Figure 4.11, Figure 4.12 and Figure 4.13. There is a high-pressure region around shoulder and thermal boundary layer signs high temperatures as much as 1680 K. These are the main differences from inviscid CFD.

Figure 4.12 and Figure 4.13 are presented to observe isolator flow field in details. Shock train is formed along isolator. However, this shock train can be considered as reflections of weak shocks other than a classical shock trains at low Mach numbers. They only draw a straight zigzag path. The model is designed such that the isolator is longer than average isolator deliberately because present thesis is also a numerical investigation study and longer isolator presents more opportunity to observe special flow field.

As it is mentioned in supersonic combustion requirements, values above 50 kPa are enough to ignite fuel-air mixture and burn it stable. Therefore, isolator length can be kept shorter depending on application. [22] also explains that L/H ratio of isolator design can be very large for real flight application. Here, the priority is validation of the design tool compared to viscous CFD results and results demonstrate that predictions of design tool is sufficiently accurate. Detailed numerical comparisons will be given in comparison section.

Figure 4.14 and 4.15 present velocity vector profiles around shoulder and the isolator exit. The adverse pressure gradients exist around shoulder bubble and velocity vectors mirror this situation as well. Calm and uniform flow profile exists around isolator exit so it can be said that isolator does its work well. The shape of vector profiles for both regions indicate that boundary layer is well-resolved.

Figures 4.16 and 4.17 demonstrate static pressure distributions along bottom wall surfaces of the geometry. There is a smooth jump from Ramp 1 to Ramp 2 while there is a sharp jump and decrease from Ramp 2 to bottom of isolator. The reason is SBLI, expansion fan and separation bubble interactions. Then, pressure fluctuations are getting weaker along isolator bottom surface as expected from an isolator. When isolator top surface is observed, there is a strong pressure rise at the entrance because the reflected shock from the shoulder impinges on this location. Then, this effect is getting weaker along surface as expected from an isolator.

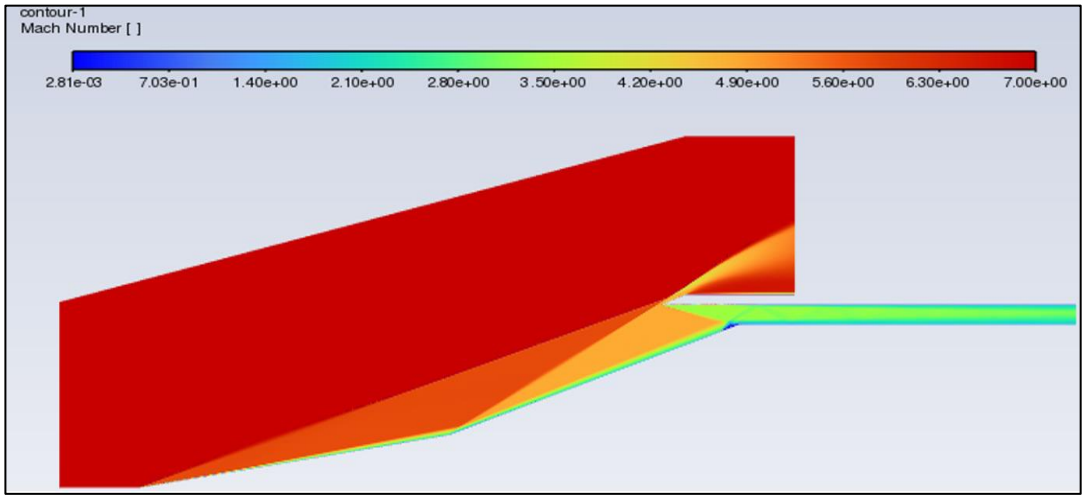

Figure 4.8. Mach Contour of Viscous CFD Result

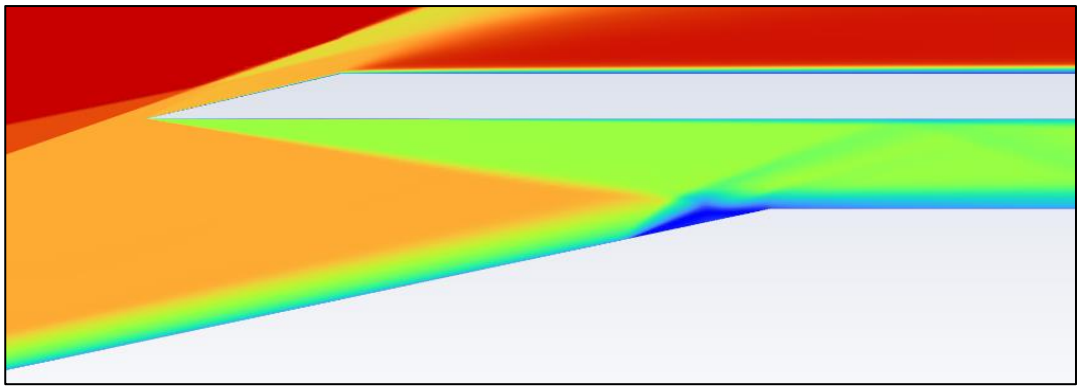

Figure 4.9. Zoomed View of Mach Contour around Shoulder Bubble

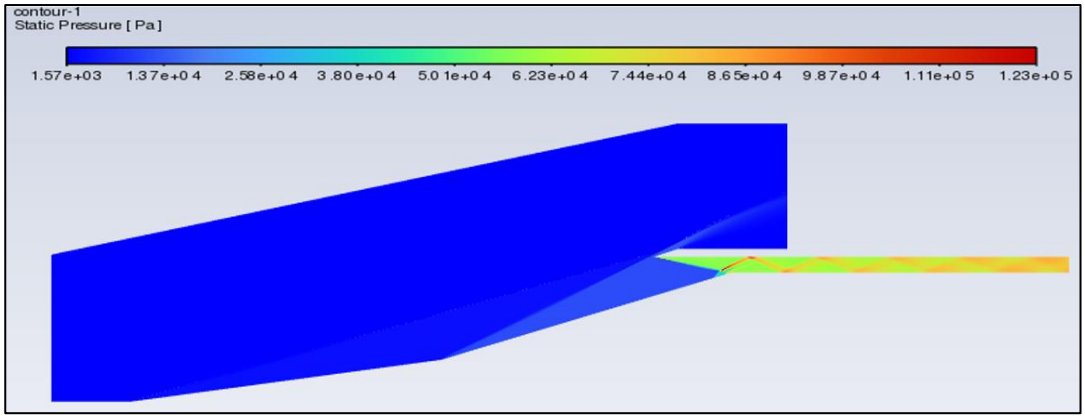

Figure 4.10. Static Pressure Contour of Viscous CFD Result

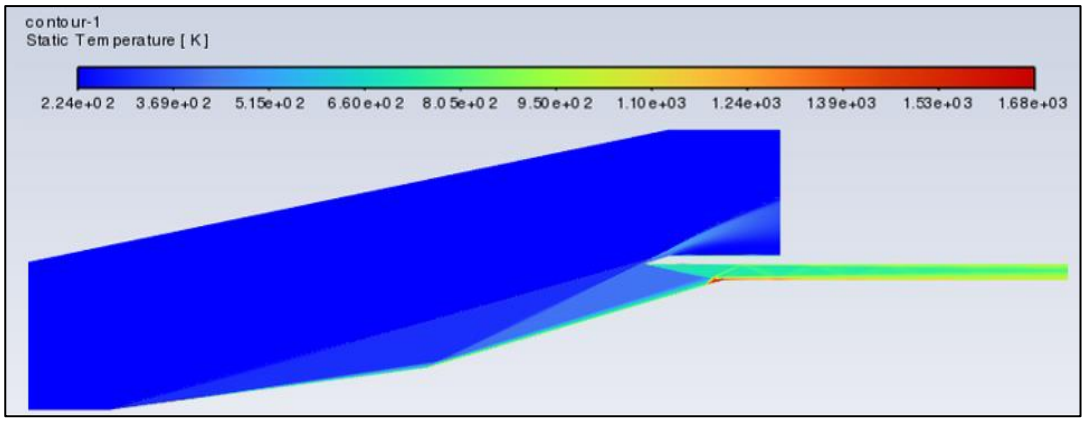

Figure 4.11. Static Temperature Contour of Viscous CFD Result

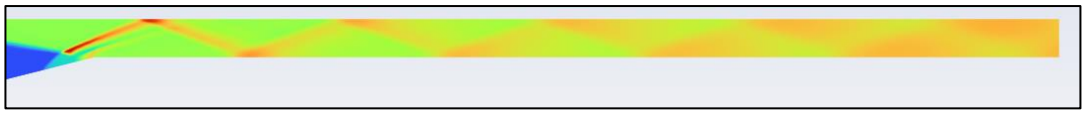

Figure 4.12. Zoomed View of Static Pressure Contour along the Isolator

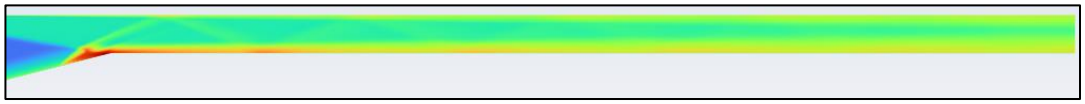

Figure 4.13. Zoomed View of Static Temperature Contour along the Isolator

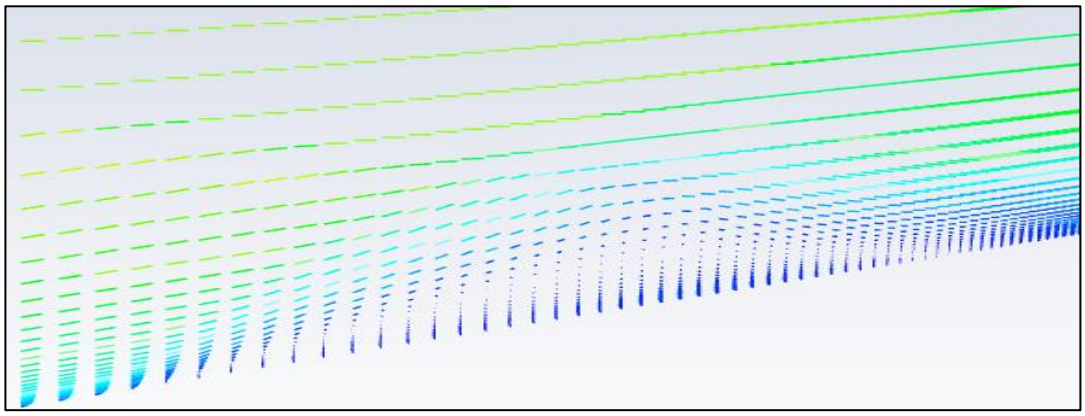

Figure 4.14. Zoomed View of Velocity Vector Profile around Shoulder Bubble

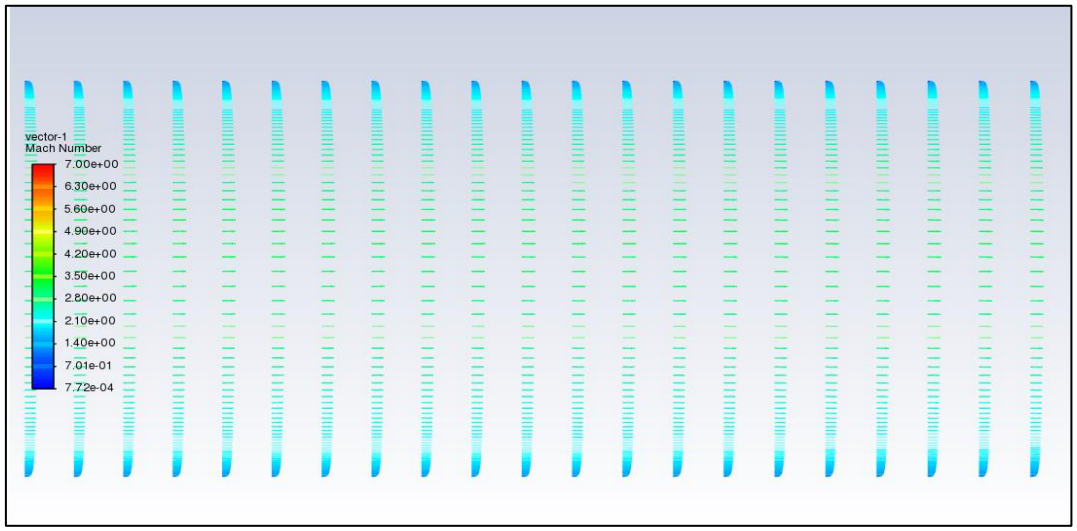

Figure 4.15. Zoomed View of Velocity Vector Profile towards Isolator Exit

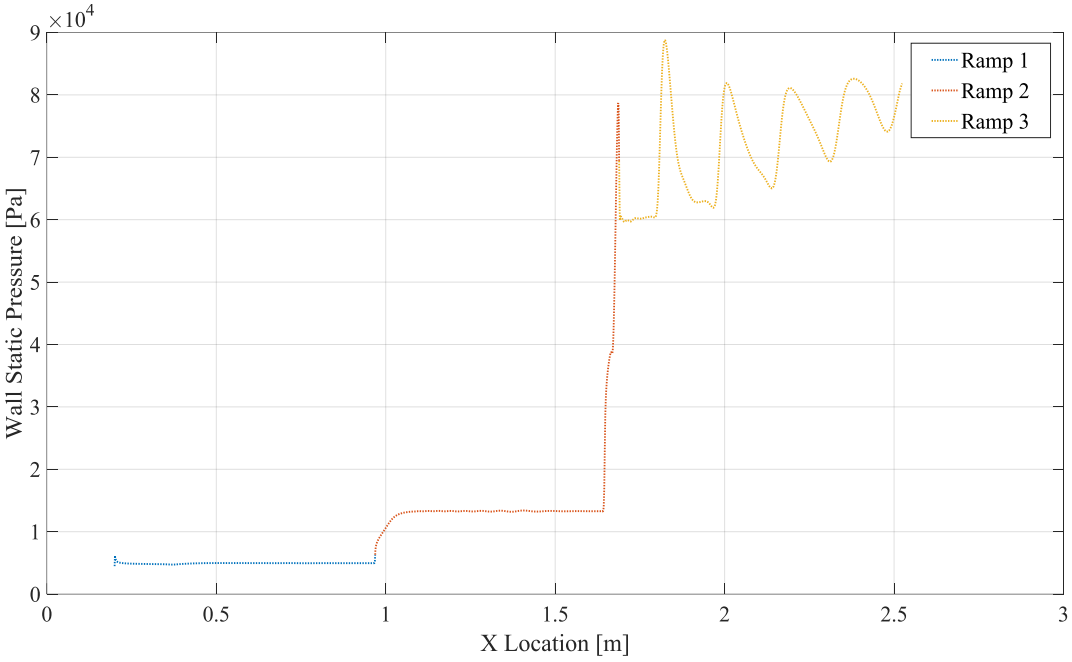

Figure 4.16. Static Wall Pressure Distribution from Ramp 1 to Isolator Exit

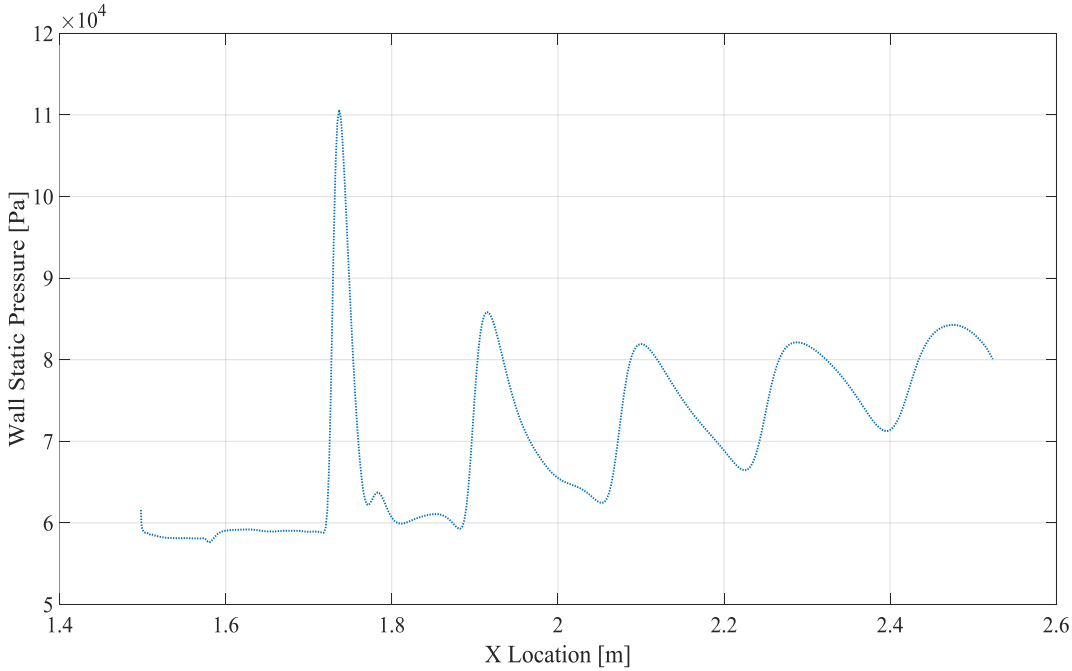

Figure 4.17. Static Wall Pressure Distribution along Top of Isolator Surface

4.3 Comparison of Results of Design Tool and CFD

After qualitative observations of contour plots, quantitative results are required for a scientific judgement. Firstly, the results until isolator will be investigated for the design tool, inviscid CFD and viscous CFD.

Table 4.4 compares **Mach numbers** for 3 different regions. Fluent gives a margin of calculated data for selected regions, and % of differences are calculated for average of these values. For all regions, design tool calculations and inviscid CFD predictions agree with a difference below %1. Design tool and viscous CFD predictions agree with a maximum difference of %1.3.

Table 4.4. Comparison of Mach Numbers Downstream Regions of Shocks

	Mach Number		
Methodology	After 1st Shock	After 2nd Shock	After 3rd Shock
Analytical (Design Tool)	5.8546	4.8547	3.5098
Inviscid CFD	5.8799	4.8670	3.5018
Viscous CFD	5.7774	4.8673	3.4671
% Difference 1-2	%0.43	%0.25	%0.23
% Difference 1-3	%1.33	%0.26	%1.22

Table 4.5 compares **static pressure** for 3 different regions. Again, average of Fluent data is used for comparisons. Differences between the tool and inviscid CFD are well below %1 and negligible. Differences between the tool and viscous CFD are acceptable below %6 up to maximum deviation.

Table 4.5. Comparison of Static Pressure Downstream Regions of Shocks

	Static Pressure [Pa]		
Methodology	After 1st Shock	After 2nd Shock	After 3rd Shock
Analytical (Design Tool)	4699.2	12901	55180
Inviscid CFD	4693.3	12837.3	55185.6
Viscous CFD	4711.1	13507.6	58747.1
% Difference 1-2	%0.13	%0.50	%0.01
% Difference 1-3	%0.25	%4.59	%6.26

Table 4.6 compares **static temperature** for 3 different regions. Again, average of Fluent data is used for comparisons. Differences between the tool and inviscid CFD are well below %1. Differences between the tool and viscous CFD are acceptable below %3.3 up to maximum deviation. As it will be discussed in the parametric analysis section, these results are a sign of the correct decision of constant wall temperature. If adiabatic wall BC is selected, such an agreement between methods would be impossible.

Table 4.7 compares **total pressure** for 3 different regions. Again, average of Fluent data is used for comparisons. Differences between the tool and inviscid CFD are below %2.54 up to maximum deviatition. Differences between the tool and viscous CFD are acceptable below %1.9 up to maximum deviation for the first two regions. However, 3rd region has %9.3 deviation. This difference can be expected because flow conditions significantly change after 3rd shock such as the appearance of small bubble around shoulder and SoL-SoS deviations compared to inviscid cases. Nevertheless, even this difference is less than expectations because viscous effects may create worse results such as flow blockage and unstart for bad designs. Contraction ratio of present design has some margin against such disturbances.

Table 4.6. Comparison of Static Temperature Downstream Regions of Shocks

	Static Temperature [K]		
Methodology	After 1st Shock	After 2nd Shock	After 3rd Shock
Analytical (Design Tool)	308.41	423.59	699.75
Inviscid CFD	308.55	421.25	694.96
Viscous CFD	318,84	420.92	712.07
% Difference 1-2	%0.04	%0.55	%0.68
% Difference 1-3	%3.33	%0.63	%1.74

Table 4.7. Comparison of Total Pressure Downstream Regions of Shocks

	Total Pressure [Pa]		
Methodology	After 1st Shock	After 2nd Shock	After 3rd Shock
Analytical (Design Tool)	6345600	5728700	4261600
Inviscid CFD	6507839	5839765	4303342
Viscous CFD	6320168	5820392	4678270
% Difference 1-2	%2.52	%1.92	%0.97
% Difference 1-3	%0.40	%1.59	%9.32

Numerical comparisons are made for the exit of intake until this point and overall agreement exists for different methods. Starting from this point, it is better to compare design tool with viscous results because theoretical formulation of isolator design and flow properties include skin friction coefficient depending on flow conditions such as turbulent Reynolds number. Furthermore, flow conditions along isolator change with horizontal location due to ODE formulation.

Here, the explanation is shortly given to remind but detailed explanation can be found in previous chapter. Already, inviscid flow with SoL and SoS carry the same properties from isolator entrance to exit so there is no need to follow inviscid results for isolator. Also, total pressure recovery factors at the intake exit for design tool and viscous CFD are 0.606 and 0.665, respectively. This factor can be thought as an indicator of performance or efficiency.

Figure 4.18, Figure 4.19, and Figure 20 are presented to investigate isolator exit flow profiles under inviscid or viscous flow conditions. These figures state that inviscid flow field is almost uniform because this is the result of SoL and SoS design constraints. Viscous flow field demonstrates a changing flow profile from walls to the centerline. X-axis of these figures are nondimensional, and it starts from the bottom wall of isolator to the top wall of isolator. It should be noted that static pressure and temperature are higher for viscous flow because of the shock train existence and weak shock waves. Therefore, exit Mach number is less than inviscid results. Figure 4.21, Figure 4.22 and Figure 4.23 demonstrate the difference of flow profiles between the entrance of isolator and exit. As expected, isolator entrance indicates a chaotic flow field due to SBLI and flow separation. Therefore, pressure fluctuates along vertical axis while isolator exit shows slight change around 80 kPa and profile is uniform enough. When temperature plot is considered, bottom wall of entrance is quite hot and chaotic due to the existence of SBLI and shoulder bubble. The exit temperature profile has an accepted change between walls. Wall temperature effects will be investigated in parametric study, but present result agrees with [10].

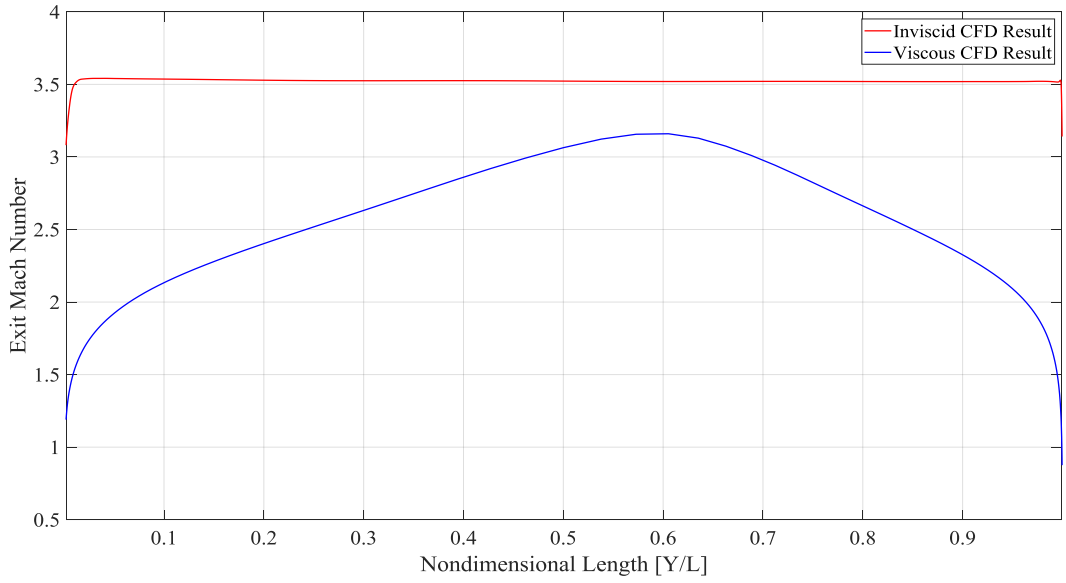

Figure 4.18. Comparison of Isolator Exit Mach Number Profiles along Isolator Y-Axis

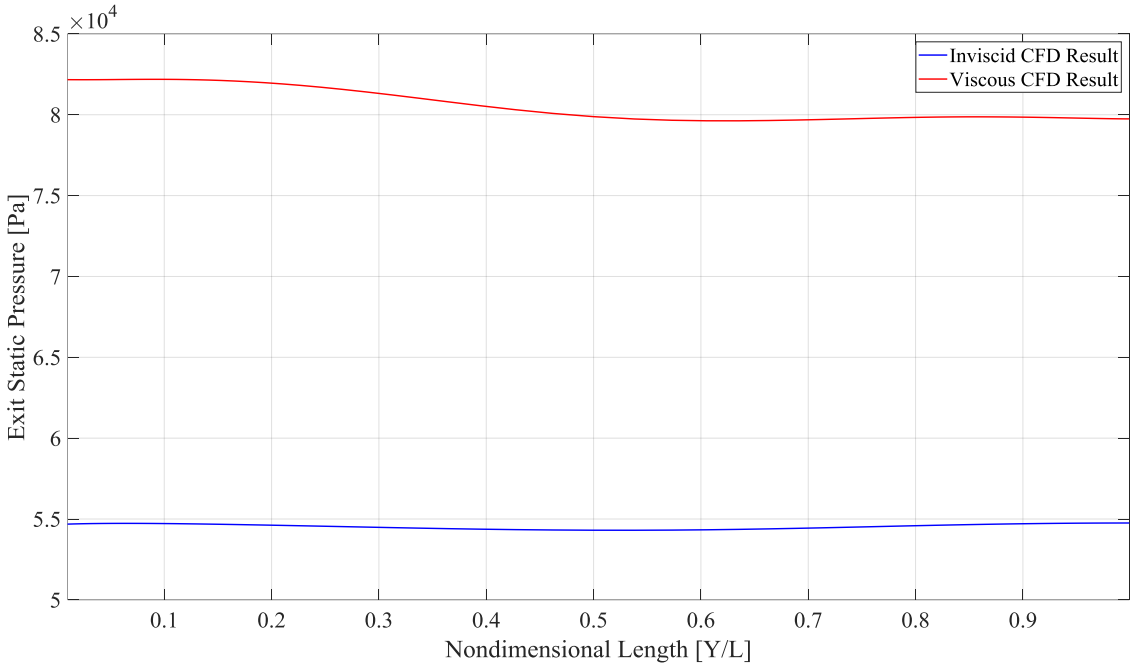

Figure 4.19. Comparison of Isolator Exit Static Pressure Profiles along Isolator Y-Axis

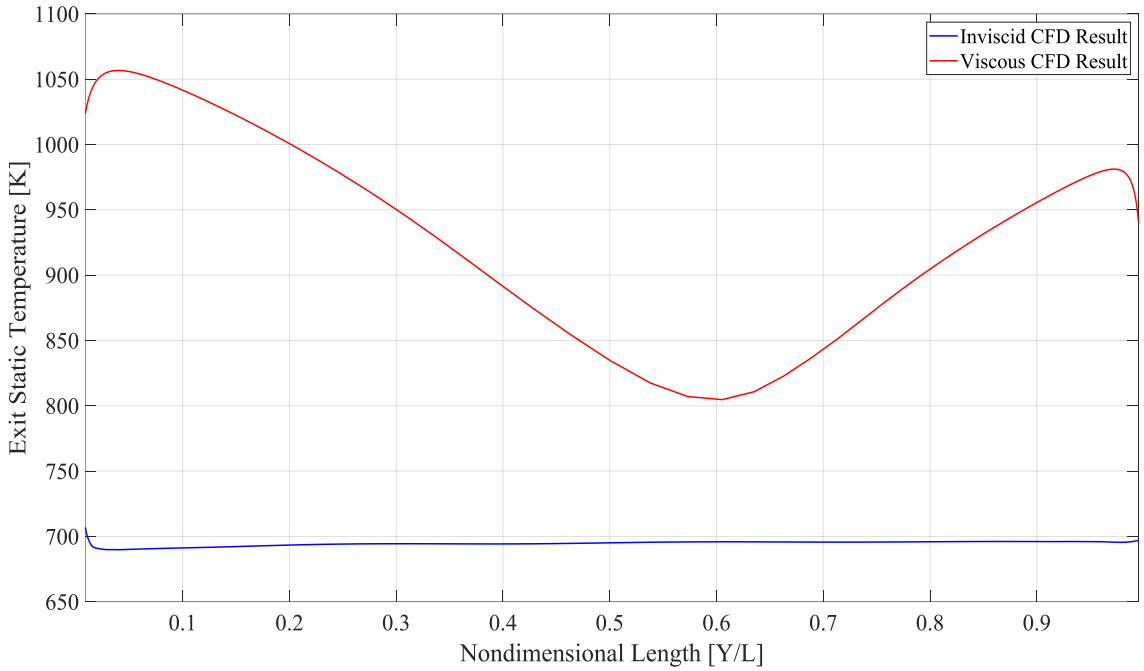

Figure 4.20. Comparison of Isolator Exit Static Temperature Profiles along Isolator Y-Axis

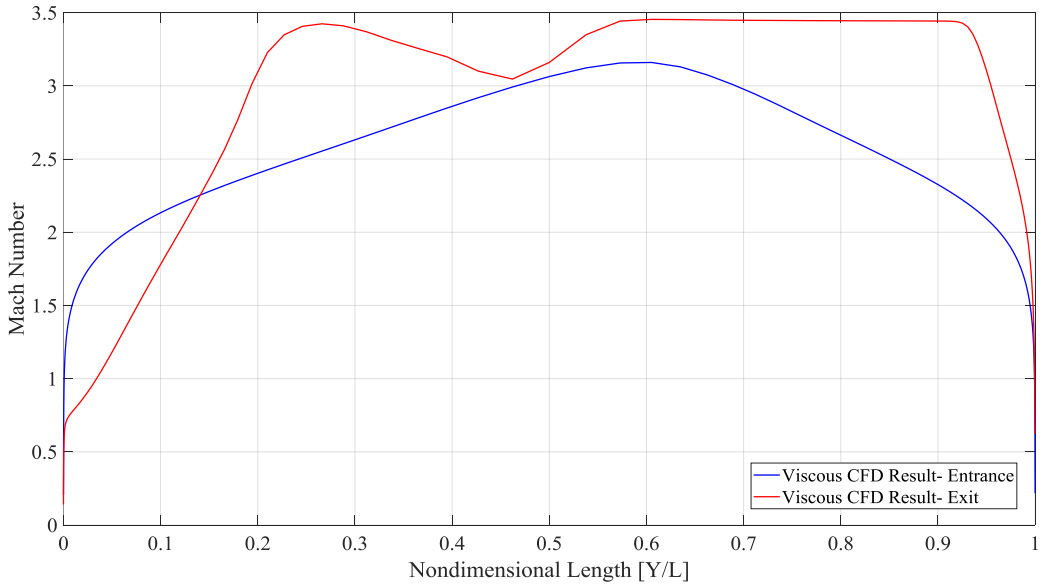

Figure 4.21. Comparison of Isolator Exit and Entrance Static Pressure Profiles along Isolator Y-Axis

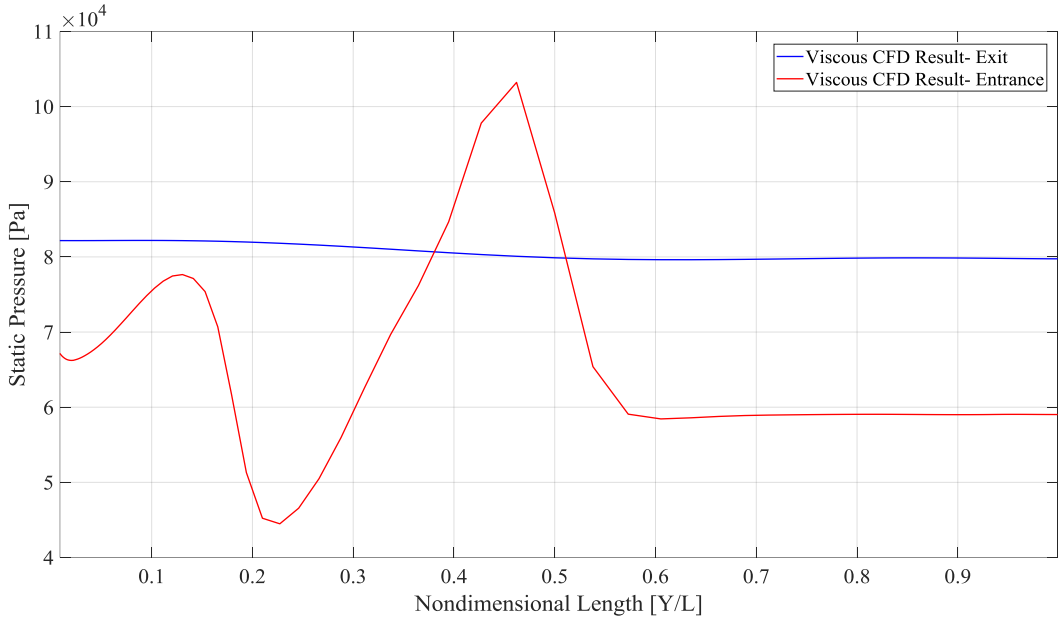

Figure 4.22. Comparison of Isolator Exit and Entrance Static Pressure Profiles along Isolator Y-Axis

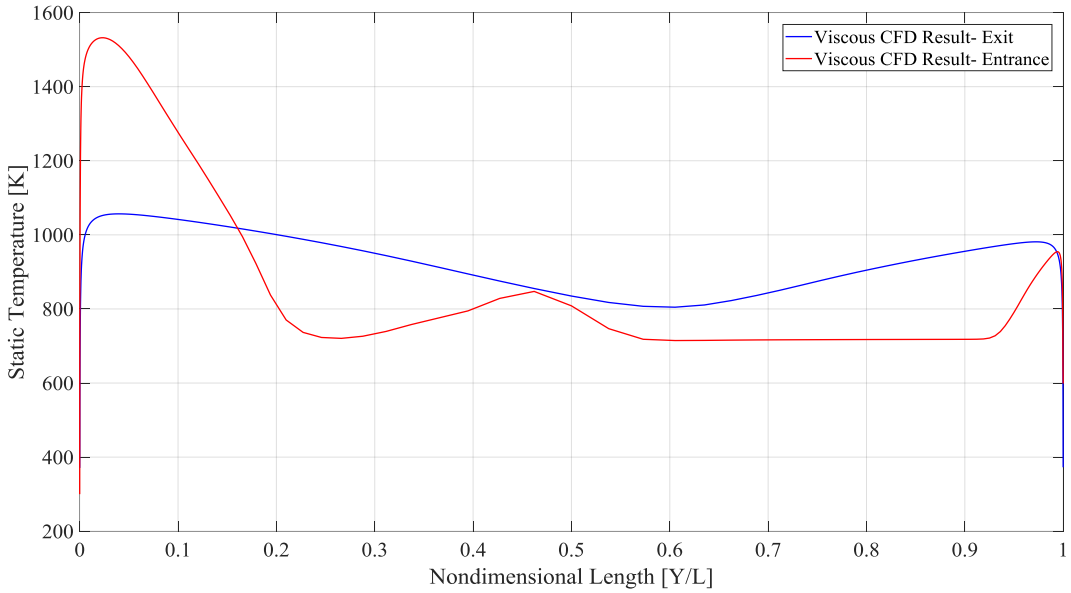

Figure 4.23. Comparison of Isolator Exit and Entrance Static Pressure Profiles along Isolator Y-Axis

Viscous isolator-exit flow profiles can be compared with design tool results by averaged data. Fluent can give many types of averaged flow properties along defined lines such as exit. In present thesis, widely used mass averaged properties are chosen for Mach number, static temperature, and total temperature. Area averaged properties are only used for pressure because area averaging is more suitable for pressure. Comparison and % of differences can be seen at Table 4.8. Results are better than expected because the nature of scramjet flows and especially isolator region still carry many uncertainities in theory, and even experimental measurements have uncertainity levels above %5 [25]. Considering these facts, all of parameters are below %10 difference and surprisingly Mach number is below %1 difference.

Table 4.8. Comparison of Isolator Exit Mass Averaged Values between Design Tool and Viscous CFD for Present Geometry

Parameter	Design Tool	Viscous CFD	% Difference
Mach Number	2.66	2.6796	%0.73
Static Pressure [Pa]	87125	80480	%9.20
Static Temperature [K]	1007	925	%8.86
Total Pressure [Pa]	1900674	1912000	%5.96
Total Temperature [K]	2427	2211	%9.77

Additional investigations to confirm the success of design tool can be made at different lengths of the geometry. To be more precisely, the design tool and isolator strategy depends on the length of the isolator and outputs can be taken from 500 mm or 300 mm. If the length of scramjet isolator is decreased and CFD is repeated for these lengths, design tool and CFD can be compared again. Ultimately, results should agree for different lengths so that design tool can be fully confirmed.

Table 4.9 and Table 4.10 compares analytical results and averaged viscous CFD results. Differences are below %6 at maximum deviation. One can observe such a trend that Mach number deviation decreases at the end of isolator while temperature and pressure deviation increase at the end of isolator. The reason of this trend is related to the formulation of the analytical method. Isolator's exit Mach number is a constraint as a function of isolator inlet Mach number and the best result occurs at the exit. However, temperature and pressure are related to viscous dynamics, which is natural to deviate from a simple analytical tool with distance. In other words, the best agreement occurs at the exit for Mach number while the worst agreement occurs at the entrance. The deviation does not extend %9.77 level at any place of domain.

Table 4.9. Comparison of Isolator Exit Mass Averaged Values between Design Tool and Viscous CFD for Isolator of 500 mm

Parameter	Design Tool	Viscous CFD	% Difference
Mach Number	2.9268	2.8481	%2.76
Static Pressure [Pa]	74951	74809.55	%0.02
Static Temperature [K]	894	872.13	%2.52

Table 4.10. Comparison of Isolator Exit Mass Averaged Values between Design Tool and Viscous CFD for Isolator of 300 mm

Parameter	Design Tool	Viscous CFD	% Difference
Mach Number	3.1388	2.9688	%5.72
Static Pressure [Pa]	66822	70983.03	%.6.20
Static Temperature [K]	817	844.72	%3.32

This additional investigation proves that the agreement of design tool and CFD results. Isolator can be shorter or longer, but ODE solution of the tool keeps accuracy with an acceptable margin. Moreover, the reason of choosing longer isolator for the design was numerical investigation of shock train properly. Otherwise, shorter isolators also provide necessary exit conditions for proper combustion with a pressure well over 50 kPa, but static temperature should also be considered.

CHAPTER 5

RESULTS FOR PARAMETRIC ANALYSIS

In this chapter, the purpose is investigation of off-design conditions of present design. It is known that scramjet powered hypersonic vehicles generally have a narrow operational band. Also, engine components should be adjusted using the geometry or special techniques. For a preliminary study, it is beneficial to investigate off-design flight Mach numbers, flight altitude, different wall temperature conditions and AoA.

5.1 Off-Design Flight Conditions

5.1.1 Mach Number Effects

Off-design flight conditions mean lower-higher flight Mach numbers and lower-higher flight altitudes. Since design is directly related to SoL and SoS conditions for present design, off-design conditions vanish them as expected. Higher flight Mach number flow pushes shock waves inside the isolator and shock waves impinge on cowl wall surfaces away from tip. Lower Mach number flow has a big spillage over the cowl and shock waves do not impinge on tip.

Figure 5.1 and 5.2 present the contour plot of Mach 8.25 flow. This speed is over the design point and SoL condition is disturbed as expected. Since the shock is stronger due to Mach number, there is a slight separation on the upper isolator surface.

It also increases the structural and thermal loads on this small impingement area. However, the intake still works and there is no fatal result as long as combustion dynamics is suitable for such a flow.

Figure 5.3 and Figure 5.4 presents contour plot of Mach 5.75, which is below the design point. This time SoL condition is disturbed towards the upstream of cowl lip. There is a flow spillage over the cowl lip. Such a flow situation is more related to engine start-unstart other than additional loads of higher Mach numbers.

Since Mach 5.75 does not create a fatal result, Mach 4.50 is tried. After some iterations, isolator flow starts to come back, and the isolator flow is totally disturbed. Such a flow causes the formation of a very big bubble around shoulder and two other separations at upper wall surface. Ultimately, all these bubbles and SBLI cause divergence and intake can no longer operate under these conditions.

It should be noted that Figure 5.5 and Figure 5.6 are captured just to illustrate the situation of extreme off-design condition. At the end of iterations, the flow would probably be corrupt. Such unstarted flows should be investigated using unsteady RANS simulations other steady RANS. URANS is not the scope of this study.

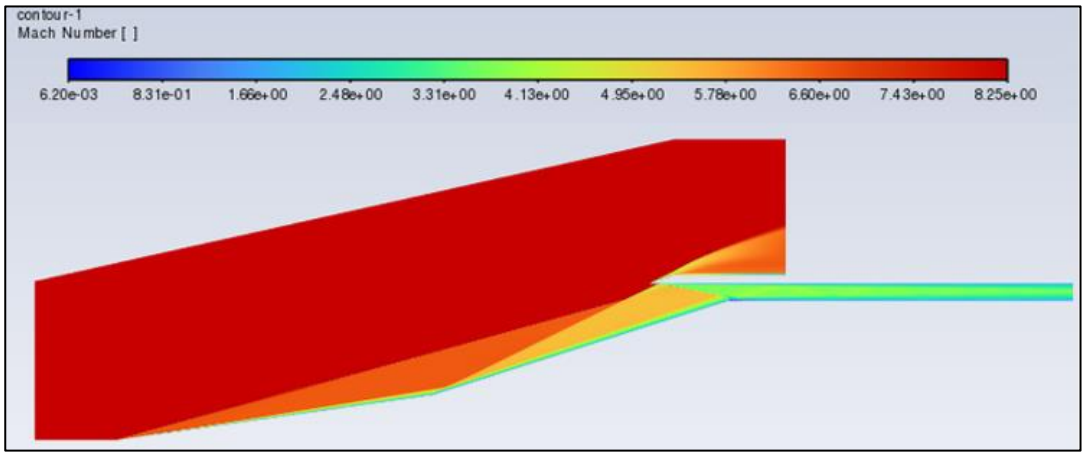

Figure 5.1. Off-Design Mach Contour of M=8.25

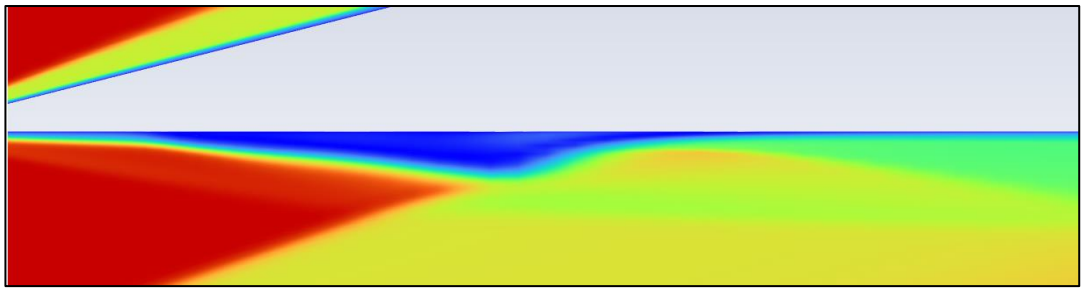

Figure 5.2. Zoomed View for Cowl Separation at M=8.25

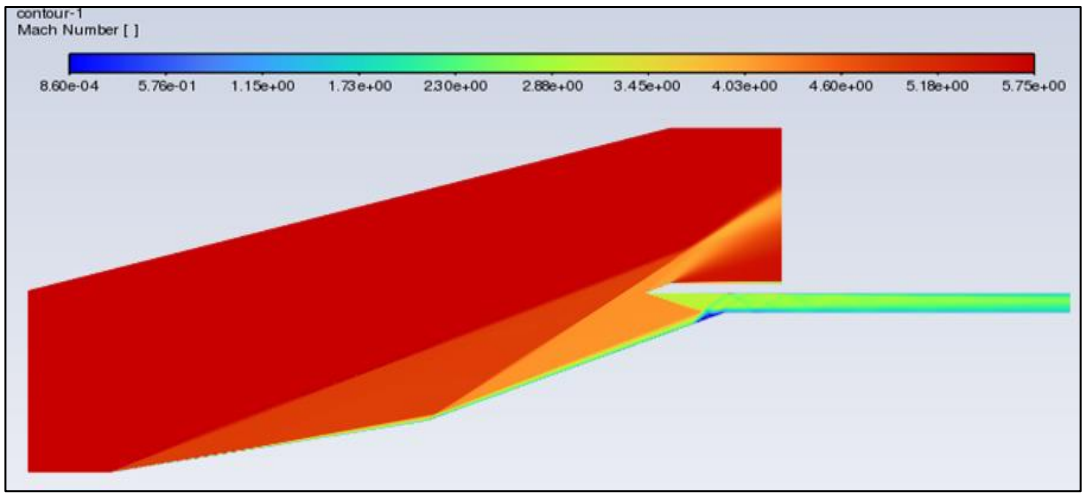

Figure 5.3. Off-Design Mach Contour of M=5.75

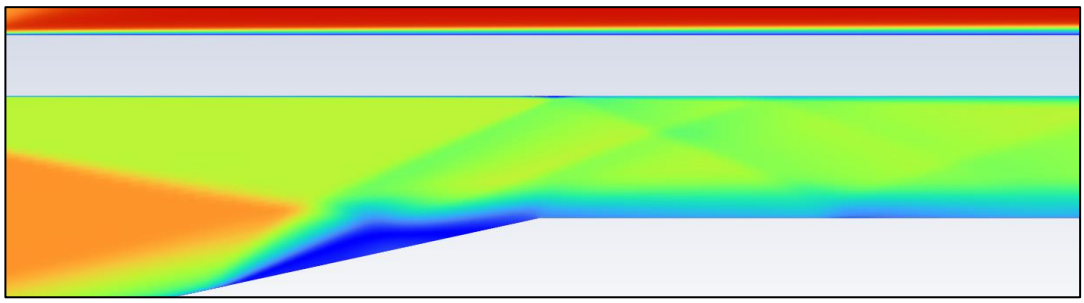

Figure 5.4. Zoomed View for Flow State around Shoulder at M=5.75

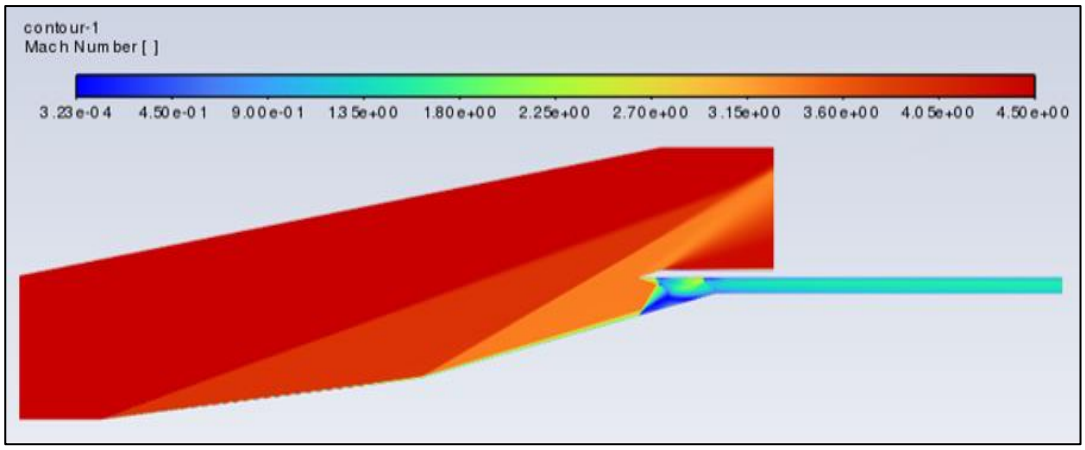

Figure 5.5. Off-Design Disturbed Mach Contour of M=4.5

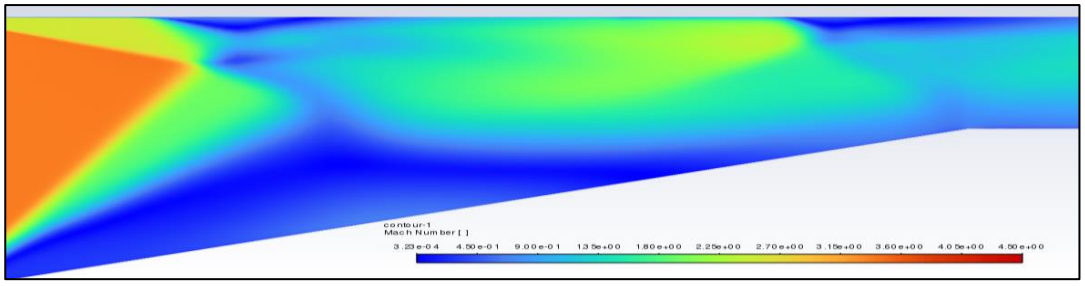

Figure 5.6. Zoomed View for Cowl-Shoulder Region at M=4.5

5.1.2 Flight Altitude Effects

The next evaluation about flight corridor is the altitude. The base design is developed for 27500 m. This point is near the lower bound of design box given in Figure 5.7. Therefore, 33500 m near the upper bound of the design box for Mach 7 is investigated. The lower bound generally means structural limits and upper bound means combustor blowout limit. Flight altitude has a significant impact on pressure other than temperature because even 500 m changes the static temperature quite a lot.

Figure 5.7, Figure 5.8 and Figure 5.9 present how the change of flight altitude for Mach 7 affects the isolator exit conditions. There is no remarkable change on exit Mach number other than slight decrease. However, there is a moderate increase at exit static temperature and striking decrease on exit static pressure. This is an expected result because even little changes on flight altitude changes freestream pressure quite a lot. This result indicates that off-design flight altitude limits should be arranged carefully not to have any issue on stable combustion.

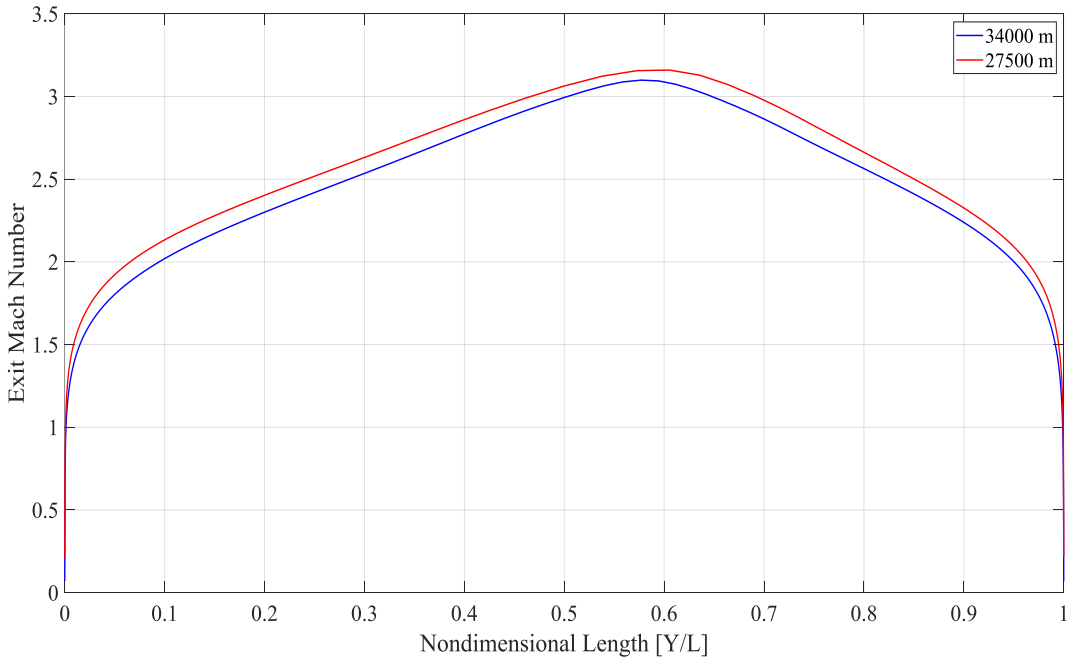

Figure 5.7. Effect of Flight Altitudes on Isolator Exit Mach Number

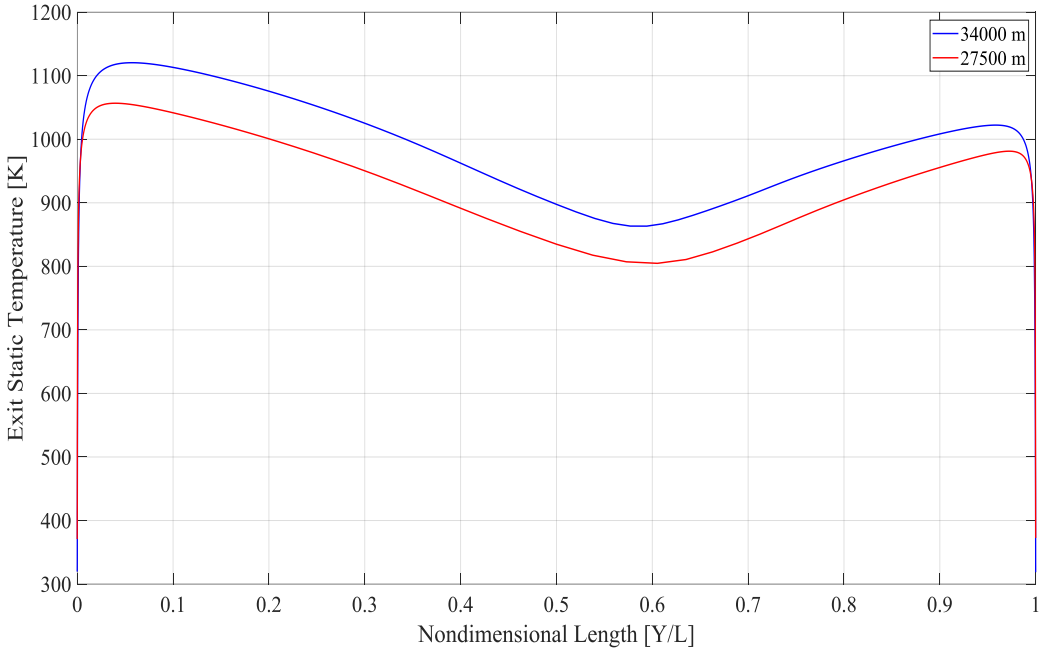

Figure 5.8. Effect of Flight Altitudes on Isolator Exit Static Temperature

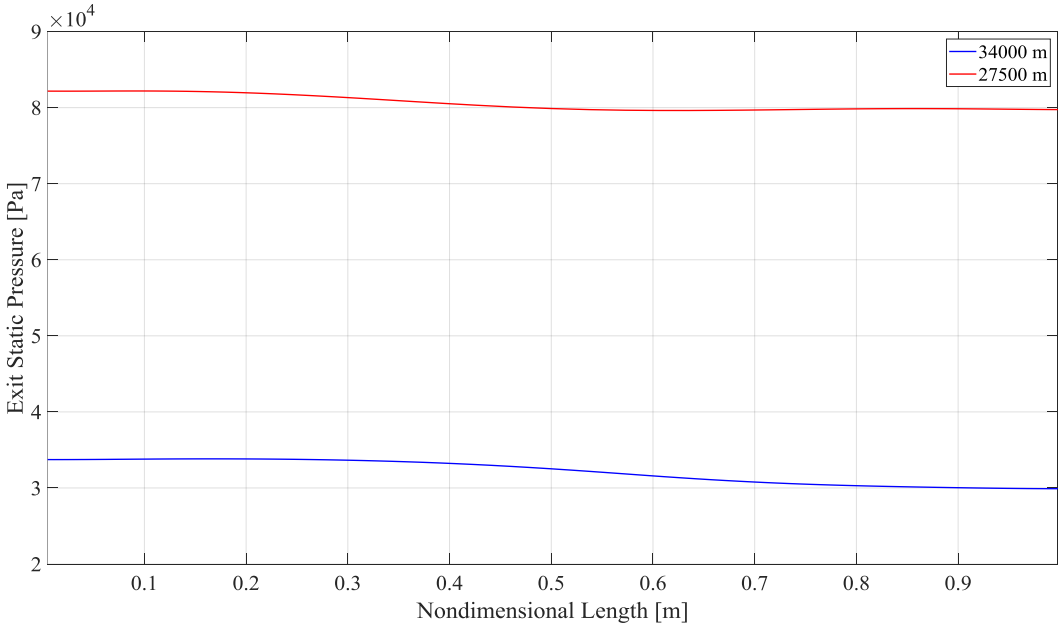

Figure 5.9. Effect of Flight Altitudes on Isolator Exit Static Pressure

5.1.3 Wall Temperature Effects

It is beneficial to investigate the effect of wall thermal conditions on the solution because much research on this field parametrically observes these effects. Firstly, applying adiabatic wall BC is investigated because results given by [10] indicate negative effects on the solution. Similarly, present results agree to that finding. Adiabatic wall BC causes extremely high temperatures up to 2000-2500 K next to surface and this is not sensible physically as discussed by [10]. Trends for 300 K and 750 K are consistent and physically sensible. Wall temperature for 750 K condition reaches temperatures around 1250 K at exit while 300 K condition reaches around 1050 K. This situation naturally affects averaged exit conditions, and the comparison is given in Table 5.1 and Figure 5.10.

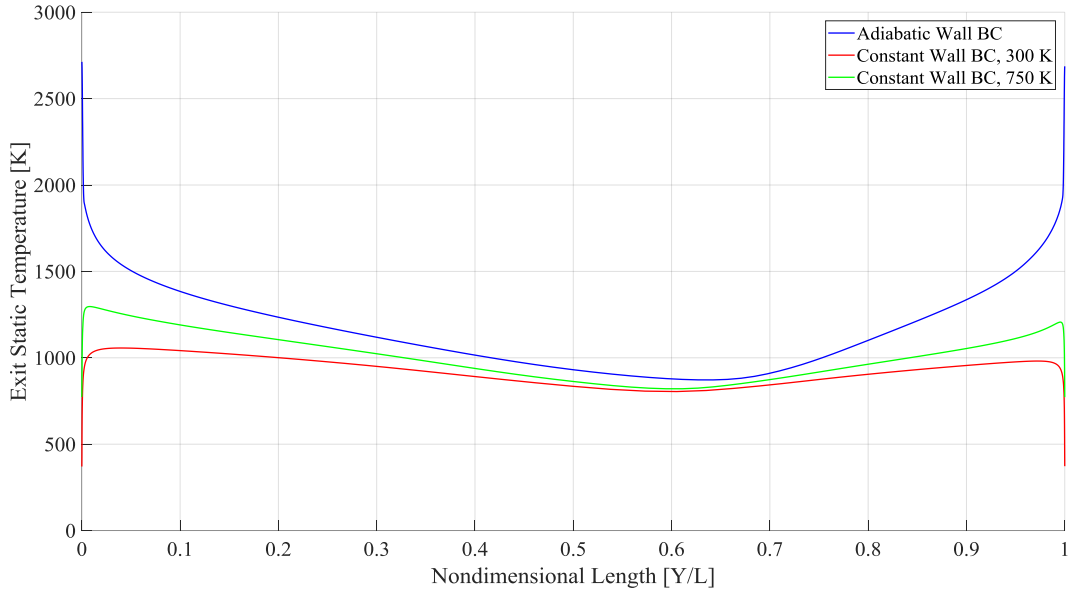

Figure 5.10. Effect of Different Wall Thermal Conditions on Isolator Exit Temperature Profile

Table 5.1. Comparison of Wall Temperatures for Isolator Entrance and Exit

Parameter	300 K-Isolator Entrance	750 K-Isolator Entrance	300 K-Isolator Exit	750 K-Isolator Exit	Adiabatic Wall-Isolator Entrance	Adiabatic Wall-Isolator Exit
Exit Mach Number (Averaged)	3.1542	3.1386	2.6604	2.6201	3.0786	2.5196
Exit Static Temperature (Averaged)	805.43	821.80	925.03	976.03	858.62	1084.27

5.1.4 AoA Effects

Airbreathing hypersonic vehicles and scramjet engines have limited AoA margin during flights. It is generally preferrable to have small AoA values and to keep the vehicle under straight path because of air capture, shock dynamics and start-unstart issues. Therefore, AoA parametric study is conducted using 2° and 4°. The margin is like the validation experiment of present thesis. [25]

Table 5.2. Isolator Exit Averaged Properties of AoA=2° Flow

Parameter	Exit Mach Number (Averaged)	Exit Static Pressure [Pa] (Averaged)	Exit Static Temperature [Pa] (Averaged)	Exit Total Pressure [Pa] (Averaged)
AoA= 2°	2.52	99303.46	969.05	1867272
AoA= 4°	2.36	120326.04	1034.74	1759539

As it can be seen from Table 5.2, increasing AoA causes higher temperature and pressure values at exit while Mach number is lower. This is an expected result, and it agrees with [25] although intake geometries are different.

The vital point here is that a designer should consider overall effects of such changes on the performance and constraint. The peak temperature of 1726 K on the domain is captured around the shoulder separation bubble. This temperature is not over the material limits, but it can affect weight, bleeding, or cooling systems of the vehicle. Also, increasing AoA causes higher wall static pressure around the impingement location of shoulder reflected shock wave. This is another consideration for structural limits. Since it is assumed to be in preliminary design phase, these are just initial investigations. Figure 5.11, Figure 5.12 and Figure 5.13 demonstrate how change of AoA influences isolator exit profiles other than averaged values. AoA increase has a decreasing effect on Mach number, while temperature and pressure work in opposite direction. These profiles are consistent with averaged values. However, it should be noted that there is a different effect on exit temperature at AoA=4°. While bottom wall pressure is higher than upper wall for AoA=0° and 2°, it is the opposite for 4°. The reason is caused by the direction of reflected shock waves along isolator.

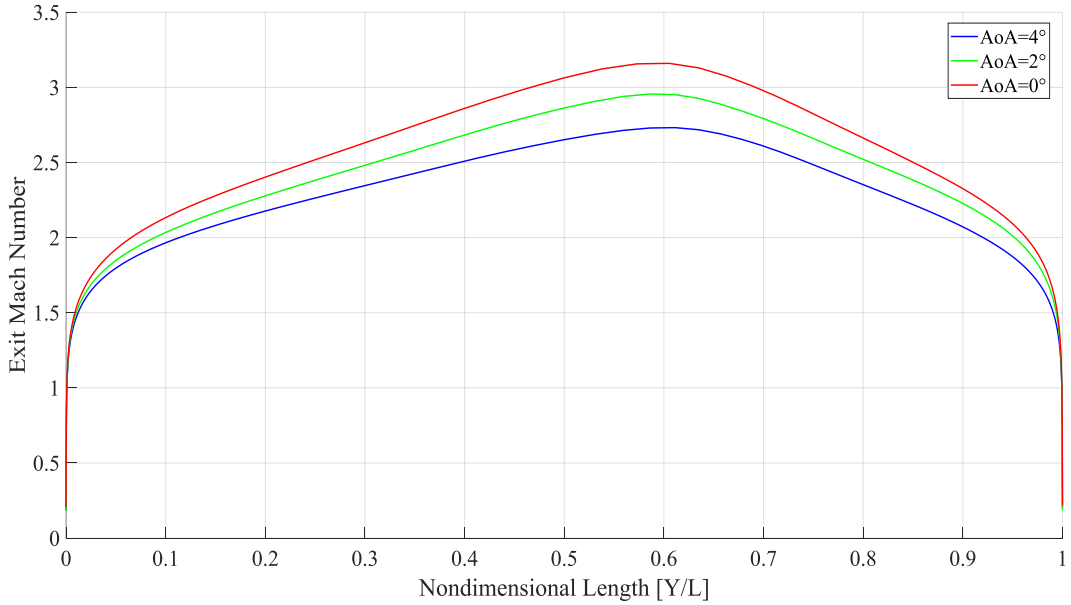

Figure 5.11. Comparison of Exit Mach Number Profiles for Different AoAs

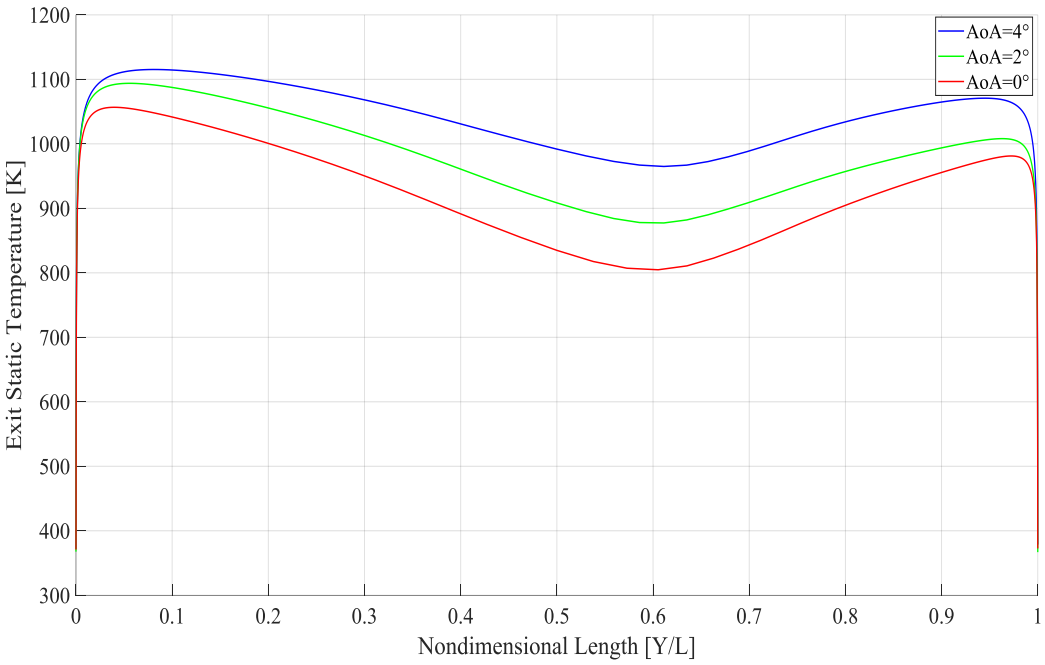

Figure 5.12. Comparison of Exit Static Temperature Profiles for Different AoAs

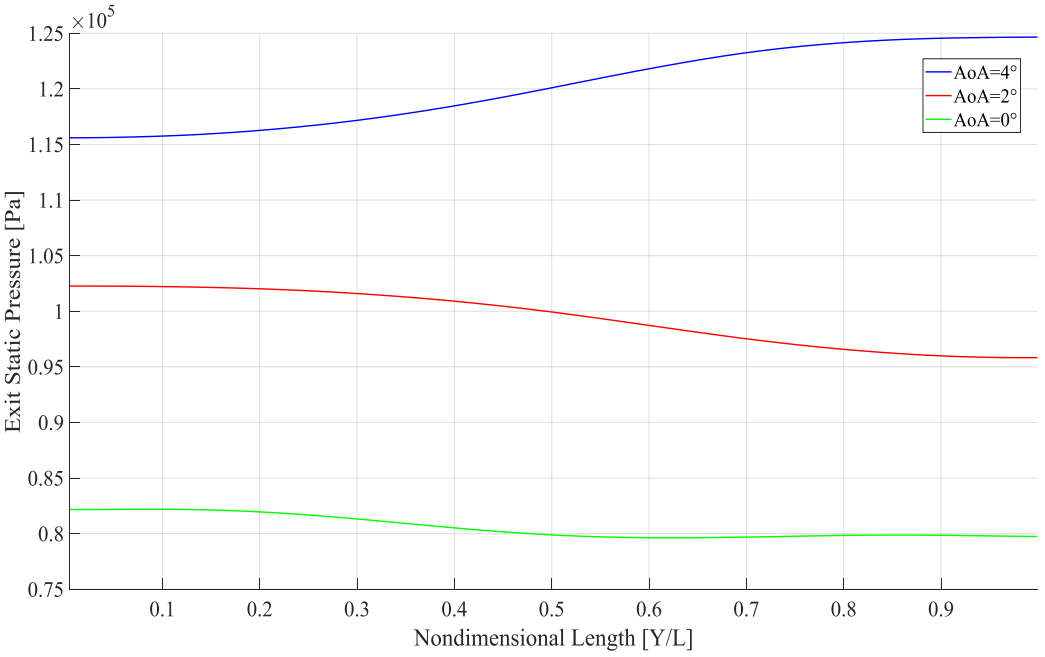

Figure 5.13. Comparison of Exit Static Pressure Profiles for Different

CHAPTER 6

CONCLUSIONS

6.1 Conclusion on Present Thesis

In this thesis, the design and analysis of hypersonic intake are studied. Since the topic includes many connected details on aerodynamics and propulsion fields, an intense literature survey is conducted. A design tool is created to obtain a scramjet intake geometry with two ramps and isolator. The design tool follows the oblique shock wave formulations and TBM relations for the intake part. Although the idea is simple, these relations can create required geometries with SoL and SoS conditions under inviscid flow assumption. In addition to intake ramp geometries, another set of relations and ODE set are used to create isolator geometry. The whole geometry and resultant flow properties at stations follow the pre-defined constraints and rules. Then, the design tool is coupled with CFD metholody and compared with each other. During the present thesis, MATLAB is used for analytical processes and ANSYS Fluent is used for CFD processes.

Before further studies are conducted, the CFD metholody is validated using an experiment whose results are published as open-source. The mesh independence study with 5 different grids is performed to have grid-independent solutions. Satisfying the mesh indepence, turbulence model study is performed to reach closer results compared to experiment. Also, settings of CFD solver is tuned for current studies in this step.

In the analytical study, a design point with its justifications is defined. Flight corridor inputs and aerodynamic constraints are given to the inviscid design tool. Geomtetry of the model and thermodynamic properties are taken in return. Frictional effects are included in the isolator formulation to converge viscous case.

In the next phase, intense CFD study is conducted to understand the usability of design tool for further prelimary designs of scramjet intakes. Firstly, inviscid CFD method with energy equation is applied. Then, viscous CFD method with KW-SST turbulence model is applied. Results are considered quite promising because scramjet intakes have many challenging physical phenomena and remarkable uncertainities exist in the literature. Results of design tool, inviscid CFD and viscous CFD are in strong harmony with each other until isolator entrance. SoL and SoS design criterias are satisfied for inviscid CFD, and negligible deviations around cowl tip and shoulder exist for viscous CFD. After isolator exit, it is observed that inviscid CFD loses accuracy as expected because viscous effects and boundary layer flow dominate the isolator. Isolator flow is solved considering frictional effects in design tool so it is able to follow viscous solution under maximum %10 deviation for all thermodynamic paramaters. Some parameters are even closer. These results demonstrate that such a tool can be very beneficial for preliminary design phase because viscous CFD is computationally expensive and some factors such as mesh treatment and tuning solver make it inefficient despite its accuracy. It is clear that even little separation bubbles or deviations from SoL-SoS condition create differences on flowfield but initial design phases do not require such level of details.

In additon to these comparisons, parametric off-design studies are conducted to investigate what kind of changes occur away from design point because scramjet cycles operate in a narrow band. Effects of Mach number change and flight altitude change indicates that variable geometry is needed to keep optimum performance. In fact, fatal results may occur if certain Mach number limits are passed such as engine unstart. Also, the effect of wall temperatures on overall performance is mentioned in many references; therefore, this effect is observed. While higher wall temperature can have positive impacts, adiabatic wall condition suffers from accuracy.

In conclusion, present thesis combines the deisgn and numerical investigation of a generic scramjet intake. The main finding is that proposed design tool can be used for preliminary design phase with an acceptable accuracy, and the present CFD settings can be used for research in the future.

6.2 Further Works and Recommendations

As it is mentioned many times in present thesis, scramjet intake-isolator flows have many challenges and uncertainties about both numerically and experimentally. Steady RANS simulations are sufficient, but they are not perfect without additional studies. Unsteady flow physics is the core of this field and successful experiences of this study should be used for unsteady cases. Start-unstart investigations can boost the understanding of intake design. Moreover, 3D CFD simulations can be observed to see effects of three dimensionality on flow field and exit properties.

Scramjet propelled hypersonic vehicles follow the integrated design methodology. In other works, every component of scramjet and carrier vehicle are strongly coupled with each other. In present design, design constraints at the exit of isolator provide some coupling with the rest of the engine. Optimization cycles can be used to find optimum geometry for defined design point. Evolutionary algorithms seems promising to change the sizing of the model. Viscous CFD contours demonstrate that there are local regions with bubbles or excessive temperatures, especially away from design point. Multi-Objective optimizations can decrease these effects without losing the overall performance.

Lastly, the design tool is open to developments based on new information or techniques. Intake part already does its tasks fine, but isolator part can include advanced modules. In addition to frictional effects, heat transfer effects can be included to increase accuracy. Wall temperature increase makes viscous CFD results closer to design tool. This situation can be a good sign to investigate further.

REFERENCES

[1] Anderson, J. (2016). *Fundamentals of Aerodynamics*. Mcgraw-Hill.

[2] Andreadis, D. (n.d.). *SCRAMJET ENGINES ENABLING THE SEAMLESS INTEGRATION OF AIR & SPACE OPERATIONS* . Retrieved from https://www.kimerius.com/app/download/5784275952/Scramjet+engines+enabling+the+seamless+integration+of+air++space+operations.pdf

[3] ANSYS Inc. (2017). *ANSYS Fluent Tutorial Guide Release 18.0*.

[4] Araújo, P. P. B., Pereira, M. V. S., Marinho, G. S., Martos, J. F. A., & Toro, P. G. P. (2021). Optimization of Scramjet Inlet based on temperature and Mach number of supersonic combustion. *Aerospace Science and Technology*, *116*, 106864. https://doi.org/10.1016/j.ast.2021.106864

[5] Başaran, M. (2019). *Adjoint-based design optimization of a hypersonic inlet* (thesis). Ankara.

[6] Berto, F., Benini, E., Wyatt, C., & Quinn, M. K. (2020). Time-accurate experimental investigation of Hypersonic Inlet Buzz at mach 5. *AIAA Journal*, *58*(5), 2197–2205. https://doi.org/10.2514/1.j058764

[7] Biasca, R. J. (1988, July). *Chemical Kinetics of SCRAMJET Propulsion*. Master of Science. Retrieved from https://core.ac.uk/download/pdf/4400852.pdf

[8] Billig, F. S. (1993). Research on supersonic combustion. *Journal of Propulsion and Power*, *9*(4), 499–514. https://doi.org/10.2514/3.23652

[9] Bouchez, M. (2013). *Scramjet Thermal Management (tenue thermique des superstatoreacteurs): Semantic scholar*. Retrieved from https://www.semanticscholar.org/paper/Scramjet-Thermal-Management-(Tenue-thermique-des-Bouchez/f211b0ebf91198f04b880ce16d5485c3f4a77575

[10] Cardoso, I. M. da C. (2021, January). *Aerodynamic Analysis of a Scramjet Inlet and Isolator*. Retrieved from https://fenix.tecnico.ulisboa.pt/downloadFile/1126295043838809/93819_Thesis.pdf

[11] Cecchetto, P. (2021). *Hypersonic air intake design using multi-objective optimisation based on CFD data*. Universita degli Studi di Padova Master of

Science in Aerospace Engineering. Retrieved from https://thesis.unipd.it/bitstream/20.500.12608/10103/1/Cecchetto_Pietro.pdf

[12] Cengel, Y. A., & Cimbala, J. M. (2018). *Fluid Mechanics: Fundamentals and Applications*. McGraw-Hill Education.

[13] Curran, E. T., & B., M. S. N. (2000). *Scramjet Propulsion*. American Institute of Aeronautics and Astronautics.

[14] Denman, Z., Wheatley, V., Smart, M. K., & Veeraragavan, A. (2016). *Fuel injection and mixing in a Mach 8 hydrocarbon-fuelled scramjet*. Proceedings of the 20th Australasian Fluid Mechanics Conference, AFMC 2016. Retrieved from https://espace.library.uq.edu.au/view/UQ:435074

[15] Ferguson, F., Dhanasar, M., Grant, J., Uitenham, L., & Blankson, I. (2011). CFD analysis of an inlet-isolator combination for dual mode scramjet applications. *49th AIAA Aerospace Sciences Meeting Including the New Horizons Forum and Aerospace Exposition*. https://doi.org/10.2514/6.2011-404

[16] Fischer, C. M. (2014). *Investigation of the isolator flow of scramjet engines*. DNB. Retrieved from https://portal.dnb.de/opac.htm?method=simpleSearch&cqlMode=true&query=idn%3D1059796627

[17] Flock, A. K. (2017). *Design and Performance Analysis of Three-Dimensional Air Intakes for Supersonic Combustion Ramjet Engines*. eLib. Retrieved from https://elib.dlr.de/111146/

[18] Frauholz, S., Behr, M., Reinartz, B., & Müller, S. (2012). Numerical simulation of hypersonic air intake flow in scramjet propulsion using a mesh-adaptive approach. *18th AIAA/3AF International Space Planes and Hypersonic Systems and Technologies Conference*. https://doi.org/10.2514/6.2012-5976

[19] Geerts, J. S., & Yu, K. H. (2016). Shock train/boundary-layer interaction in rectangular isolators. *AIAA Journal*, *54*(11), 3450–3464. https://doi.org/10.2514/1.j054917

[20] Häberle, J., & Gülhan, A. (2006). Investigation of the performance of a scramjet inlet at mach 6 with Boundary Layer Bleed. *14th AIAA/AHI Space Planes and Hypersonic Systems and Technologies Conference*. https://doi.org/10.2514/6.2006-8139

[21] Häberle, J., & Gülhan, A. (2008). Investigation of two-dimensional Scramjet Inlet Flowfield at mach 7. *Journal of Propulsion and Power*, *24*(3), 446–459. https://doi.org/10.2514/1.33545

[22] Heiser, W. H., & Pratt, D. T. (1994). *Hypersonic Airbreathing Propulsion*. AIAA.

[23] Henrotin, J. (2021, June 18). *Hypersonic weapons: What are the challenges for the Armed Forces - Ifri*. Security Studies Center. Retrieved from https://www.ifri.org/sites/default/files/atoms/files/henrotin_hypersonic_weapons_2021.pdf

[24] Hong Quan, L. (2016). Analysis and design of a scramjet engine inlet operating from mach 5 to mach 10. *International Journal of Mechanical Engineering and Applications*, *4*(1), 11. https://doi.org/10.11648/j.ijmea.20160401.12

[25] Idris, A. C. (2014, September). *Characterization of High Speed Inlets Using Global Measurement Techniques*. Manchester eScholar Services. Retrieved from https://www.escholar.manchester.ac.uk/item/?pid=uk-ac-man-scw%3A235518

[26] Idris, A., Saad, M., Zare-Behtash, H., & Kontis, K. (2014). Luminescent Measurement Systems for the investigation of a Scramjet Inlet-Isolator. *Sensors*, *14*(4), 6606–6632. https://doi.org/10.3390/s140406606

[27] Jeong, E., O'Byrne, S., Jeung, I.-S., & Houwing, A. F. P. (2020, January 1). *The effect of fuel injection location on supersonic hydrogen combustion in a cavity-based model scramjet combustor*. MDPI. Retrieved from https://www.mdpi.com/1996-1073/13/1/193

[28] João Felipe de Araujo Martos, Renan Guilherme Santos Vilela, Bruno Coelho Lima, Sérgio Nicholas Pachon Laiton, Thiago Victor Cordeiro Marcos, Israel da Silveira Rego, & Paulo Gilberto de Paula Toro. (2016). Experimental investigation of the Brazilian 14-X B hypersonic scramjet aerospace vehicle. *IX Congresso Nacional De Engenharia Mecânica*. https://doi.org/10.20906/cps/con-2016-1150

[29] John, B., Sarath, G., Kulkarni, V., & Natarajan, G. (2014). Performance comparison of flux schemes for numerical simulation of high-speed inviscid flows. *Progress in Computational Fluid Dynamics, An International Journal*, *14*(2), 83. https://doi.org/10.1504/pcfd.2014.060142

[30] Kang, S., Shin, H. C., Park, S. H., Park, J., & Park, D. (2021). Comparative assessment of modified X models for scramjet intake flow analysis. *International Journal of Aerospace Engineering*, *2021*, 1–24. https://doi.org/10.1155/2021/9916416

[31] Kellecy, F. J. (2021, April). *Adjoint Shape Optimization for Aerospace Applications*. *NASA Ames Research Center*.

[32] Khan, D. A., Hassan, M. H., & Qamar, I. (2019). Design of Hypersonic Scramjet Engine Operating between Mach 5 to Mach 9. *2019 Sixth International Conference on Aerospace Science and Engineering (ICASE)*. https://doi.org/10.1109/icase48783.2019.9059159

[33] Krieger, A. T. E. (2019). *Numerical Simulation of the Start and Unstart Behaviour of a Ram- or Scramjet* (thesis). RWTH Aachen University.

[34] Krause, M., & Ballmann, J. (2009). Enhanced design of a scramjet intake using two different Rans Solvers. *Shock Waves*, 589–594. https://doi.org/10.1007/978-3-540-85168-4_94

[35] Krause, M., Reinartz, B., & Ballmann, J. (2006). *Numerical Computations for Designing a Scramjet Intake*. 25th INTERNATIONAL CONGRESS OF THE AERONAUTICAL SCIENCES. Retrieved from http://icas.org/ICAS_ARCHIVE/ICAS2006/PAPERS/194.PDF

[36] Krishnan, M., Ray, A., & Peetala, R. (2022). Numerical Analysis of high speed flow applications using various flux schemes. *Trends in Sciences*, *19*(18), 5813. https://doi.org/10.48048/tis.2022.5813

[37] Launder, B. E., & Spalding, D. B. (1974). The numerical computation of turbulent flows. *Computer Methods in Applied Mechanics and Engineering*, *3*(2), 269–289. https://doi.org/10.1016/0045-7825(74)90029-2

[38] Lee, J., & Kang, S. H. (2019). Numerical study on the start and unstart phenomena in a scramjet inlet-isolator model. *PLOS ONE*, *14*(11). https://doi.org/10.1371/journal.pone.0224994

[39] Li, N., Qu, F., Sun, D., & Wu, G. (2022). An effective AUSM-type scheme for both cases of low Mach number and high Mach number. *Applied Sciences*, *12*(11), 5464. https://doi.org/10.3390/app12115464

[40] Mahoney, J. (1991). Inlets for Supersonic Missiles. https://doi.org/10.2514/4.403799

[41] Markell, K. C. (2005). *Exergy methods for the generic analysis and optimization of Hypersonic Vehicle Concepts* (thesis). Virginia Tech.

[42] Mateu, M. M., & Dalmases, J. O. L. (2013, September). *Study of an air-breathing engine for hypersonic flight*. Technical Report. Retrieved from https://upcommons.upc.edu/bitstream/handle/2099.1/20295/Technical%20Report.pdf

[43] Menter, F. R., Lechner, R., & Matyushenko, A. (2021). *Best Practice: Rans Turbulence Modeling in Ansys Cfd*. *Turbulence Modeling for Aerodynamic Flows*.

[44] Mingbo, S., Bin, A., Hongbo, W., & Chenglong, W. (2022, March 18). *Numerical simulation of the scramjet engine: From numerical flight to Intelligent Numerical Flight*. Retrieved from https://lxxb.cstam.org.cn/en/article/doi/10.6052/0459-1879-21-397

[45] Moura, A. F., & Rosa, M. P. (2014, July). *A Numerical Investigation of Scramjet Engine Air Intakes for the 14-X Hypersonic Vehicle*. WCCM XI - ECCM V - ECFD VI. Retrieved from https://www.researchgate.net/publication/264691543_A_numerical_investigation_of_scramjet_engine_air_intakes_for_the_14-X_hypersonic_vehicle

[46] Musielak, D. (2022). *Scramjet Propulsion: A practical introduction* (1st ed.). Wiley.

[47] Neuenhahn, T. (2010, March). *Investigation of the Shock Wave Boundary Layer Interaction of Scramjet Intake Flows*. RWTH Publications. Retrieved from https://publications.rwth-aachen.de/record/94607/

[48] Nguyen, T. Q. T., & Behr. (2011, December). *Numerical Investigations of Relaminarization in Scramjet Flows*. Numerical investigations of relaminarization in scramjet flows - RWTH Publications. Retrieved from https://publications.rwth-aachen.de/record/50136/

[49] Oliden, D. (2013, December). *Parametric Analysis of a Hypersonic Inlet Using Computational Fluid Dynamics*. ASU Electronic Theses and Dissertations. Retrieved from https://keep.lib.asu.edu/items/152249

[50] Pletcher, R. H., Tannehill, J. C., & Anderson, D. A. (2021). *Computational Fluid Mechanics and heat transfer*.

[51] Qu, F., Sun, D., Liu, Q., & Bai, J. (2021). A review of Riemann solvers for Hypersonic flows. *Archives of Computational Methods in Engineering*, *29*(3), 1771–1800. https://doi.org/10.1007/s11831-021-09655-x

[52] Reardon, J. P. (2019, November 26). *Computational Analysis of Transient Unstart/Restart Characteristics in a Variable Geometry, High-speed Inlet*. VTechWorks Home. Retrieved from https://vtechworks.lib.vt.edu/handle/10919/95883

[53] Rumsey, C. (n.d.). *Langtry-Menter 4-equation transitional SST model*. Langley Research Center Turbulence Modeling Resource. Retrieved from https://turbmodels.larc.nasa.gov/langtrymenter_4eqn.html

[54] Sanders, B. W., & Weir, L. J. (2008). Aerodynamic Design of a Dual-Flow Mach 7 Hypersonic Inlet System for a Turbine-Based Combined-Cycle Hypersonic Propulsion System. *NASA/CR—2008-215214, 20080030791*.

[55] Sarout, Y., R, T. K., & Paramasivam, S. (2020). Numerical simulation of flow through Scramjet Inlet - isolator model with pressure feedback. *AIAA Scitech 2020 Forum*. https://doi.org/10.2514/6.2020-0650

[56] Segal, C. (2009). The Scramjet engine. *Processes and Characteristics*. https://doi.org/10.1017/cbo9780511627019

[57] Seleznev, R. K. (2018). History of Scramjet Propulsion Development. *Journal of Physics: Conference Series*, *1009*, 012028. https://doi.org/10.1088/1742-6596/1009/1/012028

[58] Sen, D., Pesyridis, A., & Lenton, A. (2018). A scramjet compression system for Hypersonic Air Transportation Vehicle Combined Cycle Engines. *Energies*, *11*(6), 1568. https://doi.org/10.3390/en11061568

[59] Smart, M. K. (2010). Scramjet Inlets . *RTO-EN-AVT-185* .

[60] Smart, M. K. (2012). How much compression should a scramjet inlet do? *AIAA Journal*, *50*(3), 610–619. https://doi.org/10.2514/1.j051281

[61] Smart, M., & Stalker, R. (2010, September). *Scramjet Combustion Processes - DTIC*. RTO-EN-AVT-185. Retrieved from https://apps.dtic.mil/sti/pdfs/ADA581903.pdf

[62] Song, W.-yan, Li, M., Cai, Y.-hu, Liu, W.-xiong, & Bai, H.-chen. (2004). Experimental investigation of hydrocarbon-fuel ignition in Scramjet Combustor. *Chinese Journal of Aeronautics*, *17*(2), 65–71. https://doi.org/10.1016/s1000-9361(11)60216-1

[63] Spalart, P., & Allmaras, S. (1992). A one-equation turbulence model for aerodynamic flows. *30th Aerospace Sciences Meeting and Exhibit*. https://doi.org/10.2514/6.1992-439

[64] Sullins, G., & Mclafferty, G. (1992). Experimental results of shock trains in rectangular ducts. *AlAA 4th International Aerospace Planes Conference*. https://doi.org/10.2514/6.1992-5103

[65] Thaw, P. W., & Thu, Z. W. (2018, September). *Development and Validation of Hypersonic Engine Inlet Design Code*. International Journal of Research and Scientific Innovation (IJRSI). Retrieved from https://www.rsisinternational.org/journals/ijrsi/digital-library/volume-5-issue-9/108-115.pdf

[66] The Times. (2018, August 10). *Need for speed: Why the US is spending billions in a hypersonics arms race*. World | The Times. Retrieved from https://www.thetimes.co.uk/article/need-for-speed-why-the-us-is-spending-billions-on-hypersonics-fr977p8jq

[67] Tran, K. (2011, January 8). *One Dimensional Analysis Program for scramjet and Ramjet Flowpaths*. VTechWorks Home. Retrieved from https://vtechworks.lib.vt.edu/handle/10919/30857

[68] Urzay, J. (2018). Supersonic combustion in air-breathing propulsion systems for hypersonic flight. *Annual Review of Fluid Mechanics*, *50*(1), 593–627. https://doi.org/10.1146/annurev-fluid-122316-045217

[69] Van Wie, D. M., White, M. E., & Corpening, G. P. (1990). *John Hopkins APL Technical Digest*, *11*, 353–362.

[70] Walet, N. (2022, July 4). *Explicit boundary conditions*. Mathematics LibreTexts. Retrieved from https://math.libretexts.org/Bookshelves/Differential_Equations/Book%3A_Partial_Differential_Equations_(Walet)/03%3A_Boundary_and_Initial_Conditions/3.02%3A_Explicit_Boundary_Conditions

[71] Waltrup, P. J., & Billig, F. S. (1973). Structure of shock waves in cylindrical ducts. *AIAA Journal*, *11*(10), 1404–1408. https://doi.org/10.2514/3.50600

[72] Versteeg, H. K., & Malalasekera, W. (2011). *An introduction to computational fluid dynamics: The Finite Volume Method*. Prentice Hall.

[73] Yao, Y. F. (2013). Scramjet Flow and intake SBLI: Technical challenges and case study. *Applied Mechanics and Materials*, *315*, 344–348